ABSTRACT

FIDAN, EMINE. Understanding Hurricane-Induced Water Quantity and Quality Dynamics Using Machine Learning and Environmental Data Analytics Approaches. (Under the direction of Dr. Natalie G. Nelson).

Hurricanes are disruptive and alter water quantity and quality dynamics in surface waters. Process based models are commonly used to assess flood extent and water quality changes. However, these models typically require sophisticated boundary conditions, an understanding of complex drainage systems, abundance of validation data, expert domain knowledge, and high computational power. This dissertation focuses on advancing the use of machine learning, statistical modeling, and data analytics to evaluate flood dynamics and water quality trends induced by extreme events.

The specific objectives of this research were to (1) evaluate the application of the Random Forest, a machine learning algorithm, for daily flood extent modeling in low-lying and flat terrains using rainfall and physiographic characteristics as predictors, (2) explain floodwater nutrient concentrations as a function of watershed characteristics using Bayesian statistical learning methods, and (3) quantify hurricane impacts on dissolved oxygen trends within different estuaries using data analytics.

Objective 1 was accomplished by processing satellite imagery and delineating landscape characteristics to produce a timeline of pluvial flooding from Hurricanes Matthew (2016) and Florence (2018). A Random Forest model was trained within the North Carolina (NC) Coastal Plain and results indicated that the model predicts pluvial flooding well, with overall accuracy of 0.96 and F1 score of 0.83. An evaluation of model variables indicated that physically-based predictor variables, distance to the nearest

stream, distance to the nearest road, and height above nearest drainage, were the most important in flood extent prediction. Objective 2 identified the nutrient water quality signatures in Hurricane Florence (2018) floodwaters and characterized the potential drivers of nutrient pollution as a function of different environmental variables using geostatistical Bayesian modeling techniques. Results showed that rainfall and pollution point sources were important variables in explaining nutrient responses, with concentrated animal feeding operations (CAFOs) and wastewater treatment plant (WWTP) variables being important factors influencing floodwater nutrient concentrations. This study suggests that better management of CAFOs and WWTPs for extreme storm events may be necessary to reduce nutrient pollution in floodwaters. Study 3 quantified how hurricanes affect dissolved oxygen trends within different estuaries along the U.S. Atlantic coast using data science tools. Our findings revealed no change in dissolved oxygen concentrations after hurricane impact within the tidal estuaries in our study region. We believe that the short residence time within the estuaries in this study likely induced freshwater flushing and dilution of nutrients and organic matter entering the coastal basins; this effect may have feasibly muted the DO response.

These three studies above explore hurricane impacts on surface water quantity and quality, as well as the potential drivers of surface water dynamics. These studies reveal how extreme events sometimes impact our rivers and estuaries, but not always, and the variables that potentially drive the observed impacts.

Understanding Hurricane-Induced Water Quantity and Quality Dynamics Using Machine Learning and Environmental Data Analytics Approaches

By
Emine Fidan

A dissertation submitted to the Graduate Faculty of
North Carolina State University
in partial fulfillment of the
requirements for the degree of
Doctor of Philosophy

Biological and Agricultural Engineering

Raleigh, North Carolina
2023

APPROVED BY:

_____	_____
Dr. Natalie Nelson Committee Chair	Dr. Ryan Emanuel
_____	_____
Dr. Angela Harris	Dr. Barbara Doll

DEDICATION

For myself.
Because all that hard work finally produced this.

BIOGRAPHY

Emine Fidan grew up in Tennessee loving the environment around her. She pursued a Bachelor's of Science in Biosystems Engineering at the University of Tennessee, graduating in 2018. Upon graduating that year, she joined the Department of Biological and Agricultural Engineering at North Carolina State University as a doctoral student under the supervision of Dr. Natalie Nelson. Emine's research interests are on quantifying surface water dynamics using data science tools. Outside of research, Emine enjoys travelling, being outdoors, crafting, and gardening.

ACKNOWLEDGMENTS

Thank you to my advisor, Dr. Natalie Nelson, for your endless support. I could not have asked for a better mentor to guide me through the PhD process. You are selfless, supportive, engaging, brilliant, and my role model. I want to be the type of professor you are: one who cares, who puts herself in the student's shoes, who maintains open communication, who can take a joke and laugh out loud, who enjoys working, who sees the good in everyone, and who knows when to take a break and enjoy the little things. I am a better researcher because of you.

I also want to acknowledge my awesome committee members for their applied knowledge, patience, and inspiration. Drs. Barbara Doll, Angela Harris, and Ryan Emanuel, I am so lucky to have committee members who always look forward to seeing and hearing from me. You all have challenged me to think on my feet and seeing your excitement for my research gives me the motivation to keep going. Thank you for shaping me into the scholar I am now.

I will always be grateful for my best friends, Molly Landon, Riley Lawson, Megan Carr, Emma Tobin, and Enrique Peña. Thank you for being my best supporters throughout my PhD! I also could not have handled the stress of my PhD without all the graduate students and friends I have made while here– so thank you!

Special thanks to my siblings, Kemal and Esma Fidan! Thank you for making me laugh, putting up with me, and keeping me grounded. Additionally, I am deeply thankful for my parents, who instilled the value of education and hard work.

Finally, thank you to my pup, Goose. Goose, you are the best companion I didn't know I needed. Thank you for the cuddles and attention and unconditional love.

TABLE OF CONTENTS

LIST OF TABLES

LIST OF FIGURES

CHAPTER 1: INTRODUCTION

1. HURRICANE IMPACTS ON PUBLIC AND ENVIRONMENTAL HEALTH

Hurricanes are extreme events that create devastating impacts to people, property, and the environment. High speed winds, intense rainfall, flooding, and physical devastation from these extreme storm events have the capacity to influence biogeochemical cycling, water quality, biodiversity, and even human health.

Strong winds from extreme storm events have been shown to resuspend and transport sediments, which affect downstream salinity and water quality (Schafer et al., 2020). Flooding and rainfall-driven runoff induced by hurricanes has the capacity to increase discharge and pollutant loads, which in return can lead to eutrophication, harmful algal blooms, and disease outbreaks among the public (Ahern et al., 2005; Paerl et al., 2018). Additionally, the disturbances from strong storm events have been shown to detrimentally affect trees, birds, and aquatic life (Chambers et al., 2000; Marsh & Wilkinson, 1991; Tabb & Jones, 1962; Tanner et al., 1991).

Many studies have investigated the impacts of stormwater on surface water dynamics (e.g., Bedan & Clausen, 2009; Jefferson et al., 2017; Makepeace et al., 1995; Tsihrintzis & Hamid, 1997; Vogel & Moore, 2016). However, the impacts of major storm events, such as hurricanes and tropical storms, are comparably understudied. Major storm events are destructive and dangerous, creating logistical challenges for obtaining data. Modeling and data analytics methods have the capabilities to convert our limited data into knowledge and insights on surface water dynamics.

Overall, it is anticipated that as climate change progress, the risks associated with hurricanes and flooding will increase as well (Milly et al., 2002); thus, it is important

to characterize the impacts associated with hurricanes and understand the potential drivers of those impacts. In return, quantifying these impacts can inform the development of management actions and policies focused on minimizing the effects of hurricane disasters on the public and the environment.

2. USING DATA ANALYTICS AND MODELING TO UNDERSTAND HURRICANE IMPACTS ON SURFACE WATER RESOURCES

Quantifying the factors that influence surface water dynamics is important in explaining the drivers of water quality and planning effective water management. Anthropogenic activities, natural catchment characteristics, and weather/climate variability heavily influence the spatio-temporal variability of flood extent and water quality constituents (Arheimer & Lidén, 2000; Lintern et al., 2018; Meybeck & Helmer, 1989; Song et al., 2022; Varanka et al., 2015). In particular, surface water hydrology and hydraulics are complex during hurricane events and involve inputs from landscapes that are typically not hydrologically connected to surface waters. While we have an understanding of the variables that influence runoff in non-flooded conditions, there is a lack in understanding of the degree in which different landscape, watershed, and weather characteristics influence pluvial flooding, flood water contamination, and the quality of receiving waters at varying spatio-temporal scales.

At present, approaches for modeling surface water dynamics include using process-based modeling and data-driven modeling methods. Physically based models apply the laws of fluid motion to simulate hydrodynamic processes, thus making this class of models an ideal choice for characterizing surface water processes. Despite their strengths, many studies have also highlighted the challenges with process-based

modeling techniques– generally speaking, physically based models require sophisticated boundary conditions, an understanding of complex drainage systems, abundance of validation data, expert domain knowledge, and use of high computational power (Choubin et al., 2019; Zakaria et al., 2021). On the other hand, data-based or empirical methods are able to model surface water processes without explicit physical process representation and serve as valuable alternatives to physically-based models.

With the increase of environmental data collection year by year, the need to reveal hidden trends in data using data analytics is growing more important (Szalay & Gray, 2006). Data science tools, such as machine learning, have revolutionized the extraction of meaning information within environmental data by revealing patterns that would otherwise be challenging to deduce. Despite the advancements in data analysis approaches, such concepts have not been widely adopted within the environmental sciences (Zhong et al., 2021). Here, we present research that applies data science tools to extract knowledge from environmental data and create actionable insights. By utilizing the increasing amount of environmental data, we can provide insights into surface water trends and drivers, and inform effective management strategies that tackle environmental problems.

3. RESEARCH FRAMEWORK AND ORGANIZATION OF DISSERATATION

The research presented in this doctoral dissertation applied modeling and data analytics to understand how hurricanes impact the quantity and quality of surface water resources. Specifically, we evaluated the following research studies:

Study 1 (Chapter 2): Machine Learning Approach for Modeling Daily Pluvial Flood Dynamics in Agricultural Landscapes.

The aim of this research was to develop a pluvial flood training and validation set using high spatiotemporal resolution optical remote sensing observations, test the suitability of Random Forest for pluvial flood extent modeling in low-lying and flat agricultural terrain using rainfall and physiographic characteristics as predictors, analyze predictor importance to understand key variables in the model, and generate pluvial flood time series of Hurricanes Matthew and Florence using the trained model. The study area consisted of a region within the NC Coastal Plain, which faced record-breaking flooding from Hurricanes Matthew and Florence.

Study 2 (Chapter 3): Key Descriptors of Nutrient Concentrations in Flood-Impacted Surface Waters

The goals of this study were to generate a spatio-temporal dataset of floodwater nutrient concentrations after Hurricane Florence impact, develop a model that explains nutrient concentrations as a function of watershed characteristics, identify the variables that best explain the nutrient water quality signatures in flood-impacted surface waters. Water quality samples obtained across the NC Coastal Plain were assessed for different N and P constituents at four different time points after Hurricane Florence.

Study 3 (Chapter 4): The Impacts of Hurricane Strength and Watershed Characteristics on Estuarine Dissolved Oxygen (DO) Dynamics

Our goal was to quantify the trends, if any, in DO dynamics after hurricane impact across different estuarine systems. Specifically, we evaluated the trends in DO before, during, and after hurricane impact in different tidal estuaries

spanning the southeast Atlantic coast of the US, a region routinely impacted by hurricanes and where long-term water quality data are available.

4. REFERENCES

Ahern M, Kovats RS, Wilkinson P, Few R, & Matthies F. (2005). Global Health Impacts of Floods: Epidemiologic Evidence. *Epidemiologic Reviews*, 27(1), 36-46. doi: 10.1093/epirev/mxi004

Arheimer, B., & Lidén, R. (2000). Nitrogen and phosphorus concentrations from agricultural catchments—Influence of spatial and temporal variables. *Journal of Hydrology*, *227*(1–4), 140–159. https://doi.org/10.1016/S0022-1694(99)00177-8

Bedan, E.D. & Clausen, J.C. (2009). Stormwater Runoff Quality and Quantity From Traditional and Low Impact Development Watersheds. Journal of the American Water Resources Association (JAWRA), 45(4), 998-1008. https://doi.org/10.1111/j.1752-1688.2009.00342.x

Chambers, J.Q., Fisher, J.I., Zeng, H., Chapman, E.L., Baker, D.B., Hurtt, G.C. (2007). Hurricane Katrina's carbon footprint on U.S. Gulf Coast forests. *Science*, 318(5853), 1107. doi: 10.1126/science.1148913

Choubin, B., Moradi, E., Golshan, M., Adamowski, J., Sajedi-Hosseini, F., & Mosavi, A. (2019). An ensemble prediction of flood susceptibility using multivariate discriminant analysis, classification and regression trees, and support vector machines. *Science of the Total Environment*, 651, 2087–2096. https://doi.org/10.1016/j.scitotenv.2018.10.064

Jefferson, A.J., Bhaskar, A.S. Hopkins, K.G., Fanelli, R., Avellaneda, P.M., & McMillan, S.K. (2017). Stormwater management network effectiveness and implications for urban watershed function: A critical review. *Hydrological Processes*, 31(23), 4056-4080. https://doi.org/10.1002/hyp.11347

Lintern, A., Webb, J. a., Ryu, D., Liu, S., Bende-Michl, U., Waters, D., Leahy, P., Wilson, P., & Western, A. W. (2018). Key factors influencing differences in stream water quality across space. *WIREs Water*, *5*(1), e1260. https://doi.org/10.1002/wat2.1260

Makepeace, D.K., Smith, D.W., Stanley, S.J. (1995). Urban stormwater quality: Summary of contaminant data. Critical Reviews in Environmental Science and Technology, 25(2), 93-139. https://doi.org/10.1080/10643389509388476

Marsh, C. P., & P. M. Wilkinson. (1991). The impact of Hurricane Hugo on coastal bird populations. *Journal of Coastal Research*, 8:327–334.

Meybeck, M., & Helmer, R. (1989). The Quality of Rivers: From Pristine Stage to Global Pollution. *Global and Planetary Change*, *75*(4), 283–309. https://doi.org/10.1016/0921-8181(89)90007-6

Milly, P. C. D., Wetherald, R. T., Dunne, K. A., & Delworth, T. L. (2002). Increasing Risk of Great Floods in a Changing Climate. *Nature*, 415, 514−517.

Paerl, H. W., Crosswell, J. R., Van Dam, B., Hall, N. S., Rossignol, K. L., Osburn, C. L., Hounshell, A. G., Sloup, R. S., & Harding, L. W. (2018). Two decades of tropical cyclone impacts on North Carolina's estuarine carbon, nutrient and phytoplankton dynamics: Implications for biogeochemical cycling and water quality in a stormier world. *Biogeochemistry*, *141*(3), 307–332. https://doi.org/10.1007/s10533-018-0438-x

Schafer, T., Ward, N., Julian, P., Reddy, K.R., & Osborne, T.Z. (2020). Impacts of Hurricane Disturbance on Water Quality across the Aquatic Continuum of a

Blackwater River to Estuary Complex. *Journal of Marine Science and Engineering*, 8(6), 412. doi.org/ 10.3390/jmse8060412

Song, Z., Chomicki, K. M., Drouillard, K., & Weidman, R. P. (2022). A statistical framework for testing impacts of multiple drivers of surface water quality in nearshore regions of large lakes. *Science of The Total Environment*, *811*, 152362. https://doi.org/10.1016/j.scitotenv.2021.152362

Szalay, A., Gray, J., 2006. Science in an exponential world. *Nature*, 440, 413–414. https://doi.org/10.1038/440413a

Tabb, D. C., & A. C. Jones. (1962). Effect of Hurricane Donna on aquatic fauna of North Florida Bay. *Transactions of the American Fisheries Society,* 91, 375–378. https://doi.org/10.1577/1548-8659(1962)91[375:EOHDOT]2.0.CO;2

Tanner, E. V. J., Kapos, V., & Healy, J. R. (1991). Hurricane effects on forest ecosystems in the Caribbean. *Biotropica,* 23(4), 513–521. doi.org/ 10.2307/2388274

Tsihrintzis, V.A., & Hamid, R. (1997). Modeling and Management of Urban Stormwater Runoff Quality: A Review. *Water Resources Management,* 11, 136–164. https://doi.org/10.1023/A:1007903817943

Varanka, S., Hjort, J., & Luoto, M. (2015). Geomorphological factors predict water quality in boreal rivers. *Earth Surface Processes and Landforms*, *40*(15), 1989–1999. https://doi.org/10.1002/esp.3601

Vogel, J.R. & Moore, T.L. (2016). Urban Stormwater Characterization, Control, and Treatment. Water Environment Research, 88(10), 1918-1950. https://doi.org/10.2175/106143016X14696400495938

Zakaria, M. N. A., Abdul Malek, M., Zolkepli, M., & Najah Ahmed, A. (2021). Application of artificial intelligence algorithms for hourly river level forecast: A case study of Muda River, Malaysia. *Alexandria Engineering Journal*, 60(4), 4015–4028. https://doi.org/10.1016/j.aej.2021.02.046

Zhong, S., Zhang, K., Bagheri, M., Burken, J.G., Gu, A., Li, B., et al. (2021). Machine Learning: New Ideas and Tools in Environmental Science and Engineering. *Environmental Science & Technology,* 55, 12741– 12754. https://doi.org/10.1021/acs.est.1c01339

CHAPTER 2: MACHINE LEARNING APPROACH FOR MODELING DAILY PLUVIAL FLOOD DYNAMICS IN AGRICULTURAL LANDSCAPES

Abstract

Despite rural, agricultural landscapes being exposed to pluvial flooding, less research has been conducted on predicting flooding in such regions. To improve and extend pluvial flood modeling approaches for use in agricultural regions, we built a machine learning model framework that uses remotely sensed imagery, gridded rainfall data, and open-access geospatial landscape characteristics to produce a pluvial flood timeline. A Random Forest model was trained and daily flood timelines were generated for Hurricanes Matthew (2016) and Florence (2018) at a 10-m resolution. The results show the model predicts pluvial flooding well, with overall accuracy of 0.96 and F1 score of 0.83. Further evaluation of model outputs highlighted that croplands, specifically corn, soybean, and tobacco fields, were most impacted by the pluvial flooding. Therefore, the model may be used to emphasize agricultural areas susceptible to pluvial flooding, crops that may be potentially impacted, and characteristics of areas that experience pluvial flooding.

Keywords: Random Forest, inundation, surface water flooding

1. INTRODUCTION

Floods are the most common and costliest natural hazard in the United States (USA) and world (NOAA NSSL, n.d.; WHO, n.d.). In the USA, many people are impacted by flood disasters, with financial losses from flood exposure amounting to over 2.5 billion dollars in 2021 alone (NOAA NCEI, 2021). Flooding can occur in different forms: fluvial, coastal, and pluvial. Fluvial flooding is the result of water overflowing the boundaries of a channel, coastal flooding is induced by tides and storm events, and pluvial flooding occurs when heavy rainfall introduces more water than the drainage capacity of the landscape. In particular, pluvial flooding (sometimes referred to as surface water flooding) is often used to describe inundation that occurs outside of floodplains surrounding river networks. Historically, research on flooding has focused on fluvial and coastal mechanisms with pluvial flooding being understudied in comparison (Muthusamy et al., 2019). As a result, more effort has been invested towards analyzing and mitigating fluvial and coastal flooding impacts (Muthusamy et al., 2019). Moreover, of studies that have aimed to advance understanding of pluvial flood dynamics, most have used urban areas as study systems (e.g., Abebe et al., 2018; Guerreiro et al., 2017; Li et al., 2021; Palla et al., 2018; van Dijk et al., 2013).

Although characterizing pluvial flooding in urban settings is important for protecting public health and safety, rural areas also face comparable risks. In particular, crops are sensitive to waterlogging and anaerobic soil conditions; thus, the agricultural sector is prone to detrimental pluvial flood impacts ranging from economic loss to food insecurity at local and global scales (Tanir et al., 2021). With pluvial flooding leading to damages to crops and livestock, having the ability to predict pluvial flood extent in

agricultural landscapes is necessary for identifying vulnerable areas and preparing for flood-driven impacts. Flood models are used by natural resource managers, insurance companies, emergency responders, and policymakers to better understand historical flood dynamics, as well as identify areas of future flood risk. Model outputs, in return, can inform the development of management actions and policies to minimize the impact of flood disasters, as recent studies show that more areas are vulnerable to flooding than current flood maps show (First Street Foundation, 2020; Tellman et al., 2021). Despite the benefits of modeling pluvial flood dynamics, reliably quantifying pluvial flood extent in agricultural landscapes is challenging due to agricultural lands often spanning flat terrains outside of delineated floodplains, and including drainage networks that are poorly mapped relative to natural river channels and tributaries. In addition, modeling pluvial flooding in flat terrains outside of delineated floodplains is often difficult due to the complex and chaotic nature of flood hydraulics (Bernet et al., 2018; Bulti & Abebe, 2020).

Approaches for modeling flooded areas include using process-based modeling and data-driven modeling methods (Teng et al., 2017). Physically based models like HEC-RAS and MIKE FLOOD apply the laws of fluid motion to simulate hydrodynamic processes, thus making this class of flood models an ideal choice for producing dynamic flood estimates. Applications of process-based flood models have been reviewed by Kauffeldt et al., 2016, Teng et al. (2017), Jain et al., (2018), Bulti and Abebe (2020), and Qi et al. (2021). Despite their strengths, many studies have also highlighted the challenges with process-based modeling techniques– generally speaking, physically based models require sophisticated boundary conditions, an

understanding of complex drainage systems, abundance of validation data, expert domain knowledge, and use of high computational power (Choubin et al., 2019; Zakaria et al., 2021).

Data-based or empirical methods in flood modeling are able to provide flood extent estimates without explicit physical process representation and serve as valuable alternatives to physically-based flood models. Traditionally, data-driven flood models have consisted of time-series statistical models, such as linear regression, autoregressive moving average, and auto-regressive integrated moving average (Zakaria et al., 2021). However, recent research has moved away from time-series statistical methods due to their inability to capture non-linear hydrological dynamics, and underlying assumptions regarding normality and stationarity (Zakaria et al., 2021). Machine learning-based data-driven models have gained momentum, particularly as they are well-suited to capture non-linear flood dynamics and often outperform traditional flood modeling methods (Mosavi et al. 2018). Recent studies have demonstrated how support vector machines (e.g. Tehrany et al., 2019), multilayer perceptrons (e.g. Zakaria et al., 2021), decision trees (e.g. Tehrany et al., 2019; Khosravi et al., 2018), adaptive neuro-fuzzy inference systems (e.g. Zakaria et al., 2021; Tabbussum and Dar, 2021), wavelet neural networks (e.g. Yeditha et al., 2020), ensemble prediction systems (e.g. Towfiqul Islam et al., 2021), and other machine learning approaches (e.g. Costache et al., 2020; Kan et al., 2020; Kabir et al., 2021) are effective at predicting flooding using minimal inputs and low computational cost as compared to process-based modeling methods, showing promise for their use as predictive tools of flooding. Although machine learning models require substantial

training data, we can obtain this data readily through remote sensing, which is accessible and does not require *in situ* data collection.

Overall, we sought to improve and extend previous urban pluvial flood modeling approaches for use in rural agricultural regions, specifically by building a machine learning flood model that uses satellite remote sensing, rainfall, and readily-available geospatial landscape characteristics to produce flood extent maps. Our objectives were to 1) develop a pluvial flood training and validation set using high spatiotemporal resolution optical remote sensing observations, 2) test the suitability of Random Forest for pluvial flood extent modeling in low-lying and flat agricultural terrain using rainfall and physiographic characteristics as predictors, 3) analyze predictor importance to understand key variables in the model, and 4) generate pluvial flood time series using the model. We specifically focus on a community in the flat, agriculturally-dominated landscape of the North Carolina (NC) Coastal Plain, USA, as a representative study system, and analyzed flooding across two recent major flood events that occurred as a result of Hurricane Matthew (2016) and Hurricane Florence (2018). The methodological framework developed here is transferable to other agricultural areas, particularly those in low terrain landscapes, and demonstrates how satellite remote sensing observations and machine learning can be used to produce pluvial flood extent time series in rural catchments.

2. METHODS

2.1 Study Area

We focused on Kinston, NC, USA and surrounding rural areas (study region area of 671 km^2) which is located in the low-lying Coastal Plain of eastern NC (Figure 1).

Kinston was selected as the study area due to its vulnerability to extreme flooding, the spatial extent of available remotely sensed data, and extensive agricultural land (row crops and animal production). The predominant land cover in the study area consists of cultivated crops, followed by woody wetlands, evergreen forests, developed open spaces, shrub/scrub lands, and low intensity developed lands; these land cover classes are defined by the US National Land Cover Database 2016 product (Dewitz, 2019).

Hurricanes Matthew and Florence created massive flooding in Kinston in October 2016 and September 2018, respectively. Hurricane Matthew initially impacted the Greater Antilles as a category 5 storm before making landfall along the central coast of South Carolina and bringing heavy rainfall (Stewart, 2017). Hurricane Florence, a long standing category 4 storm, made landfall along the southern coast of North Carolina as a category 1 hurricane (S.R. Stacy & R. Berg, 2019). Despite being downgraded to a category 1 storm, Hurricane Florence caused historic flooding within the region due to its low traveling speed; Hurricane Florence hovered over eastern NC for about 3 days after landfall, delivering 1000-year rainfall in some locations of southeastern NC (NDSC, 2018).

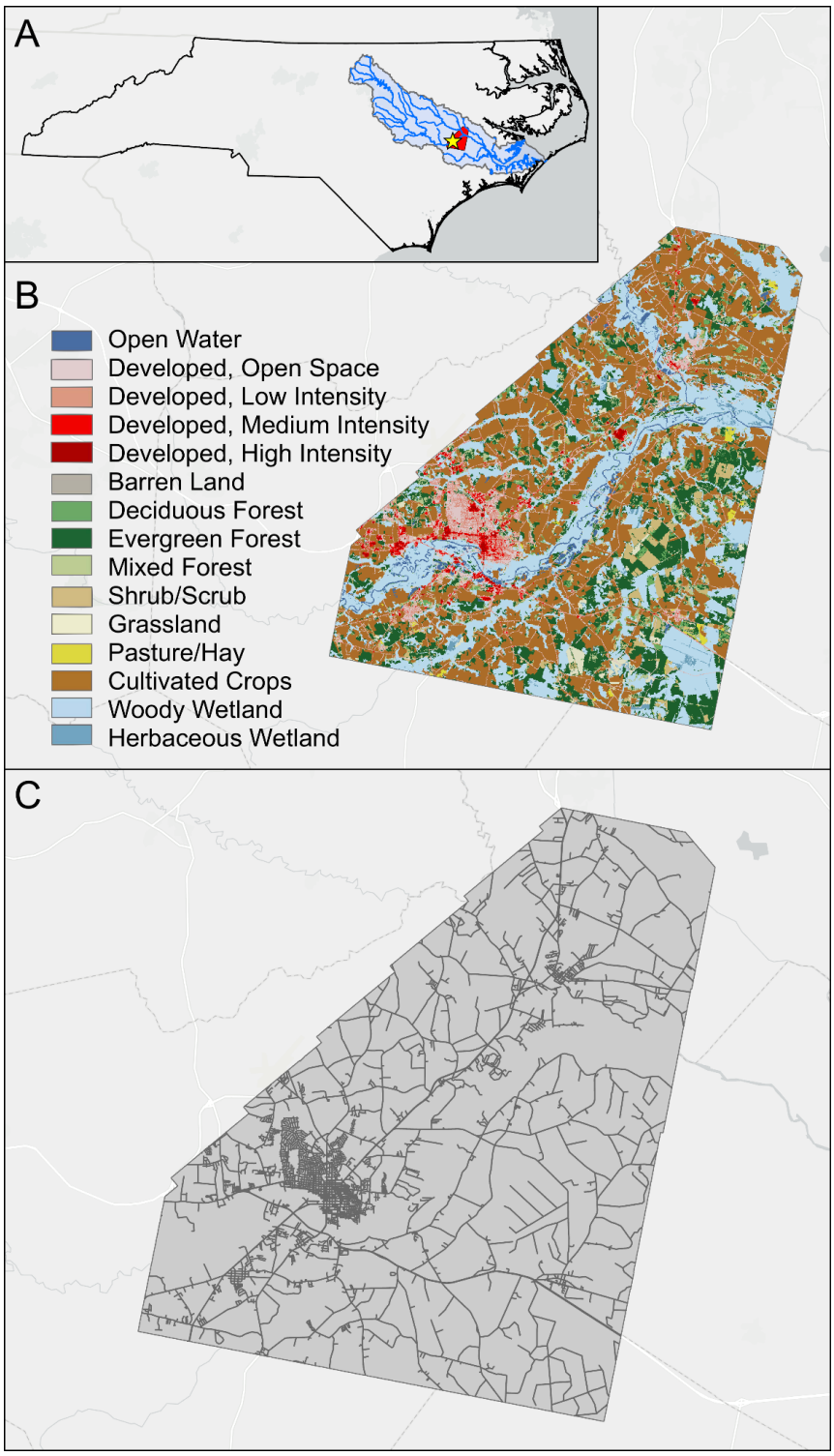

Figure 2- 1. Map of the study area showing (a) the extent of North Carolina with the red region representing the location of the study area, the yellow star indicating the town of Kinston, the light blue area showing the Neuse watershed, and the blue lines showing the Neuse River, (b) the different land cover classifications (Dewitz, 2019) in the study area, (c) the road network in the study area (U.S. Census Bureau, 2015).

2.2 Delineating flooded areas from Planet Labs imagery

In order to create a dynamic flood model, remotely sensed imagery was processed into flood maps that serve to train the model and test it. Planet Labs imagery was selected for this study as it offers daily optical imagery around the world at high resolutions (< 5-m). Optical surface reflectance data from Planet Labs, specifically PlanetScope and RapidEye imagery, were selected instead of radar imagery due to the high spatio-temporal resolution, accessibility, and processing ease of these products. PlanetScope and RapidEye products offer imagery at 3-5 meter resolution almost daily, which was resampled to 10 meters to match the resolution of the predictor variable rasters. Imagery was downloaded for the flooding events following Hurricane Matthew (October 8 - 15, 2016) and Hurricane Florence (September 14 - 19, 2018). Although Planet Labs imagery is available nearly every day, due to cloud cover obstruction from hurricane events, not all daily imagery could be used in this study. Images with greater than 30% cloud coverage were excluded. After excluding data with poor quality due to cloud cover, four remotely sensed images were available for Hurricanes Matthew and Florence (Figure 2). Optical imagery presents issues with canopy penetration; therefore, inundation within forested and woody areas could not be analyzed with this product and were consequently masked from this analysis. Additionally, to avoid capturing the fluvial flood dynamics, the floodplain areas were masked from the training data using the gridded FEMA National Flood Hazard Layer dataset (FEMA, 2019). Lastly, a scene classification (SCL) file was available for Planet Lab imagery; however, due to this product being inadequate in capturing cloud detection, the cloud and cloud shadow pixels had to be masked manually.

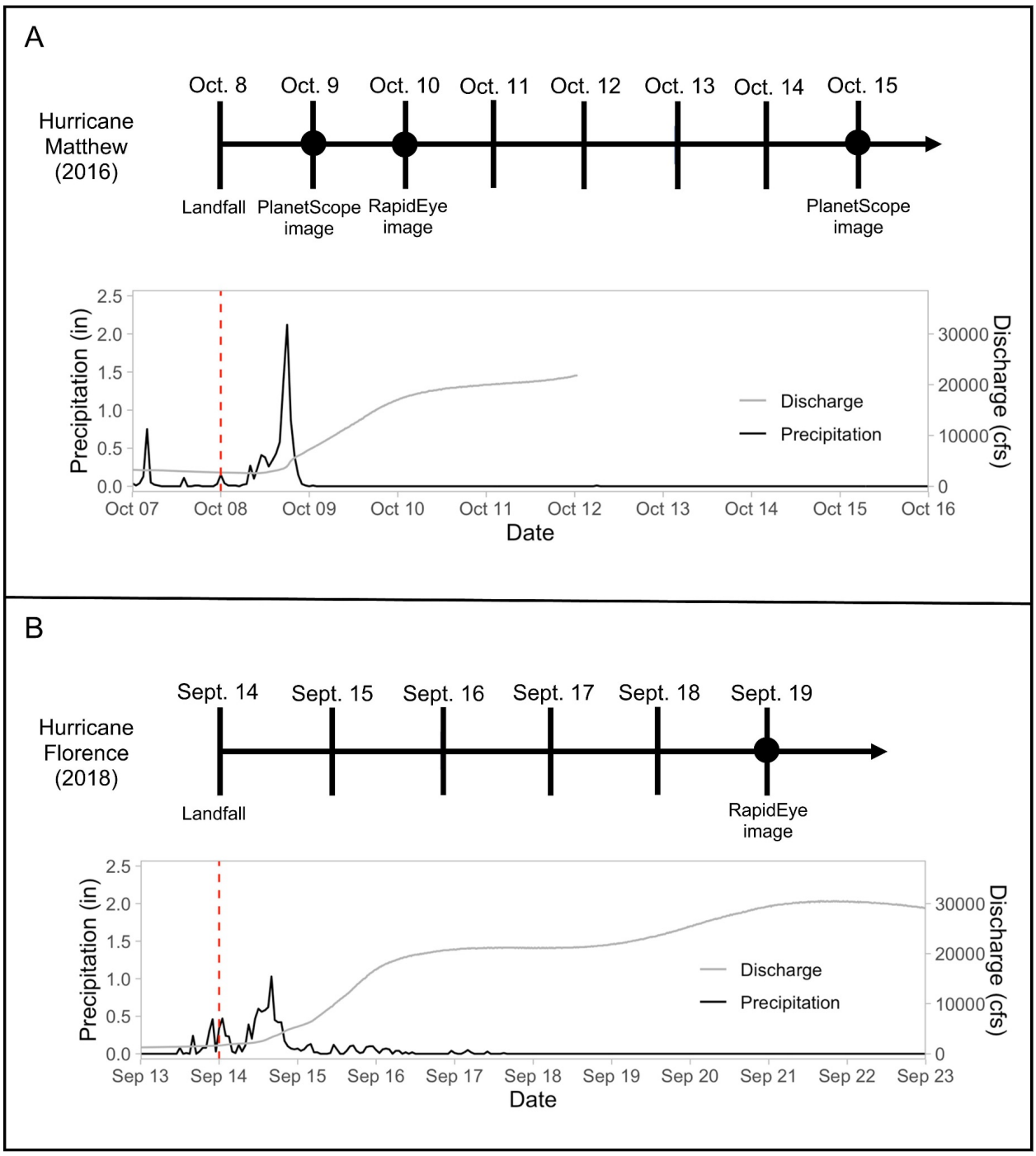

Figure 2- 2. The progression of rainfall and discharge with the corresponding Planet Labs imagery for Hurricanes Matthew (A) and Florence (B) in the Kinston, NC area. The red dotted line represents the date of landfall. The timeline dates with dots represent days in which imagery was available. Note that there is missing discharge data for Hurricane Matthew after Oct. 12.

From the available Planet Labs images, the Normalized Difference Water Index (NDWI) was applied to delineate standing water (Equation 1; McFeeters 1996). The NDWI ranges from values of -1 to 1, in which values closer to -1 indicate dry/vegetative pixels and values closer to 1 indicate water pixels.

$$NDWI = \frac{green - nir}{green + nir} \quad (1)$$

In Equation 1, green is the green band (typically ranging from 500-590 nm) and nir is the near infrared band (ranging from 760-860 nm). The equation was applied to each pixel in each image.

Although the NDWI index highlights areas of standing water, a threshold value must be set in order to classify areas as either flooded or not flooded. To obtain a threshold value, high-resolution (15 cm) aerial imagery sparsely collected by the US National Oceanographic and Atmospheric Administration (NOAA) Emergency Response program was separately analyzed to determine which areas were flooded/non-flooded, and then compared to the satellite imagery NDWI values. NOAA Emergency Response aerial imagery for Hurricane Florence was collected in the Kinston area on September 19, 2018, a date for which Planet Labs imagery was also available for NDWI value comparisons. A total of 2,500 10-m by 10-m sample tiles were randomly generated from the NOAA aerial imagery and manually labeled as either flooded or not flooded depending on whether the floodwater fraction was ≥50% flooded or <50% not flooded, respectively (Figure A-1). 2,500 samples were chosen according to Equation 2, which estimates the standard error of the overall accuracy, i.e., the classification accuracy (CA), given a number of samples (n), assuming that the samples are a small proportion of the entire dataset such that this proportion is effectively zero.

To determine the number of samples required, we solved for n in Equation 2, using a conversative CA of 0.5 and a standard error (SE) of 0.01.

$$SE = \sqrt{CA * (1 - CA)/n} \qquad (2)$$

Using the labeled NOAA aerial imagery data and NDWI values calculated from Planet Labs imagery, a receiver operator characteristic (ROC) analysis was performed to determine which NDWI value would be the best threshold when partitioning flood/non-flood conditions. The ROC analysis balanced sensitivity and specificity to find the optimum NDWI threshold value for separating pixels into flood and non-flood classes. Specifically, the ROC analysis works by calculating the true positive rate and false positive rate of the data at different NDWI thresholds and summarizing which threshold has the highest true positive and lowest false positive rate. Using this threshold, binary flood extent maps were created using NDWI from the Planet imagery. Figure 3 represents the complete workflow used to generate the training data.

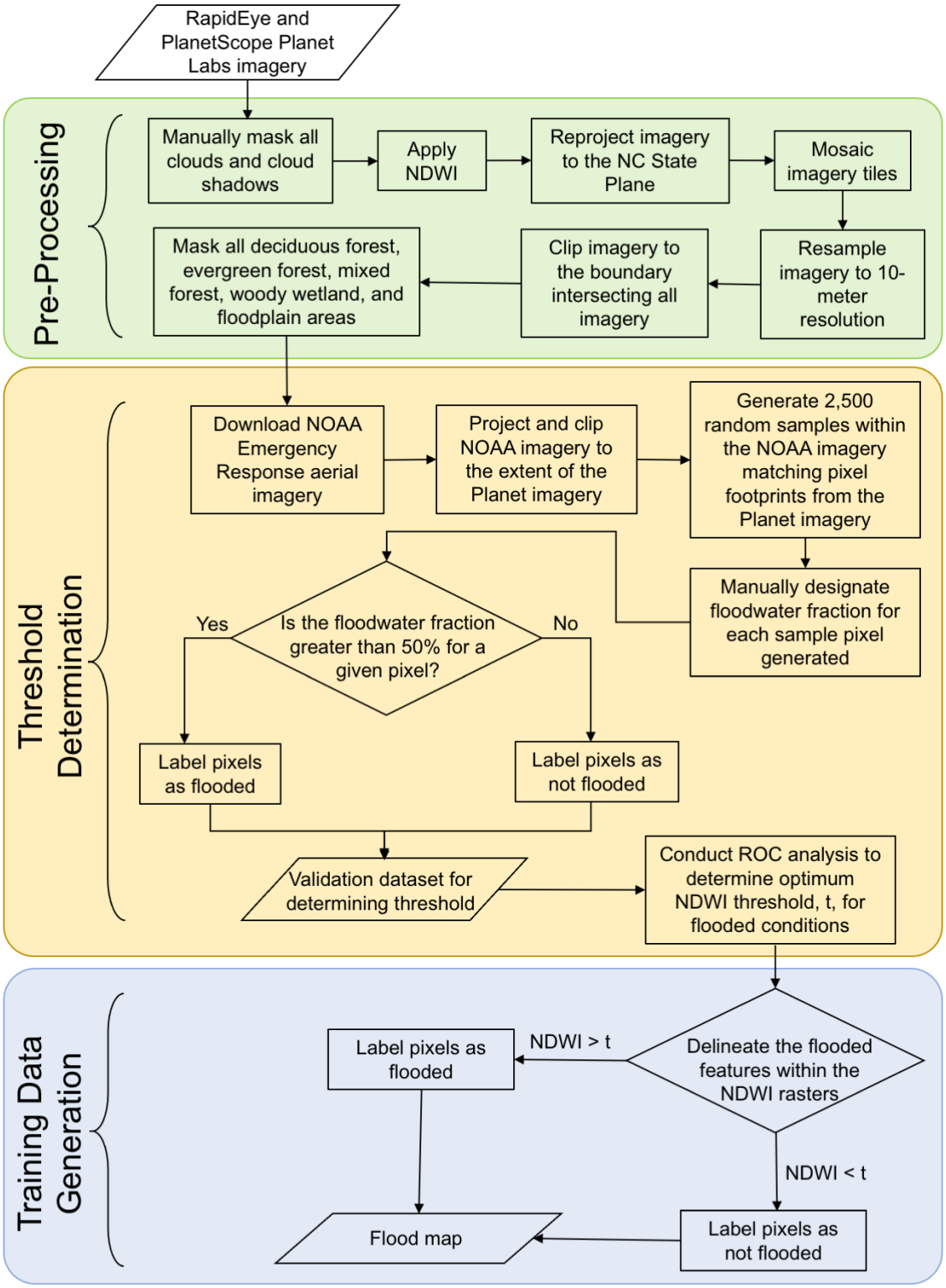

Figure 2- 3. Workflow used to generate pluvial flood maps from remotely sensed imagery. Rectangles correspond to processing steps, parallelograms indicate data products, and diamonds indicate decision steps.

2.3 Processing predictor variable data

In building the machine learning model, predictor variables must be supplied to generate relationships between the response and the predictors. However, prior to supplying the predictor variables and building the model, the variables were screened for multicollinearity by analyzing the variance inflation factor (VIF; Marquardt, 1970). Screening predictor variables for multicollinearity is important since high multicollinearity between two variables implies that one of those features is redundant. The predictor variables screened within the model were a combination of geophysical and socio-environmental geospatial rasters (Table 1). The geophysical variables screened for the model were land cover, flood frequency, drainage class, elevation, height above nearest drainage, slope, topographic wetness, distance to nearest stream, and distance to nearest road. The socio-environmental variables were social vulnerability and population density. In addition, a dynamic variable, precipitation, was included to capture the daily dynamics of flooding since all other variables are temporally static.

Table 2- 1. Predictor variables screened during model development. References are not included for derivative products created for this study.

Variable	Product Name/Source	Property	Data type	Reference
Land Cover	National Land Cover Database 2016 - Multi-Resolution Land Characteristics consortium	static	categorical	Dewitz, 2019
Flood Frequency	Gridded Soil Survey Geographic (gSSURGO) - Natural Resources Conservation Service	static	categorical	Soil Survey Staff, n.d.

Table 2- 1. (continued)

Drainage Class	Gridded Soil Survey Geographic (gSSURGO) - Natural Resources Conservation Service	static	categorical	Soil Survey Staff, n.d.
Elevation	National Elevation Dataset - U.S. Geological Survey	static	continuous	U.S. Geological Survey, n.d.
Height Above Nearest Drainage	Calculated using Elevation	static	continuous	
Slope	Calculated using Elevation	static	continuous	
Topographic Wetness Index	Calculated using Elevation	static	continuous	
Distance to Nearest Stream	National Hydrography Dataset - U.S. Geological Survey	static	continuous	U.S. Geological Survey, n.d.
Distance to Nearest Road	U.S. Census Bureau	static	continuous	U.S. Census Bureau, n.d.
Social Vulnerability	Social Vulnerability Index - Centers for Disease Control	static	continuous	CDC/ATSDR Social Vulnerability Index 2018 Database North Carolina, n.d.
Population Density	LandScan 2019 - Oak Ridge National Lab	static	continuous	Rose et al., 2020
Precipitation	DayMet v3 - Oak Ridge National Lab	dynamic	continuous	Thornton et al., 2020

A combination of geophysical and socio-environmental variables were considered in the model in order to capture both potential physical drivers of flooding

and socio-environmental conditions that have been correlated with flooding (Ajiboye & Orebiyi, 2021; Rufat et al., 2015; Zahran et al., 2008). Although socio-environmental variables, like social vulnerability, are not causal drivers of flooding, they were screened due to the correlations between these factors and flooding. For example, as population density increases and a city grows, more impervious surfaces are developed; in return, the impervious surfaces create high amounts of runoff that discharge quickly without typical infiltration into soils, which creates an increased likelihood of flooding. Since flooding has historically impacted marginalized communities more than others (Rufat et al., 2015), the social vulnerability index (SVI) produced by the U.S. Centers for Disease Control was considered in the model

The national land cover dataset (NLCD) was used since the surface of the land has a strong influence on the capability of rain to infiltrate or generate runoff. The NLCD is a categorical product produced by a group of federal agencies known as the Multi-Resolution Land Characteristics (MRLC) consortium at a 30-m resolution. This product was resampled from 30-m to 10-m to maintain the flood model at a 10-m resolution. The land cover pixels are classified as being Open Water; Developed, Open Space; Developed, Low Intensity; Developed, Medium Intensity; Developed, High Intensity; Barren Land; Deciduous Forest; Evergreen Forest; Mixed Forest; Shrubs; Grassland; Pasture Land; Crop Land; Woody Wetland; or Herbaceous Wetland. Since forested and woody areas were masked from this analysis, deciduous forest, evergreen forest, mixed forest, and woody wetland land cover classifications were masked.

The flood frequency dataset, derived from the gSSURGO soils data product, was used to indicate documented susceptibility to flooding. gSSURGO flood frequency

classes ranged from none (i.e., no history of flooding), very rare, rare, occasional, frequent, and very frequent. Similarly, drainage class was also derived from the gSSURGO product and it was used within the model since areas with poor drainage are prone to standing water and inundation. The drainage classes ranged from excessively drained, somewhat excessively drained, moderately well drained, well drained, somewhat poorly drained, poorly drained, and very poorly drained.

Elevation and derivative products were screened as predictors within the model to capture the physical processes of flooding, as elevation, height above nearest drainage, slope, and topographic wetness are all important indicators of flow movement and accumulation. Elevation was used as a predictor since lower elevations experience more flooding and higher elevations hardly ever flood (Botzen et al. 2012), but it was also used to derive other terrain variables: height above nearest drainage, slope, and the topographic wetness index. Slope is an important terrain variable used as a proxy for runoff potential and infiltration time (Tehrany et al., 2015); it was calculated using the Slope tool within ArcGIS Pro. The height above nearest drainage and topographic wetness index variables were calculated and screened as predictor variables. Height above nearest drainage represents the difference in elevation between an area and its nearest drainage source (Rennó et al. 2008). Topographic wetness index highlights an area's potential to retain water and considers terrain influences on hydrological processes (Tehrany et al., 2015). To create these variables, the elevation dataset was first processed to fill sinks, then flow direction and flow accumulation were calculated using ArcGIS Pro version 2.3.0 to finally derive the height above nearest drainage and topographic wetness index.

In addition, distance to nearest stream and distance to nearest road were variables considered as predictors within the model. The distance to nearest stream variable was considered since high flows from riverine discharge have the capability to store water in a manner that affects the drainage capacity of nearby soils outside the delineated floodplain. Additionally, distances to nearest road data were used since roads typically drain water to the shoulders to avoid pooling on the surface of the pavement. Within North Carolina, roadway design standards indicate shoulder slopes on the outer edges of roads must allow for drainage (NCDOT, 2002; NCDOT, 2018). Thus, roads serve as important first order drainage systems within areas such as Kinston. The distance to nearest road and distance to nearest stream were calculated using the ArcGIS Pro Euclidean Distance tool, and then rasterized using the Vector to Raster tool.

The social vulnerability index (SVI) was also screened as a correlate of flooding. The SVI dataset is produced by the U.S. Centers for Disease Control and ranges from 0 to 1, in which 0 indicates communities with no vulnerability and 1 indicates the maximum amount of social vulnerability. This dataset is available as a vector file, thus it was rasterized to a 10-m resolution dataset. The social vulnerability index considers socio-economic status, household composition, minority status, and housing conditions. Social vulnerability refers to a community's ability to respond to and recover from public health threats, such as natural hazards. Although social vulnerability does not cause flooding, we include this variable within the model to capture the correlations between vulnerable communities and flooding. Additionally, population density was used as a possible predictor since areas with more people are highly correlated with the increase

in flood cases (Jongman et al., 2012). The population density variable was a 1-km resolution raster produced at a global extent. This dataset was resampled to a 10-m resolution to match the resolution of the other datasets.

Lastly, precipitation data was used as a dynamic predictor variable to capture day-to-day changes in flooding. Precipitation data was derived from the Oak Ridge National Laboratory DayMet product (Thornton et al., 2020). This gridded product measures daily precipitation at 1-km resolution, thus the raster was resampled down to 10-m resolution. DayMet v3 reports rainfall between 0-200 mm, and areas that received greater than 200 mm (7.9 inches) of rainfall were assigned the maximum value of 200 mm. DayMet data are available at a daily timestep, and were used to generate seven predictor variables that were screened in the model: daily, 2-day antecedent, 3-day antecedent, 4-day antecedent, 5-day antecedent, 6-day antecedent, and 7-day antecedent rainfall. All precipitation variables were totals, i.e. the 2-day antecedent variable consisted of the total rainfall over a 2-day period. The antecedent rainfall derivatives were calculated using R software version 4.0.2 (R Core Team, 2020). These products were used to capture the compounding influence of precipitation and rainfall runoff on pluvial flooding.

2.4 Model training and testing

2.4.1 Random Forest

A Random Forest model was chosen due to its versatility, relatively low computational power demands, and ability to handle high dimensional data (e.g. Chen et al., 2020; Hou et al., 2021; Kabir et al., 2021; Motta et al., 2021). The Random Forest algorithm is a machine learning model that randomly subsets a sample of the data and

predictors and trains a decision tree to the sampled values, and repeats the sampling and training process n times (Breiman, 2001). The final model consists of many decision trees that are individually unskilled, but collectively effective at predicting (Dietterich, 2000). To train the Random Forest algorithm, the ranger package in R version 4.0.2 was used due to its computational efficiency as compared to other Random Forest packages (Wright & Ziegler, 2017). The Random Forest model was trained as a binary classifier of flooding, and processed using the Henry2 High Performance Computing services at NC State University.

Building a Random Forest model requires the specification of several hyperparameters. To determine the number of trees needed in the model, the model was trained using up to 1000 trees and the out of bag error was evaluated for the models with differing numbers of trees. The number of variables to possibly split at each node was determined by dividing the predictor variables by three and rounding down per Feng et al. (2015), which resulted in a value of 6. All other model hyperparameters were left constant at default values (minimum node size of 1; maximum tree depth of 0).

2.4.2 Data splitting

Due to the large amount of non-flooded area (10,813,041 pixels) relative to flooded area (1,677,896 pixels), the data could not be split randomly, as such a split would have resulted in the model having fewer flooded observations in the training data, resulting in an imbalanced training set. To avoid an imbalanced training set, a balanced training dataset of 1,000,000 non-flooded pixels and 1,000,000 flooded pixels was created, and the leftover data were reserved as a holdout set. Upon training the model and testing it with the holdout set, model testing revealed a large rate of

misclassification among non-flooded pixels; thus, the training dataset was adjusted to increase the number of non-flooded pixels represented in the training set. The final training set consisted of 3,000,000 non-flooded observations and 1,000,000 flooded observations.

2.4.3 Model performance metrics

To assess model performance, accuracy metrics were calculated based on the model's predictability on the holdout testing dataset. Overall accuracy (OA), Cohen's kappa coefficient (κ), precision (P), recall (R), specificity (S), and F1 score (F1) were calculated (Table 2). Here, OA calculates the model's overall ability to predict flood and non-flood conditions and ranges from values between 0 to 1, in which 1 is complete accuracy. κ captures the model's ability to predict considering the possibility of random agreement and values range from -1 to 1, in which values below 0 represent agreement worse than random chance, while values closer to 1 indicate that the model has better performance than a random classifier (Cohen, 1960). F1 is another accuracy metric that balances precision and recall for data with uneven class distributions. R is a metric ranging from 0 to 1 that highlights the model's ability to capture all flooded areas; while P quantifies the proportion of flood observations that were accurately predicted. Lastly, S was calculated to indicate how well the model could capture all the non-flood areas.

Table 2- 2. Model performance metrics and the associated equations, range of values, and variables.

Metric	Equation	Range of values	Variables
Overall Accuracy	$OA = \frac{TP + TN}{TP + TN + FP + FN}$	0,1	TN ~ true negative count TP ~ true positive count FN ~ false negative count FP ~ false positive count
F1 Score	$F1 = \frac{2\ P \times R}{P + R}$	0,1	P ~ precision R ~ recall
Cohen's Kappa	$\kappa = \frac{p_o - p_e}{1 - p_e}$	-1, 1	p_o ~ observed agreement among the two classes p_e ~ probability of random agreement.
Precision	$P = \frac{TP}{TP + FP}$	0,1	TP ~ true positive count FP ~ false positive count
Recall	$R = \frac{TP}{TP + FN}$	0,1	TP ~ true positive count FN ~ false negative count
Specificity	$S = \frac{TN}{TN + FP}$	0,1	TN ~ true negative count FP ~ false positive count

2.4.4 Variable importance

Variable importance was assessed using the permutation, or "accuracy-based," method. This method calculates importance for a variable by first reserving an out of bag sample for a tree and calculating the standard error. Then, the variable of interest is randomized while all other variables stay constant. The standard error measurement is re-calculated using the new dataset containing the permuted variable. The change in error is averaged across all trees and scaled to yield the scaled permutation importance for the predictor variables. The greater the change in accuracy, the greater the importance of the variable in the model.

3. RESULTS

3.1 Predictor variable selection

Prior to building the machine learning model, the predictor variables were screened for multicollinearity through a VIF analysis. Elevation and height above nearest drainage were highly collinear, thus elevation was omitted. Once elevation was excluded, the VIF values were less than 2 for all predictors and were used in model building.

3.2 Delineating flooded areas from Planet Labs imagery

An ROC analysis was conducted to determine the best NDWI threshold value that partitions flooded and non-flooded conditions in satellite imagery taken along the Kinston landscape. An NDWI value of 0 most effectively segregated the flood and non-flooded pixels (Figure A-2). Thus, when determining which NDWI pixels are standing water and which are not, the index values greater than 0 served to indicate inundation and values less than 0 represented dry, non-flooded areas. In return, these delineated NDWI rasters yielded pluvial flood maps for training the machine learning model.

3.3 Random Forest model training and testing

The model was re-trained with up to 1000 trees and out of bag error was calculated on each iteration to determine the optimal number of trees. After 750 trees, the error stabilized (Figure A-3), thus the final model used for analysis contained 750 trees.

3.4 Model performance

Model performance was assessed by calculating the P, S, R, F1, OA, and κ coefficient. These results show that the model has high S (0.97), R (0.93), F1 (0.83) and

OA (0.96) values, while the P (0.75) and Cohen's kappa (0.80) indicate moderate agreement between predicted and observed values.

The model was also assessed for its performance, based on OA and F1, within each land cover class (Figure 4). OA was high for every class, and lowest in medium intensity developed landscapes. According to the F1 values, model performance was lowest in open space and low intensity developed areas. Although there were some discrepancies between OA and F1, there was agreement between OA and F1 in open water, medium and high intensity development, and barren land. Misclassifications within open water areas occurred primarily surrounding edges of water bodies, where mixed pixels (a pixel containing multiple different surfaces within the pixel area) may present complications with flood classification.

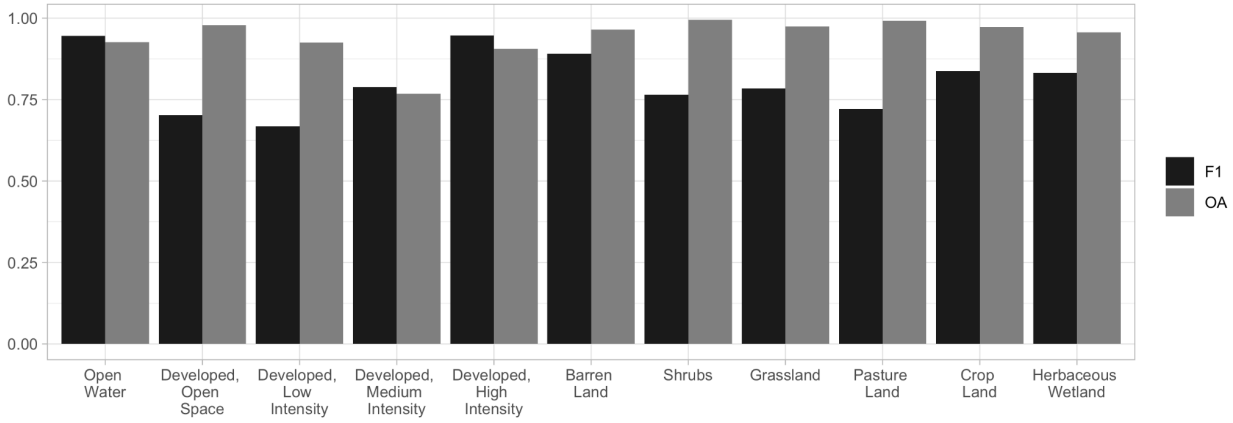

Figure 2- 4. Model performance was quantified with overall accuracy and F1 score for each land cover class in the holdout dataset.

3.5 Variable importance

Predictor variable importance was determined using the permutation method (Figure 5). Distance to the nearest river, distance to the nearest road, and height above nearest drainage were the most important variables within the model. Day-of rainfall and

flood frequency were the two least important variables within the model. Rainfall predictors were all moderately important.

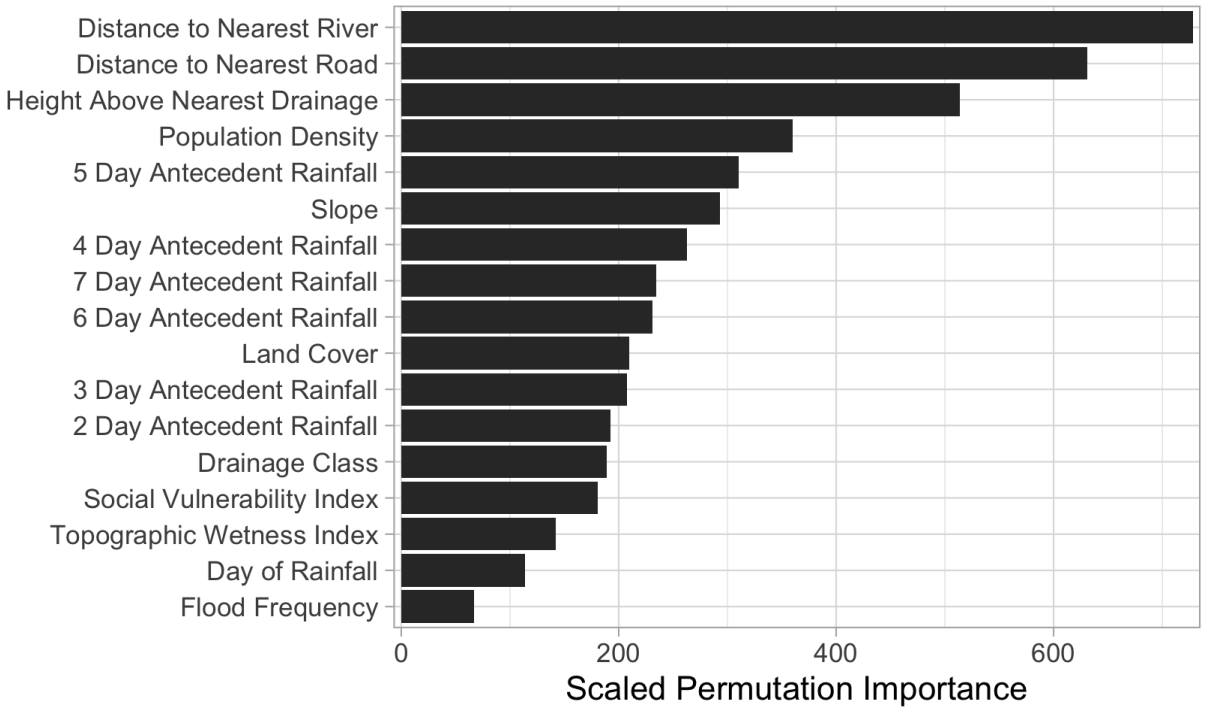

Figure 2- 5. Variable importance for the different predictors within the flood model.

3.6 Generating flood time series

The final model was applied to create the timeline of pluvial flooding immediately after Hurricanes Matthew and Florence made landfall on the Carolinas on October 8, 2016, and September 14, 2018, respectively (Figure 6). Hurricane Matthew delivered two days of heavy rainfall to the study area, while Hurricane Florence slowly rained over the region for four days. In the model output for Hurricane Matthew (Figure 6A), no flooding was predicted on the day of landfall (Oct. 8), but widespread floodwaters were predicted for the following day (Oct. 9) and model predictions estimated the floodwaters mostly dissipated by Oct. 11. For Hurricane Florence (Figure 6B), the model estimated

no inundation had occurred within the study area on the day of landfall, but within the next day pluvial flooding had affected a small area. Interestingly, the model shows that widespread surface water flooding for Hurricane Florence occurred on Sept. 19, five days after landfall.

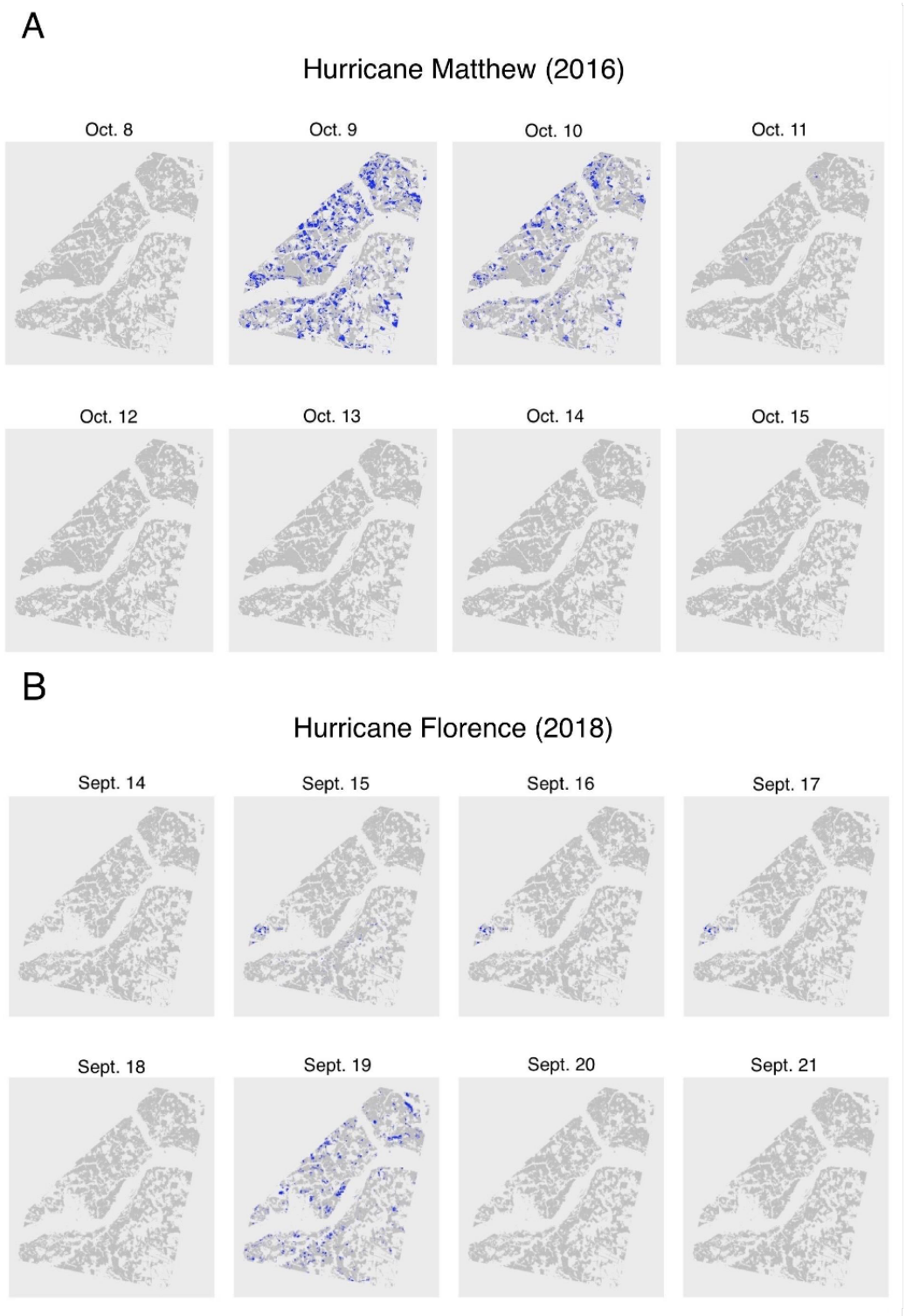

Figure 2- 6. Random Forest model outputs, which estimate the timeline of flooding for Hurricane Matthew from October 8-15, 2016 (A) and flooding for Hurricane Florence from September 14-23, 2018 (B). Blue areas represent pixels predicted to be flooded, dark gray are masked pixels (e.g., forested and floodplain areas).

4. DISCUSSION

Floods are complex natural hazards that can never be fully prevented, thus it is important to be able to predict inundation and mitigate the damage. In this study, we sought to build a flood model framework that uses remotely sensed imagery and geospatial data to create pluvial flood extent maps in a flat, agricultural landscape. We demonstrated the applicability of this method in producing daily flood maps after major storm events and evaluated key predictors in the model. Overall, the model performance metrics indicate that pluvial flooding was effectively predicted. In particular, the model was able to predict flooding in agricultural areas, with cultivated croplands encompassing over 75% of the flooded area on some dates (Figure A-4). Thus, model predictions reveal the susceptibility of croplands to pluvial flooding following extreme rainfall events, and this flood model would serve as a useful resource for flood forecasting in agriculturally dominated watersheds. Given that more flood studies have historically been conducted in urban areas as compared to rural, the presented modeling approach could prove effective at estimating flooding for stakeholders within other agricultural regions (e.g., Bulti and Abebe, 2020; Giustarini et al., 2013; Motta et al., 2021; Qi et al., 2021).

Overall, the flood model results show that the performance was good (OA of 0.96, κ of 0.80), with the errors largely attributed to false positives. The S of 0.97 and R of 0.93 indicate that the model is able to correctly predict 97% of the non-flooded pixels and 93% of the flooded pixels. However, the P of this model (0.75) is not as high as the other examined performance metrics, which indicates that there is a large presence of false positives produced from the model. False positive predictions also explain the

difference between the F1 score (0.83) and OA (0.96). We believe the large presence of false positives could be attributed to the quality of the data, as some roads and rooftops appear to have similar reflectances as water features. However, the occurrence of false positives is not necessarily a poor result in the context of disaster response, since the detection of false positives is generally considered better than false negatives. False positives are preferable to false negatives since false positives might lead to individuals in an area preparing for a flood that may not occur, which would be better than misleading individuals into thinking their area will not flood, only to have them suffer from devastating inundation. Therefore, thresholding remotely sensed imagery, as done with the NDWI in this study, works well for delineating flooding when suitable imagery is acquired, however this method would not work for generating daily flood dynamics in cases where imagery was not available (e.g. due to cloud cover from hurricanes) or in cases where obtaining continuous high spatiotemporal resolution imagery would be expensive, like in the case of using commercial imagery. Future work on improving model performance should experiment with class weighing, hyperparameter tuning, and high-quality data acquisition.

Further investigation of model performance also shows lower F1 scores compared to overall accuracy within each dominant land cover class, which included cultivated crops, open developed, low intensity developed, and shrub/scrub lands. We limit our interpretation of model performance to the dominant land cover classes, as a small number of misclassifications within a minority land class can yield a large change in accuracy metrics for that class, and it is difficult to infer trends from land cover classes that are not well represented in the study area. Within the major land cover

classes in the study area, a major decrease in F1 score, compared to overall accuracy, highlights that there is low precision and/or recall within a particular land cover classification. Because the dominant land cover classes had the largest discrepancy between F1 score and overall accuracy, it is likely these classes have the large presence of false positives, which is causing the lower F1 score in overall model performance.

An examination of predictor variable performance shows that physically-based predictors were the most important in the flood model. Distance to the nearest stream, distance to the nearest road, and height above nearest drainage were the most important predictors of flooding within the Random Forest model. Thus, the importance of these variables highlights the value of physically-based geospatial products in flood prediction. The distance to nearest road variable serves as an interesting predictor variable that we anticipate was deemed important due to how roads are designed to quickly route water off roads, which can lead to water pooling and flooding (Kalantari et al., 2014). Interestingly, land cover was not as important in the model as we anticipated. We believe that this may be due to the majority of flooding occurring in crop lands, scrub/shrub lands, and grasslands. The similarity of these land classifications, in terms of surface roughness, may be a reason why the land cover variable was not a primary predictor of flood extent.

While physical predictors were most important in the model, topographic wetness, day-of rainfall, and flood frequency were the least important variables. The topographic wetness index was a relatively poor predictor of pluvial flooding within the model; however, this is likely due to the correlation between height above nearest

drainage and topographic wetness, as both variables are derived from elevation data. Most likely, the height above nearest drainage variable is capturing the influence of elevation on flooding, thus making the topographic wetness index an ineffective addition to the model. In addition, the day-of rainfall may have carried less weight in the model since local inundation typically occurs when rainfall compounds over time to exceed the drainage capacity of soils. Accordingly, this explanation is supported by the 5-day antecedent rainfall being the most important rainfall variable. Flood frequency was consistently the least important variable within each model training iteration. However, the masking of wooded wetlands and the floodplain, which surrounded rivers in the area, likely explains why the flood frequency product was a poor predictor of pluvial flooding. The “high risk” flood frequency designations primarily occur in stream or river floodplains; thus, masking woody wetlands and floodplain areas likely would have largely removed most of the “high risk” areas from consideration during model application. Future work should experiment with combinations of physical predictor variables that avoid overfitting and produce high accuracy.

Lastly, flood timelines from Hurricanes Matthew and Florence were created by applying the final Random Forest model. Maps of model predictions show that pluvial flooding persisted in Kinston for about 5 days following Hurricane Florence while flooding during Hurricane Matthew subsided completely after 2 days. The model outputs demonstrate that the model predicted no flooding on the day of landfall of either storm, likely due the rainfall from the storms having not yet accumulated on the landscape. However, beginning the day following landfall, the model predicted that flooding began. Interestingly, the model predicted a resurgence of Hurricane Florence flooding on Sept.

19: model outputs show an initial flood peak occurring one day after landfall (Sept. 15), the floodwaters subsequently retreating, and then a second peak occurring on Sept. 19. Although model testing indicated the model had high performance, we are unable to confirm whether this resurgence actually occurred in reality. That being said, it is worth noting that each model iteration showcased this resurgence on Sept. 19. The resurgence could potentially be attributed to there being a compounding effect of several days worth of rainfall, and the model could be accounting for the time lag between heavy rainfall and downstream flooding using the antecedent rainfall variables. In addition, with Hurricane Florence receiving heavy rains for several more days than Hurricane Matthew, the predicted flooding dissipated more slowly than it did for Hurricane Matthew, thus providing some corroboration for the results.

An investigation of the flood timeline associated with Hurricanes Matthew and Florence revealed that pluvial flooding was not widespread across the landscape, leading us to believe that drainage within agricultural soils were effective in reducing the extent of waterlogging. However, the land classes that received the most flooding were cultivated croplands, shrub/scrub lands, and herbaceous grasslands, respectively, thus creating possible concerns for farmers that depend on row crops. Further evaluation of the croplands that were flooded across the landscape yielded that corn, soybean, and tobacco fields were the crops that were primarily affected by Hurricanes Matthew and Florence (Figure 7). This is an important consideration for local farmers, as flood conditions deplete soil oxygen and affect plant growth. Specifically, corn, tobacco, and soybeans are crops sensitive to waterlogging, particularly in the early stages of growth (Kaur et al., 2019; Nurhidayati et al., 2021; Purnobasuki et al, 2018; Rhine et al., 2010;

Scott et al., 1989; Walne and Reddy, 2021). In addition, the model results show that out of all the flooded lands, tobacco crops were especially impacted during Hurricane Florence. This is a valuable finding since tobacco crops encompassed only a small area of the land at the time and tobacco croplands did not flood as severely during Hurricane Matthew. Thus, the model outputs can inform stakeholders in agricultural landscapes on areas susceptible to flooding, crops that may be potentially impacted, and characteristics of areas that experience pluvial flooding.

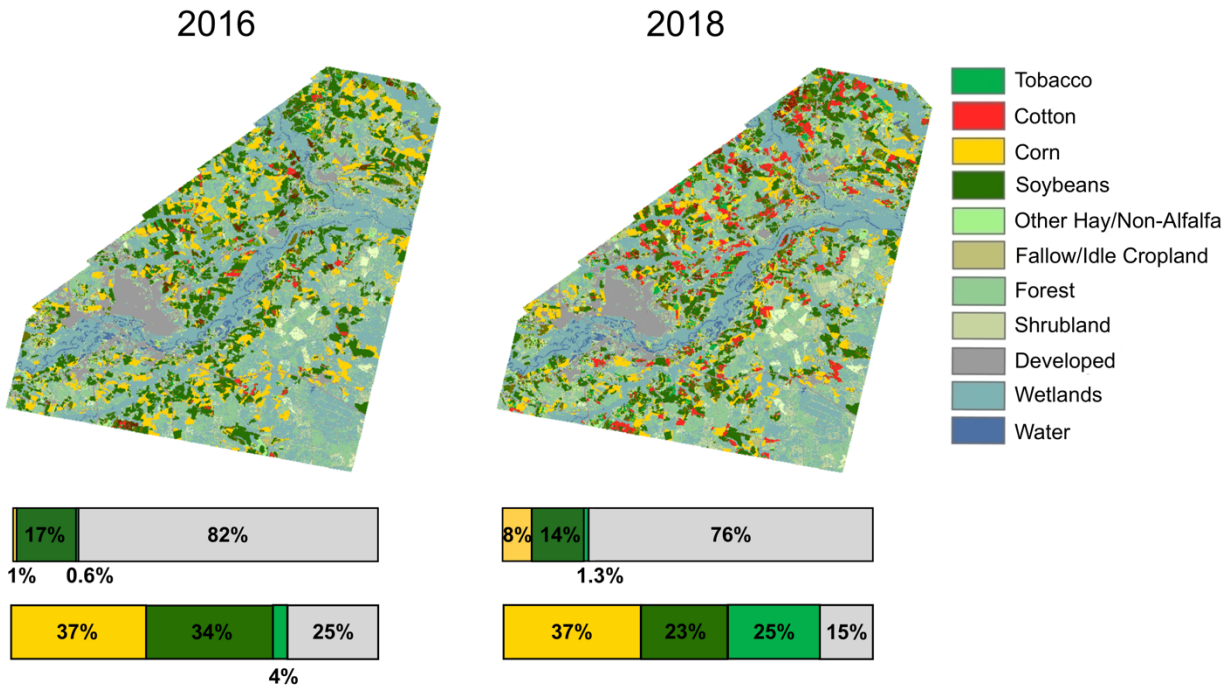

Figure 2- 7. US Department of Agriculture National Agricultural Statistics Service Cropland Data Layer product (USDA NASS) for the Kinston area during A) Hurricanes Matthew and B) Florence. The legend on the right depicts the color associated with the dominant crop. The bar charts show the percent of total area (top bar chart) and flooded area (bottom bar chart) for corn, soybeans, tobacco, and other.

In regard to transferability, it should be noted that the framework and methods presented in this study are transferable; however, model application cannot be transferred to new regions without any adaptation to the model. This is due to the

machine learning model deriving specific relationships from the data collected in rural North Carolina, which may not be characteristic of other agricultural landscapes. Additionally, although other flood models exist for fluvial, coastal, and urban flooding, the mechanisms that generate flooding in these systems are different compared to rural pluvial flooding. Thus, the approach outlined in this work presents a simplified framework for predicting pluvial flood extent and highlighting predictors of flooding in agricultural landscapes using high-resolution remotely sensed imagery and open-access geospatial data layers for an area of interest.

5. CONCLUSIONS

Flat, low-lying landscapes are notorious for flooding as well as being difficult areas in which to predict inundation. Current flood studies focus on the dynamics of flooding in urban, riverine, and coastal systems; however, agricultural landscapes are prone to flooding which can cause disruptions to food security and farmers' livelihoods. To address this problem, this study developed a Random Forest flood model for the prediction of daily flood extent in agricultural lands and evaluated characteristics of areas prone to pluvial flooding. The present work contributes to current flood modeling research by developing a machine learning model that predicts daily dynamics of pluvial flooding in a low-terrain and agricultural landscape, allowing for estimation and illustration of the surge and retreat of floodwaters. The structure of the model is such that, as more satellite imagery and flood data are generated, more training data could be fed into the model for better predictability, allowing the model to improve over time. The trained model could also be used in a forecasting context to predict flooding under future precipitation, land cover, and geophysical conditions.

The flood model performance indicated high accuracy, with errors attributed largely to false positives. The lower F1 scores within the dominant land cover classes highlight the need to improve model predictability by addressing the pitfalls in prediction for each land cover class individually. The performance of the flood model may be improved with balanced flood/non-flood classes for each land cover class. In regard to predictor performance, physically-based predictor variables, distance to the nearest stream, distance to the nearest road, and height above nearest drainage, were the most important in flood extent prediction. Meanwhile, the day-of rainfall and flood frequency were the least important variables in the model. Flood frequency was likely unimportant in the model as this variable primarily captures riverine flood frequency, rather than surface water flooding.

A key limitation of the model is the mere lack of available flood data, as even the characterization of flooding is a contemporary challenge. Therefore, it is unlikely that we were able to capture all pluvial flooding across the landscape. Despite the pitfalls, the high performance of the model indicates that this tool would be a valuable resource for flood management in agriculturally dominated watersheds. In addition, this Random Forest flood model may be used to inform farmers which areas and crops are suspected to flood, as well as the duration of flooding, when used with forecasted rainfall information.

In the future, process-based and machine learning methods may be combined to predict flooding in agricultural landscapes without the reliance of satellite imagery. The coupling of process-based and data-driving models has the potential of representing system dynamics using the complementary strengths of each modeling method. Such

process-guided machine learning models would allow for a generalizable pluvial model that is able to accurately account for unseen scenarios using the laws of mass and energy transfer.

6. REFERENCES

Abebe, Y., Kabir, G., & Tesfamariam, S. (2018). Assessing urban areas vulnerability to pluvial flooding using GIS applications and Bayesian Belief Network model. *Journal of Cleaner Production*, 174, 1629–1641. https://doi.org/10.1016/j.jclepro.2017.11.066

Ajiboye, O., & Orebiyi, E. (2021). Assessment of socio-economic effects of flooding on selected communities of Anambra West Local Government Area, Southeast, Nigeria. *Geojournal.* 10.1007/s10708-021-10400-x

Anusha, N., & Bharathi, B. (2019). Flood detection and flood mapping using multi-temporal synthetic aperture radar and optical data. *Egyptian Journal of Remote Sensing and Space Science*, 23(2), 207–219. https://doi.org/10.1016/j.ejrs.2019.01.001

Berenbrock, C., Mason, R.R., & Blanchard, S.F. (2009). Mapping Hurricane Rita inland storm tide. *Journal of Flood Risk Management*, 2(1), 76-82. 10.1111/j.1753-318X.2009.01019.x

Berens, A.S., Palmer, T., Dutton, N.D., Lavery, A., &Moore, M. (2020). Using search-constrained inverse distance weight modeling for near real-time riverine flood modeling: Harris County, Texas, USA before, during, and after Hurricane Harvey. *Natural Hazards*, 105(1), 277-292. 10.1007/s11069-020-04309-w

Bernet, D. B., Zischg, A. P., Prasuhn, V., & Weingartner, R. (2018). Modeling the extent of surface water floods in rural areas: Lessons learned from the application of various uncalibrated models. *Environmental Modelling & Software*, 109, 134–151. https://doi.org/10.1016/j.envsoft.2018.08.005

Botzen WJW, Aerts JCJH, & van den Bergh JCJM. 2012. Individual preferences for reducing flood risk to near zero through elevation. *Mitigation and Adaptation Strategies for Global Change*, 2,229–244. doi:10.1007/s11027-012-9359-5

Breiman, L. (2001). Random Forests. *Machine Learning*, 45, 5–32. https://doi.org/10.1023/A:1010933404324

Brody, S., Blessing, R., Sebastian,A., & Bedient, P. (2013) Delineating the Reality of Flood Risk and Loss in Southeast Texas. *Natural Hazards Review,* 14(2), 89-97. 10.1061/(ASCE)NH.1527-6996.0000091

Bulti, D. T., & Abebe, B. G. (2020). A review of flood modeling methods for urban pluvial flood application. *Modeling Earth Systems and Environment*, 6(3), 1293–1302. https://doi.org/10.1007/s40808-020-00803-z

Centers for Disease Control and Prevention/ Agency for Toxic Substances and Disease Registry/ Geospatial Research, Analysis, and Services Program. CDC/ATSDR Social Vulnerability Index 2018 Database North Carolina. https://www.atsdr.cdc.gov/placeandhealth/svi/data_documentation_download.html

Chen, W., Li, Y., Xue, W., Shahabi, H., Li, S., Hong, H., et al. (2020). Modeling flood susceptibility using data-driven approaches of naïve Bayes tree, alternating decision tree, and random forest methods. *Science of the Total Environment*, 701, 134979. https://doi.org/10.1016/j.scitotenv.2019.134979

Choubin, B., Moradi, E., Golshan, M., Adamowski, J., Sajedi-Hosseini, F., & Mosavi, A. (2019). An ensemble prediction of flood susceptibility using multivariate discriminant analysis, classification and regression trees, and support vector

machines. *Science of the Total Environment*, 651, 2087–2096. https://doi.org/10.1016/j.scitotenv.2018.10.064

Cohen J. (1960). A coefficient of agreement for nominal scale. *Educational and Psychological Measurement*, 20, 37-46. https://doi.org/10.1177%2F001316446002000104

Costache, R., Popa, M. C., Tien Bui, D., Diaconu, D. C., Ciubotaru, N., Minea, G., & Pham, Q. B. (2020). Spatial predicting of flood potential areas using novel hybridizations of fuzzy decision-making, bivariate statistics, and machine learning. *Journal of Hydrology*, 585, 124808. https://doi.org/10.1016/j.jhydrol.2020.124808

Dewitz, J. (2019). National Land Cover Database (NLCD) 2016 Products: U.S. Geological Survey data release, https://doi.org/10.5066/P96HHBIE

Dietterich, T.G. (2000). Ensemble methods in machine learning. *Int. Workshop on Multiple Classifier Systems*, 1–15. 10.1007/3-540-45014-9_1

FEMA. National Flood Hazard Layer. (2019). Version 1.1.1.0. https://www.fema.gov/flood-maps/national-flood-hazard-layer

FEMA National Flood Insurance Program (NFIP). (2020). Answers to Questions About the NFIP. Document F-084. https://www.fema.gov/sites/default/files/2020-05/f084_atq_11aug11.pdf

Feng, Q., Gong, J., Liu, J., & Li, Y. (2015). Flood mapping based on multiple endmember spectral mixture analysis and random forest classifier-the case of yuyao, China. *Remote Sensing*, 7(9), 12539–12562. https://doi.org/10.3390/rs70912539

First Street Foundation (2020) The First National Flood Risk Assessment: Defining America's Growing risk. https://assets.firststreet.org/uploads/2020/06/first_street_foundation__first_national_flood_risk_assessment.pdf

Giustarini, L., Matgen, P., Hostache, R., Guy, S., Bates, P. D., & Mason, C. (2013). A Change Detection Approach to Flood Mapping in Urban Areas Using TerraSAR-X. *IEEE Transactions on Geoscience and Remote Sensing*. https://doi.org/https://doi.org/10.1109/TGRS.2012.2210901

Guerreiro, S. B., Glenis, V., Dawson, R. J., & Kilsby, C. (2017). Pluvial Flooding in European Cities—A Continental Approach to Urban Flood Modelling. *Water*, 9(4), 296. https://doi.org/10.3390/w9040296

Highfield, W. E., Brody, S. D., & Norman, S. (2013). Examining the 100-year floodplain as a metric of risk, loss, and household adjustment. *Risk Analysis*, 33(2), 186–191.

Hirabayashi, Y., Mahendran, R., Koirala, S., Konoshima, L., Yamazaki, D., Watanabe, S., et al. (2013). Global flood risk under climate change. *Nature Climate Change*, 3(9), 816–821. https://doi.org/10.1038/nclimate1911

Hou, J., Zhou, N., Chen, G., Huang, M., & Bai, G. (2021). Rapid forecasting of urban flood inundation using multiple machine learning models. *Natural Hazards*, 108, 2335–2356. https://doi.org/10.1007/s11069-021-04782-x

Ireland, G., Volpi, M., & Petropoulos, G. P. (2015). Examining the capability of supervised machine learning classifiers in extracting flooded areas from landsat

tm imagery: A case study from a mediterranean flood. *Remote Sensing*, 7(3), 3372–3399. https://doi.org/10.3390/rs70303372

Jain, S. K., Mani, P., Jain, S. K., Prakash, P., Singh, V. P., Tullos, D., et al. (2018). A Brief review of flood forecasting techniques and their applications. *International Journal of River Basin Management*, 16(3), 329–344. https://doi.org/10.1080/15715124.2017.1411920

Jiang, Z., & Sainju, A. M. (2021). A Hidden Markov Tree Model for Flood Extent Mapping in Heavily Vegetated Areas based on High Resolution Aerial Imagery and DEM: A Case Study on Hurricane Matthew Floods. *International Journal of Remote Sensing*, 42(3), 1160–1179. https://doi.org/10.1080/01431161.2020.1823514

Jongman, B., Ward, P. J., & Aerts, J. C. J. H. (2012). Global exposure to river and coastal flooding: Long term trends and changes. *Global Environmental Change*, 22(4), 823–835. https://doi.org/10.1016/j.gloenvcha.2012.07.004

Kabir, S., Patidar, S., & Pender, G. (2021). A machine learning approach for forecasting and visualising flood inundation information. *Proceedings of the Institution of Civil Engineers: Water Management*, 174(1), 27–41. https://doi.org/10.1680/jwama.20.00002

Kalantari, Z. (2014). A method for mapping flood hazard along roads. *Journal of Environmental Management*, 133(15). 69-77. https://doi.org/10.1016/j.jenvman.2013.11.032

Kan, G., Liang, K., Yu, H., Sun, B., Ding, L., Li, J., et al. (2020). Hybrid machine learning hydrological model for flood forecast purpose. *Open Geosciences*, 12(1), 813–820. https://doi.org/10.1515/geo-2020-0166

Kauffeldt, A., Wetterhall, F., Pappenberger, F., Salamon, P., & Thielen, J. (2016). Technical review of large-scale hydrological models for implementation in operational flood forecasting schemes on continental level. *Environmental Modelling and Software*, 75, 68–76. https://doi.org/10.1016/j.envsoft.2015.09.009

Kaur, G.; Zurweller, B.; Motavalli, P.P.; & Nelson, K.A., 2019. Screening Corn Hybrids for Soil Waterlogging Tolerance at an Early Growth Stage. *Agriculture,* 9(2), 33. https://doi.org/10.3390/agriculture9020033

Khosravi, K., Pham, B. T., Chapi, K., Shirzadi, A., Shahabi, H., Revhaug, I., et al. (2018). A comparative assessment of decision trees algorithms for flash flood susceptibility modeling at Haraz watershed, northern Iran. *Science of the Total Environment*, 627, 744–755. https://doi.org/10.1016/j.scitotenv.2018.01.266

Kwak, Y.J., Pelich, R., Park, J., & Takeuchi, W. (2018). Improved flood mapping based on the fusion of multiple satellite data sources and in-situ data. *IEEE International Geoscience & Remote Sensing Symposium*, 3521–3523. doi.org/10.1109/IGARSS.2018.8517336

Li, Z., Liu, H., Luo, C., & Fu, G. (2021). Assessing Surface Water Flood Risks in Urban Areas Using Machine Learning. *Water*, 13(24), 3520. https://doi.org/10.3390/w13243520

Marquardt, D. W. (1970). Generalized inverses, ridge regression, biased linear estimation, and nonlinear regression. Technometrics, 12, 591-613.

Martinis, S., Kuenzer, C., & Twele, A. (2015). Flood studies using Synthetic Aperture Radar data. *Remote sensing of water resources, disasters and urban studies* (pp. 145–176). https://doi.org/10.1201/b19321-10

McFeeters (1996) The use of the normalized difference water index (NDWI) in the delineation of open water features. *International Journal of Remote Sensing*. 17(7): 1425-1432. DOI: 10.1080/01431169608948714

Milly, P. C. D., Wetherald, R. T., Dunne, K. A., & Delworth, T. L. (2002). Increasing risk of great floods in a changing climate. *Nature*, 415(6871), 514–517. https://doi.org/10.1038/415514a

Mojaddadi, H., Pradhan, B., Nampak, H., Ahmad, N., & Ghazali, A. H. (2017). Ensemble machine-learning-based geospatial approach for flood risk assessment using multi-sensor remote-sensing data and GIS. *Geomatics, Natural Hazards and Risk*, 8(2), 1080–1102. https://doi.org/10.1080/19475705.2017.1294113

Mosavi, A., Ozturk, P., & Chau, K. W. (2018). Flood prediction using machine learning models: Literature review. *Water (Switzerland)*, 10(11), 1–40. https://doi.org/10.3390/w10111536

Motta, M., de Castro Neto, M., & Sarmento, P. (2021). A mixed approach for urban flood prediction using Machine Learning and GIS. *International Journal of Disaster Risk Reduction*, 56, 102154. https://doi.org/10.1016/j.ijdrr.2021.102154

Musa, Z. N., Popescu, I., & Mynett, A. (2015). A review of applications of satellite SAR, optical, altimetry and DEM data for surface water modelling, mapping and parameter estimation. *Hydrology and Earth System Sciences*, 19, 3755–3769. https://doi.org/10.5194/hess-19-3755-2015

Muthusamy, M., Casado, M. R., Salmoral, G., Irvine, T., & Leinster, P. (2019). A Remote Sensing Based Integrated Approach to Quantify the Impact of Fluvial and Pluvial Flooding in an Urban Catchment. *Remote Sensing*, 11(5), 577. https://doi.org/10.3390/rs11050577

NC Department of Transportation (NCDOT). (2002). Roadway Design Manual General Design Information, Design Criteria and Plan Preparation Guides. https://connect.ncdot.gov/projects/Roadway/pages/roadway-design-manual.aspx

NC Department of Transportation (NCDOT). (2018). Roadway Standard Drawings. https://connect.ncdot.gov/resources/Specifications/Pages/2018-Roadway-Standard-Drawings.aspx

NOAA National Centers for Environmental Information (NCEI). (2021). U.S. Billion-Dollar Weather and Climate Disasters. https://www.ncdc.noaa.gov/billions/, DOI: 10.25921/stkw-7w73

NOAA Hydrometeorological Design Studies Center (HDSC). (2018). Hurricane Florence, 13-18 September 2018 Annual Exceedance Probabilities. https://www.weather.gov/owp/hdsc_aep

NOAA National Severe Storms Laboratory (NSSL). (n.d.) SEVERE WEATHER 101– Floods https://www.nssl.noaa.gov/education/svrwx101/floods/

Nurhidayati, T.; Safitri, W.Y.; Purnobasuki, H.; Hariyanto, S. (2021). Response of tobacco (*Nicotiana tabacum L.*) under waterlogging stress based on agronomic characters. *AIP Conference Proceedings*, 2349, 020019, https://doi.org/10.1063/5.0051852

Palaseanu-Lovejoy, M., Kranenburg, C., Barras, J. A., & Brock, J.C. (2013). Land loss due to recent hurricanes in coastal Louisiana, USA. *Journal of Coastal Research*, 63(1), 97-109. https://doi.org/10.2112/SI63-009.1

Palla, A., Colli, M., Candela, A., Aronica, G. t., & Lanza, L. g. (2018). Pluvial flooding in urban areas: The role of surface drainage efficiency. *Journal of Flood Risk Management*, 11(S2), S663–S676. https://doi.org/10.1111/jfr3.12246

Purnobasuki, H.; Nurhidayati, T.; Hariyanto, S.; & Jadid, N. (2018). Data of root anatomical responses to periodic waterlogging stress of tobacco (*Nicotiana tabacum*) varieties. *Data Brief*, 20: 2012–2016. https://doi.org/10.1016/j.dib.2018.09.046

Qi, W., Ma, C., Xu, H., Chen, Z., Zhao, K., & Han, H. (2021). A review on applications of urban flood models in flood mitigation strategies. *Natural Hazards*, (108), 31–62. https://doi.org/10.1007/s11069-021-04715-8

R Core Team (2020). R: A language and environment for statistical computing. R Foundation for Statistical Computing, Vienna, Austria. https://www.R-project.org/.

Raber, G.T., & Tullis, J.A. (2007). Rapid assessment of storm-surge inundation after hurricane katrina utilizing a modified distance interpolation approach. *GIScience and Remote Sensing*, 44(3), 220-236. 10.2747/1548-1603.44.3.220

Rahman, M. S., & Di, L. (2017). The state of the art of spaceborne remote sensing in flood management. *Natural Hazards*, 85(2), 1223–1248. https://doi.org/10.1007/s11069-016-2601-9

Rennó C.D., Nobre A.D., Cuartas L.A., Soares J.V., Hodnett M. G., Tomasella J., & Waterloo M.J. (2008). HAND, a new terrain descriptor using SRTM-DEM:

Mapping terra-firme rainforest environments in Amazonia. *Remote Sensing of the Environment*, 112, (9), 3469–3481. https://doi.org/10.1016/j.rse.2008.03.018

Rhine, M.D.; Stevens, G.; Shannon, G.; Wrather, A.; & Sleper, D. (2010). Yield and nutritional responses to waterlogging of soybean cultivars. *Irrigation Science*, 28, 135–142. https://doi.org/10.1007/s00271-009-0168-x

Rose, A. N., McKee, J.J.,Sims, K.M.,Bright, E.A.,Reith, A. E., & Urban, M.L. (2020). LandScan 2019. Oak Ridge National Laboratory.

Rufat, S., Tate, E., Burton, C. G., & Sayeed, A. (2015). Social vulnerability to floods: Review of case studies and implications for measurement. *International Journal of Disaster Risk Reduction*, 14, 470–486. https://doi.org/10.1016/j.ijdrr.2015.09.013

Schumann, G. J. P., Brakenridge, G. R., Kettner, A. J., Kashif, R., & Niebuhr, E. (2018). Assisting flood disaster response with earth observation data and products: A critical assessment. *Remote Sensing*, 10, 1230. https://doi.org/10.3390/rs10081230

Scott, H.D.; DeAngulo, J.; Daniels, M.B.; & Wood, L.S. (1989). Flood Duration Effects on Soybean Growth and Yield. *Agronomy Journal*, 81(4), 631-636. https://doi.org/10.2134/agronj1989.00021962008100040016x

Soil Survey Staff. Gridded Soil Survey Geographic (gSSURGO) Database for North Carolina. United States Department of Agriculture, Natural Resources Conservation Service. January 28, 2019. http://datagateway.nrcs.usda.gov/

Stewart, S.R. (2017). National Hurricane Center Tropical Cyclone Report: Hurricane Matthew (AL142016). https://www.nhc.noaa.gov/data/tcr/AL142016_Matthew.pdf

Stacy, S.R., & Berg, R. (2019). National Hurricane Center Tropical Cyclone Report: Hurricane Florence (Al062018). https://www.nhc.noaa.gov/data/tcr/AL062018_Florence.pdf

Tabbussum, R., & Dar, A. Q. (2021). Modelling hybrid and backpropagation adaptive neuro-fuzzy inference systems for flood forecasting. *Natural Hazards*, (0123456789). https://doi.org/10.1007/s11069-021-04694-w

Tanir, T., de Lima, A. de S., de A. Coelho, G., Uzun, S., Cassalho, F., & Ferreira, C. M. (2021). Assessing the spatiotemporal socioeconomic flood vulnerability of agricultural communities in the Potomac River Watershed. *Natural Hazards*, 108(1), 225–251. https://doi.org/10.1007/s11069-021-04677-x

Tehrany, M. S., Jones, S., & Shabani, F. (2019). Identifying the essential flood conditioning factors for flood prone area mapping using machine learning techniques. *Catena*, 175(April 2018), 174–192. https://doi.org/10.1016/j.catena.2018.12.011

Tehrany, M. S., Pradhan, B., Mansor, S., & Ahmad, N. (2015). Flood susceptibility assessment using GIS-based support vector machine model with different kernel types. *Catena*, 125, 91–101. https://doi.org/10.1016/j.catena.2014.10.017

Tellman, B.; Sullivan, J.A.; Kuhn, C.; Kettner, A.J.; Doyle, C.S.; Brakenridge, G.R.; et al. (2021). Satellite imaging reveals increased proportion of population exposed to floods. *Nature,* 596, 80–86. https://doi.org/10.1038/s41586-021-03695-w

Teng, J., Jakeman, A. J., Vaze, J., Croke, B. F. W., Dutta, D., & Kim, S. (2017). Flood inundation modelling: A review of methods, recent advances and uncertainty

analysis. *Environmental Modelling and Software*, 90, 201–216. https://doi.org/10.1016/j.envsoft.2017.01.006

Thornton, M.M., R. Shrestha, Y. Wei, P.E. Thornton, S. Kao, & B.E. Wilson. (2020). Daymet: Daily Surface Weather Data on a 1-km Grid for North America, Version 4. ORNL DAAC, Oak Ridge, Tennessee, USA. https://doi.org/10.3334/ORNLDAAC/1840

Towfiqul Islam, A. R. M., Talukdar, S., Mahato, S., Kundu, S., Eibek, K. U., Pham, Q. B., et al. (2021). Flood susceptibility modelling using advanced ensemble machine learning models. *Geoscience Frontiers*, 12(3). https://doi.org/10.1016/j.gsf.2020.09.006

U.S. Census Bureau. (2015). TIGER/Line Streets 2015 Dataset. https://www.census.gov/geographies/mapping-files/time-series/geo/tiger-line-file.html

USDA National Agricultural Statistics Service (NASS) Cropland Data Layer. (2016 & 2018). Published crop-specific data layer [Online]. USDA-NASS, Washington, DC. Available at https://nassgeodata.gmu.edu/CropScape/.

U.S. Geological Survey, 2019, National Elevation Dataset 10-Meter Resolution Digital Elevation Model (published 20200606), accessed October 23, 2019 at https://www.usgs.gov/core-science-systems/ngp/3dep/data-tools

U.S. Geological Survey, 2019, National Hydrography Dataset (ver. USGS National Hydrography Dataset Best Resolution (NHD) for Hydrologic Unit (HU) 4 - 2001 (published 20191002)), accessed October 23, 2019 at URL

https://www.usgs.gov/core-science-systems/ngp/national-hydrography/access-national-hydrography-products

van Dijk, E., van der Meulen, J., Kluck, J., & Straatman, J. H. M. (2013). Comparing modelling techniques for analysing urban pluvial flooding. *Water Science and Technology*, 69(2), 305–311. https://doi.org/10.2166/wst.2013.699

Walne, C.H., & Reddy, K.R. (2021). Developing Functional Relationships between Soil Waterlogging and Corn Shoot and Root Growth and Development. *Plants (Basel)*, 10(10), 2095. https://doi.org/10.3390/plants10102095

World Health Organization (WHO). (n.d.) Floods. https://www.who.int/health-topics/floods

Wright, M. N., & Ziegler, A. (2017). ranger: A fast implementation of random forests for high dimensional data in C++ and R. *Journal of Statistical Software*, 77, 1-17. 10.18637/jss.v077.i01

Yeditha, P. K., Kasi, V., Rathinasamy, M., & Agarwal, A. (2020). Forecasting of extreme flood events using different satellite precipitation products and wavelet-based machine learning methods. *Chaos*, 30(6), 1–12. https://doi.org/10.1063/5.0008195

Zahran S, Brody S, Peacock W, Vedlitz A, & Grover H. (2008). Social vulnerability and the natural and built environment: a model of flood casualties in Texas. *Disasters*, 32, 537–60. https://doi.org/10.1111/j.1467-7717.2008.01054.x

Zakaria, M. N. A., Abdul Malek, M., Zolkepli, M., & Najah Ahmed, A. (2021). Application of artificial intelligence algorithms for hourly river level forecast: A case study of

Muda River, Malaysia. *Alexandria Engineering Journal*, 60(4), 4015–4028. https://doi.org/10.1016/j.aej.2021.02.046

CHAPTER 3: KEY DESCRIPTORS OF NUTRIENT CONCENTRATIONS IN FLOOD-IMPACTED SURFACE WATERS

Abstract

Hurricane-induced flooding can be catastrophic and significantly impair public and environmental health. Hurricane Florence (2018) created record-breaking flooding in eastern North Carolina, which inundated many agricultural fields and animal production facilities and created surface water quality concerns. Here, we surveyed floodwaters across the North Carolina Coastal Plain at four separate time points over the span of a year for total Kjeldahl nitrogen, ammonium, nitrite and nitrate, total phosphorus, and orthophosphate concentrations. A Bayesian geostatistical model was built to explain flood water nutrient concentrations as a function of different environmental variables, such as land cover and rainfall, and the variables that best explain the nutrient water quality signatures in floodwaters were identified. Model results indicate that concentrated animal feeding operations (known as CAFOs), croplands, and wastewater treatment plants (WWTPs) were likely sources of nutrient exports into flood-affected surface waters. Rainfall was also an important variable driving nutrient concentrations, thus highlighting the transport mechanism behind nutrient runoff into surface waters. Overall, our framework highlights the presence of pollutants in floodwaters and the potential drivers of nutrient contamination.

Keywords: water quality, nitrogen, phosphorus, statical modeling, Bayesian spatial statistics

1. INTRODUCTION

Floods are one of the most frequent and detrimental natural hazards affecting the public. Along with the devastating destruction that comes with flooding, floodwaters mobilize nutrients, organic matter, sediment, and other pollutants from extensive land areas, creating public and environmental health risks. Specifically, the influx of nutrients into surface waters promotes primary production and the growth of harmful algal blooms downstream (Hagy et al., 2006; Liu et al., 2009; Paerl et al., 2006; Zhao et al., 2008). In return, harmful algal blooms and other organic matter can lead to hypoxia and massive fish deaths during decomposition and drive loss of habitat and aquatic species (Mallin et al., 1999; Tomasko et al., 2006).

Many studies have investigated connections between stormwater and downstream nutrient pollution (e.g., Carey et al., 2013; Cherry et al., 2008; Delkash et al., 2018; Haque, 2021; Malaviya & Singh, 2012; Newcomer Johnson et al., 2016). However, the water quality impacts of major storm events, such as hurricanes and tropical storms, are comparably understudied. Major flood events are destructive and dangerous, creating logistical challenges for safely sampling floodwaters and thus resulting in a lack of flood water quality data. Among the limited prior studies focused on flood water quality, most characterize contaminant profiles in floodwaters. For example, Paerl et al. (2020) evaluated 36 cyclones impacting North Carolina from 1996 to 2019 and found that tropical storm events transported significant nitrogen (N), phosphorus (P), and carbon loads downstream. Similarly, Burkholder et al. (2004), Peierls et al. (2003), Smith et al. (2009), and Wachnicka et al. (2020) evaluated surface water constituents after hurricanes and tropical storms to characterize nutrient concentrations,

hypoxia, and algal blooms, and found that extreme storm events created large nutrient loads, conditions of hypoxia, and phytoplankton growth. Additionally, other studies have evaluated the levels of pathogens, fecal indicator bacteria, antibiotic resistance genes, and heavy metals in floodwaters (Harris et al., 2021; Jiang et al., 2020; Kiaghadi & Rifai, 2019; Steichen et al., 2020; Yang et al., 2021). These studies offer critical insights into water quality constituent concentrations in flood and post-flood conditions, and questions as to which watershed characteristics explain flood water quality signatures remain.

Quantifying the factors that influence floodwater constituents is important in explaining the drivers of flood water quality and planning effective flood management. Anthropogenic activities, natural catchment characteristics, and weather/climate variability heavily influence the spatio-temporal variability of water quality constituents (Arheimer & Lidén, 2000; Lintern et al., 2018; Meybeck & Helmer, 1989; Song et al., 2022; Varanka et al., 2015). In particular, flood hydrology and hydraulics are complex and involve nutrient inputs from landscapes that are typically not hydrologically connected to surface waters. Moreover, floods may cross watershed boundaries, creating challenges for identifying areas contributing pollutants to downstream waters. While we have an understanding of the variables that influence nutrient runoff in non-flooded conditions, there is a lack in understanding of the degree in which different landscape, watershed, and weather characteristics influence floodwater nutrient contamination at varying spatio-temporal scales.

To address lack of understanding on flood water quality descriptors, we aimed to explain flood water nutrient concentrations as a function of different environmental

variables, such as land cover and rainfall. Here, we focus on nutrients as key pollutants due to research conducted over the years identifying N and P loading as a key cause in accelerated primary production, hypoxia, fish kills, altered nutrient cycling, and overall habitat decline (Paerl et al., 2006). The objectives of this study were to 1) generate a spatio-temporal dataset of flood water nutrient concentrations, 2) develop a model that explains nutrient concentrations as a function of watershed characteristics, 3) identify the variables that best explain the nutrient water quality signatures in floodwaters. To accomplish this, we collected water samples from Hurricane Florence floodwaters in eastern North Carolina (NC), where extensive flooding occurred in a predominantly agricultural landscape. Samples were assessed for N and P content of total Kjeldahl nitrogen (TKN); unionized, aqueous ammonia and ionized ammonium (referred to as total ammonia nitrogen; TAN); nitrite and nitrate (NO_{2+3}^-); total phosphorus (TP); and orthophosphate (OPO_4). The N and P responses were explained using a statistical model incorporating land characteristics, pollution point sources, and hydroclimatic factors contributing to nutrient pollution.

2. MATERIALS AND METHODS

2.1 Study area

Eastern NC received record-breaking flooding from Hurricane Florence, which made landfall in Wrightsville Beach, NC on September 14, 2018. Hurricane Florence was a category 2 hurricane with 98 mph winds upon landfall, and quickly downgraded to category 1 after reaching Wilmington, NC (International Best Track Archive for Climate Stewardship, n.d.). Despite weakening after landfall, torrential rainfall impacted eastern NC for days. Storm surge reached 9 to 13 feet with 20 to 30 inches of rainfall

accompanying the hurricane. Wilmington, NC received ~27 inches of rain, although some areas, such as Elizabethtown, received an astonishing 36 inches (U.S. Department of Commerce, 2018).

Additionally, Eastern NC is a low-lying and flat coastal plain that is frequented by hurricanes, making it susceptible to extreme flooding. The land contains a mix of poorly drained and rapidly drained soils with Group A, B, D soils that vary widely between loamy, sandy, clay (Soil Survey Staff, 2019). This region is also an agriculturally intensive area with row crops and concentration animal feeding operations (CAFOs). Thus, rainfall and flooding from Hurricane Florence created conditions in which hog farm lagoons were overtopped, wastewater treatment plants overflowed into local communities, and toxic coal ash ponds were breached (Powell, 2020; Simpson, 2018).

To understand the drivers of nutrient pollution in floodwaters, we sampled Hurricane Florence floodwaters at 51 sites in the NC coastal plain. Sites were selected to cover a range of watersheds across the region, as well as locations with spatial variability within the same watershed. Due to general differences in water quality in headwater streams compared to nearshore waters, sites were selected across different stream orders and stream types.

Additionally, many sites were contained within the Lumber, Cape Fear, and Neuse river basins. These watersheds contain different levels of anthropogenic development and consist of dense agricultural industries that are prone to non-point source nutrient inputs in surface waters (Figure B-1). Potential agricultural sources of nutrients within these watersheds include large scale soybean, corn, cotton, and wheat croplands, as well as dense swine and poultry farms (USDA NASS, 2022).

These watersheds are also home to several Native American tribes, including the Coharie, Waccamaw Siouan, and Lumbee Tribes. Tribal communities experienced inundation and received catastrophic flooding from the previous hurricane, Hurricane Matthew in 2016 (Emanuel & Wilkins, 2020; Khajehei, 2019; Roetman, 2016; Zhao et al., 2020). Thus, to identify flooding impacts on local water quality and inform underserved communities on flood preparation, several sites were selected based on proximity to the different tribal communities and site selection was informed by discussions with community leaders.

Lastly, important considerations for site selection also included accessibility to the sample location and safety concerns regarding flood conditions.

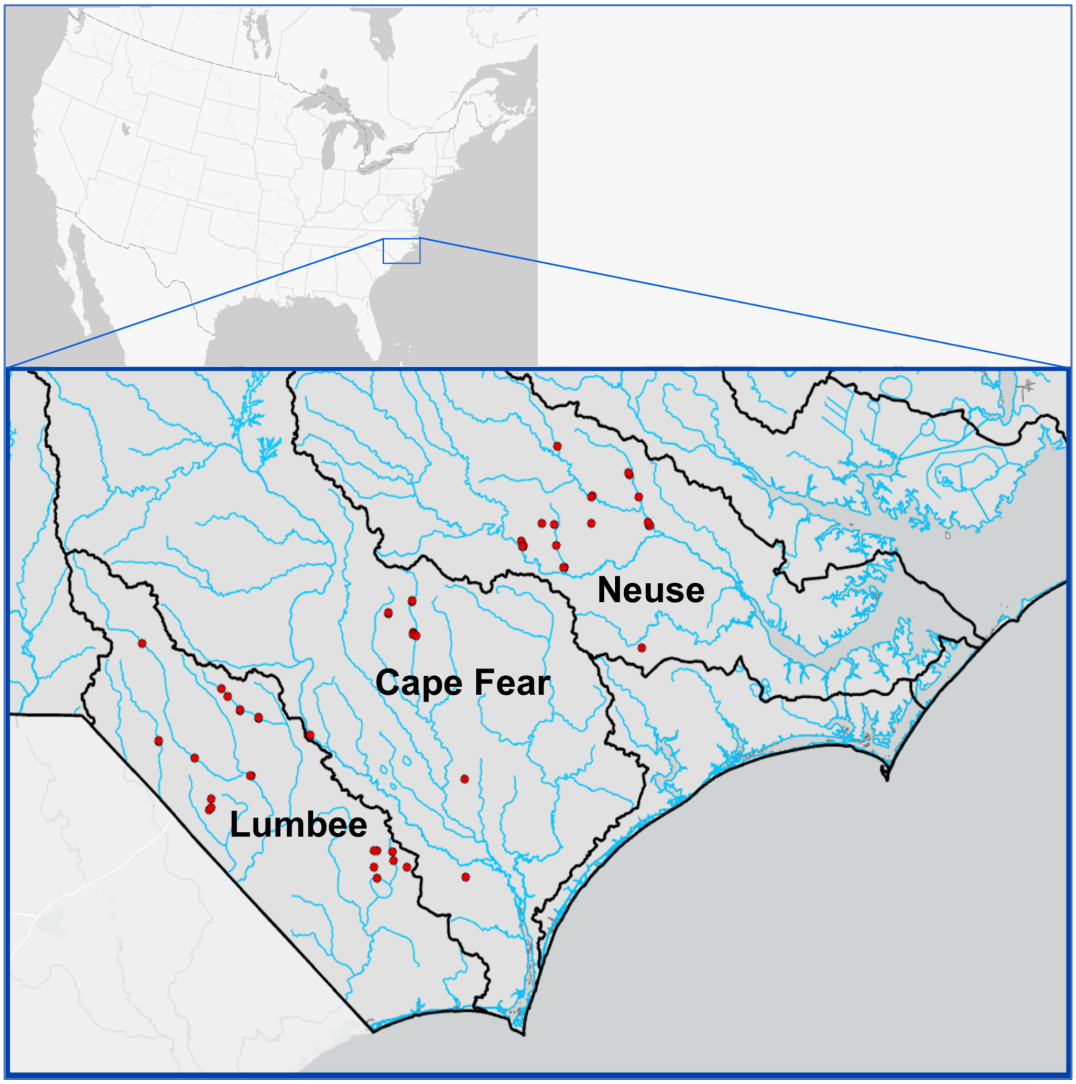

Figure 3- 1. Map of study area showing the river basins (black lines), major river systems (blue lines) and sample sites (red points, n=51). Watershed names are in bold text.

2.2 Sample collection and analyses

Each site was visited four times, referred to as phases (Table 1). Phase 1 data collection occurred a week after Hurricane Florence made impact and Phase 2 samples were collected a month after the hurricane. Phase 1 and 2 sampling occurred during post-hurricane conditions at different time points to provide insight on the variability of nutrient pollution after a hurricane. Phase 3 and 4 samples were collected a year after

Phase 1 and 2, when no hurricanes impacted the area, to serve as a baseline of water quality in this system. Figure B- 2 shows site variability of TKN, TAN, NO_{2+3}^-, TP, and OPO_4 concentrations across sampling phases.

Table 3- 1. Surface water sample dates after Hurricane Florence.

Phase	Sampling Date(s)	Days after landfall
1	September 21, 2018 – September 28, 2018	7-14
2	October 18, 2018 – October 19, 2018	34-35
3	September 28, 2019	379
4	October 18, 2019	399

Fifty-five milliliters of water were collected from each location and filtered through 0.45-µm Whatman PTFE syringe filters. All samples were placed in coolers on ice for the duration of each sampling trip and remained frozen until ready for analysis. Samples were analyzed for nutrient concentrations using the Lachat QuikChem 8500. TKN and NO_{2+3}^- were analyzed according to the United States Environmental Protection Agency methods EPA 351.2 and 353.2, respectively. TAN was analyzed using the Standard Methods 4500-NH3 G. TP and OPO_4 were analyzed using American Public Health Association (APHA) standard 4500-P and 4500-P F/G. For all N and P analyses, nutrient compounds are reported as N and P content, respectively (e.g., NH_4^+ is technically NH_4^+-N and OPO_4 is OPO_4-P).

2.3 Candidate explanatory variables

A variety of hydroclimatic factors, pollution point sources, and land characteristics were selected as candidate explanatory variables to represent mechanistic drivers of nutrient concentrations (Table 1). Candidate explanatory variables were summarized for

each sampling location's contributing watershed. To delineate watersheds, sample locations were snapped to the nearest stream grid cell (U.S. Geological Survey, n.d.) and the contributing drainage area of each sample site was calculated using the USGS StreamStats API tool (U.S. Geological Survey, 2016).

Among the candidate explanatory variables selected, several focused on proximity to nonpoint and point sources of nutrients. The primary nonpoint sources considered were croplands and developed surface area. Swine concentrated animal feeding operations (CAFOs) were specifically included as a nutrient source because swine waste in this region is stored in open-air lagoons that are prone to flooding and releasing effluent during extreme weather events. Animal production facilities like swine CAFOs have the potential to release effluent that introduces harmful animal waste and excess nutrients into surface waters (West et al., 2011). Wastewater treatment plants (WWTPs) are another major source of pollution during major storm events since they introduce human waste to the environment when their capacity is overtopped and excess wastewater spills directly onto the landscape. During major hurricane events, many WWTPs in the area are reported to overtop and spill onto the landscape (Beeson, 2018).

To construct variables summarizing the presence of point and nonpoint sources in proximity to sampling locations, swine CAFO and WWTP locations were counted within each location's watershed, and the Euclidean distances of the nearest upstream swine CAFO and WWTP to sampling locations were calculated.

Since some sites did not have any swine CAFOs or WWTPs in their contributing watersheds, the distance to nearest swine CAFO and distance to nearest WWTP

variables were transformed to categorical indicator variables representing the range of distances to nearby swine CAFOs and WWTPs. K means clustering with three bins was applied to determine the breakpoints for the distance categories (Figure 2; Lloyd, 1957). Three bins were chosen because a histogram of the data revealed three natural groupings. The result of the k means clustering analysis for the distance to nearest swine CAFO variable was used to generate three categories of distances and an additional category was created for sites that did not have swine CAFOs within their watershed. This resulted in the four categories: CAFO presence/absence, distance to nearest CAFO within 5201 m, distance to nearest CAFO within 7057 to 11807 m, and distance to nearest CAFO over 14691 m. Hereafter, the term CAFO will be used to refer to swine CAFOs specifically. The same process was repeated with the distance to nearest WWTP data to generate the four categories: WWTP presence/absence, distance to nearest WWTP within 8678 m, distance to nearest WWTP within 13152 to 17856 m, and distance to nearest WWTP over 19950 m. Within the models, each of the distance categories was included as a separate explanatory variable with a binary designation specifying if the nearest swine CAFO or WWTP fell within each distance category, and the presence/absence category was binary to indicate whether there were any swine CAFOs or WWTPs present.

The gSSURGO product (Soil Survey Staff, 2019) was used to delineate the area of a site's watershed that contains poorly draining soils and excessively draining soils. Flood extent, flooded cropland area, flooded developed area, and developed land cover area were delineated for each sample's watershed using the 2019 Multi-Resolution Land Characteristics (MRLC) National Land Cover Database (NLCD) product (Dewitz,

2019) and The Nature Conservancy Hurricane Florence flood extent product (Schaffer-Smith et al., 2020). The MRLC NLCD product is a categorical raster representing land cover classes at 30-m resolution. The flood extent product is a binary raster representing flood/non-flood conditions at 20-m resolution. Each product was clipped to the boundaries of each site's watershed and summarized according to land class and flood condition.

Additionally, cropland to wetland area ratio was considered as a model covariate due to the dense agriculture in the study area. Watersheds with more cropland than wetland area have a higher chance of agricultural pollution not being treated by wetlands (Olszewska, 2005). Thus, the cropland to wetland area was considered as an indicator of agricultural pollution potential. This variable was processed using the MRLC NLCD product and delineating the croplands, herbaceous wetlands, and woody wetlands for each site's contributing area. The cropland to wetland ratio was computed by dividing the cropland area with the sum of the herbaceous and woody wetland areas.

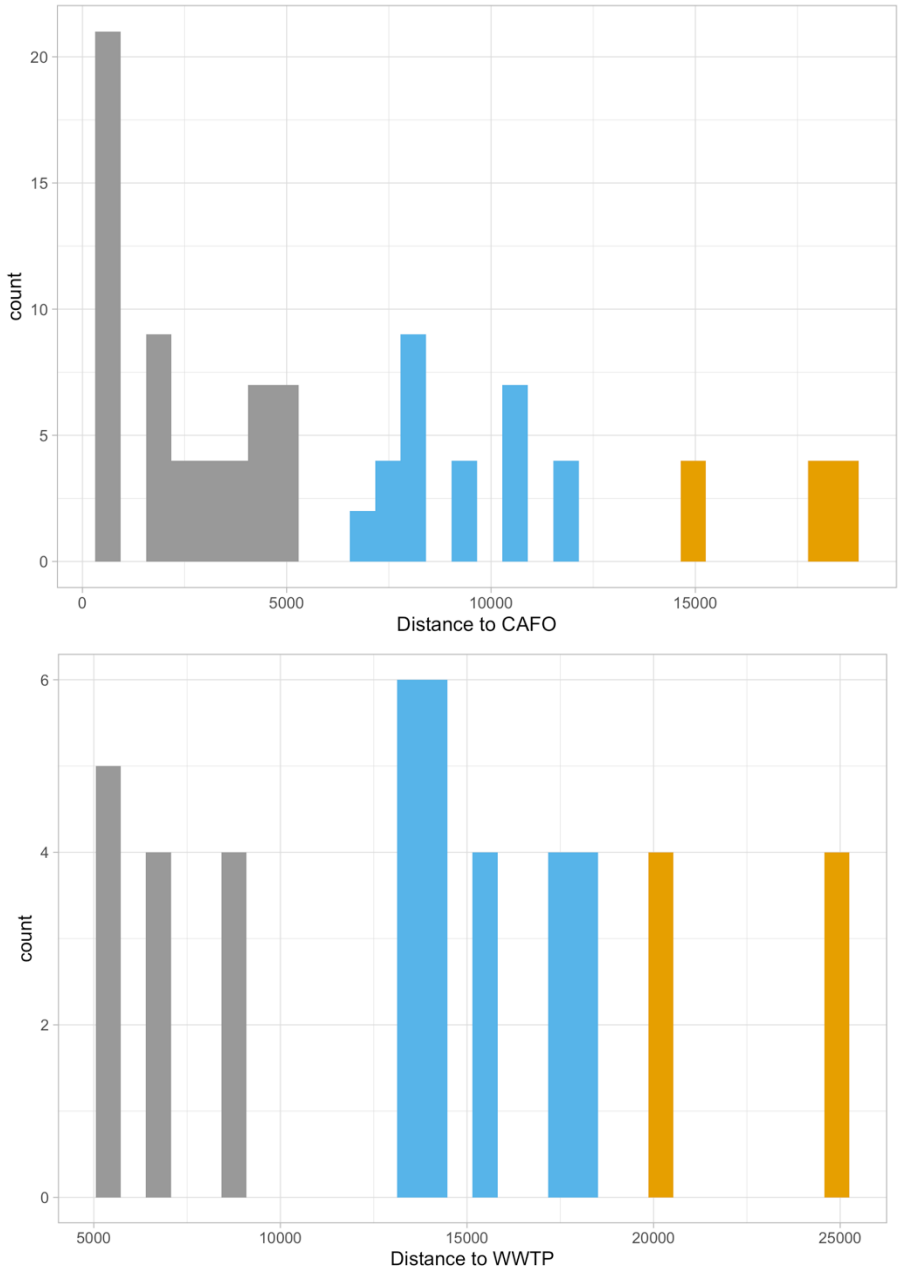

Figure 3- 2. Histogram of “Distance to nearest CAFO” (top) and “Distance to nearest WWTP” (bottom) variables. The different bar colors indicate the different groups formed through k-means clustering.

Total population also was considered as a candidate variable due to correlations between population density, flooding, and water quality (Jongman et al., 2012). This correlation is reflected as a population increases and more pervious surfaces are

developed, which generates large amounts of surface runoff that contributes to flooding and has the potential to carry pollutants with the water. High resolution gridded population data was obtained from Oak Ridge National Laboratory's LandScan product (Rose et al., 2020). Similar to the other candidate variables, total population was calculated by summing the population within each site's watershed. Figure B- 3 shows the different watersheds delineated for each site.

Table 3- 2. Summary of all candidate explanatory variables.

Variable	Data Type	Method of Calculation	Reason
Number of CAFOs	Continuous	Sum CAFOs within site's watershed area	Potential nutrient pollution point source
CAFO presence/absence	Binary	Indicator of CAFO presence within site's watershed	Potential nutrient pollution point source
Distance to closest CAFO is within 5201 m	Binary	Indicator of whether the nearest CAFO in a site's watershed was within 11707 m	Potential nutrient pollution point source
Distance to closest CAFO is within 7057 to 11807 m	Binary	Indicator of whether the nearest CAFO in a site's watershed was within 57775 to 110762 m	Potential nutrient pollution point source
Distance to nearest CAFO is over 14691 m	Binary	Indicator of whether the nearest CAFO in a site's watershed was over 128441 m away	Potential nutrient pollution point source
Number of WWTPs	Continuous	Sum CAFOs within site's watershed area	Potential nutrient pollution point source
WWTP presence/absence	Binary	Indicator of WWTP presence within site's watershed	Potential nutrient pollution point source

Table 3- 2. (continued)

Distance to closest WWTP is within 8678 m	Binary	Indicator of whether the nearest WWTP in a site's watershed was within 19950 m	Potential nutrient pollution point source
Distance to closest WTTP is within 13152 to 17856 m	Binary	Indicator of whether the nearest WWTP in a site's watershed was within 106846 to 114287 m	Potential nutrient pollution point source
Distance to nearest WWTP is over 19950 m	Binary	Indicator of whether the nearest WWTP in a site's watershed was over 133511 m away	Potential nutrient pollution point source
Poorly drained soil area	Continuous	Sum "poorly drained" and "very poorly drained" area within each site's watershed	Mechanism of flooding and nutrient transport
Excessively drained soils area	Continuous	Sum "excessively drained" area within each site's watershed	Mechanism of flooding and nutrient transport
Total population	Continuous	Sum gridded population data within site's watershed	Proxy for potential non-point source of nutrient pollution
Antecedent rainfall	Continuous	Sum total rainfall in the site's watershed area over the previous day(s)	Mechanism of flooding and nutrient transport
Flood extent	Continuous	Sum the flooded pixels within each site's watershed	Mechanism of flooding and nutrient transport
Flooded cropland area	Continuous	Sum the flooded pixels within the croplands of each site's watershed	Mechanism of flooding and nutrient transport Potential non-point source of nutrient pollution

Table 3- 2. (continued)

Flooded developed area	Continuous	Sum the flooded pixels within the developed area of each site's watershed	Mechanism of flooding and nutrient transport Potential non-point source of nutrient pollution
Developed land cover area	Continuous	Sum all developed areas within a site's contributing watershed	Mechanism of flooding and nutrient transport Potential non-point source of nutrient pollution
Cropland to Wetland Area	Continuous	Within each site's drainage area, divide the cropland area and wetland area	Mechanism of flooding and nutrient transport Potential non-point source of nutrient pollution
Watershed Area	Continuous	Site's contributing drainage area	Mechanism of flooding and nutrient transport

2.4 Explanatory variable selection

All continuous explanatory variables were screened for multicollinearity through a variance inflation factor (VIF) analysis. Variables with VIF greater than 10 were eliminated to ensure that variables used in the model are statistically independent (Marquardt, 1970; Neter et al., 1989).

Due to multicollinearity, several variables were omitted from the model. The covariates used within the model were developed flooded area, cropland to wetland area, number of CAFOs, distance to nearest CAFO, distance to nearest WWTP, day of precipitation, 2 day antecedent precipitation, 3 day antecedent precipitation, 5 day antecedent precipitation, 6 day antecedent precipitation, 7 day antecedent precipitation.

Additionally, each covariate contained two additional interaction terms associated with Phase 1 and Phase 2 sampling. The motivation behind the inclusion of phase

interaction terms was to capture the variables important in explaining water quality response during flooding, since flood conditions were present during phase 1 and 2. Then, covariates were centered around zero and scaled to enable interpretability and comparison between variables of different scales and magnitudes.

2.5 Model Structure

Bayesian statistical modeling methods have gained traction in the hydrological sciences (Clark, 2005). Bayesian modeling methods have been shown to effectively model nutrient water quality, allow for missing data, handle small sample sizes, and account for prior scientific information, thus making this class of models suited for this application (Guo et al., 2020; Qian & Reckhow, 2005). Rather than building an independent model for each nutrient response, a multivariate model was built such that one model was constructed to predict all response variables. The implementation of a multivariate model allows us to take advantage of cross correlations between nutrients and compare covariates across outcomes.

To account for spatial and multivariable response correlations we use a linear model of coregionalization (LMC). LMC models are a popular method of multivariate spatial analysis (Banerjee et al., 2014). An LMC model assumes that the observations are linear combinations of underlying latent variables that covary jointly over an area. We assume our multivariate spatial data had K= five responses: TKN, NO_{2+3}, NH_4, TP, and OPO_4. For the kth response, let $Y_k(s_i,t)$ be the response for a sample at spatial location s_i and phase t. The general set-up for the model can be represented as

$$Y_k(s_i, t) = \mu_k(s_i, t) + \omega_k(s_i, t) + \varepsilon_k(s_i, t)$$

where μ_k is the mean trend containing fixed effects, ω_k is the multivariate spatial random effects, and ε_k is the nugget error term $\varepsilon_k \sim N(0, \sigma^2)$ independent over space and time.

The mean trend of the data and is represented by a linear model of p=51 covariates

$$\mu_k(s_i, t) = \beta_{0,k} + \sum_{j=1}^{p} \beta_{j,k} X_j(s_i, t)$$

where $\beta_{0,k}$ is the intercept for response k, $X_{i,j,k}$ is a 51x51 matrix of explanatory variables, and $\beta_{j,k}$ is the regression coefficient for explanatory variable j on response k.

The regression coefficients vary by response to allow covariates to affect nutrients differently. A continuous shrinkage prior was selected so that unimportant covariates have regression coefficients that are likely to be near zero, while important covariates are assigned a larger regression coefficient. The prior for the regression coefficients is $\beta_{j,k} \sim N(0, {\tau^2}_{j,k})$, where ${\tau^2}_{j,k} = {\tau^2}_k * {\lambda_j}^2$. The λ_j term represents the importance of covariate j across k responses; if λ_j is large then the prior allows for the regression coefficient to be large as well, but if $\lambda_{j,k}$ is small the regression coefficients will be small. To determine which covariates are statistically significant for each nutrient response, the 95% credible intervals for $\beta_{j,k}$ were extracted. The covariates containing a regression coefficient with a 95% credible interval excluding zero were found to be statistically significant. Furthermore, posterior model probabilities of the statistically significant regression coefficients were examined to understand which covariates had the highest probability of being greater than zero, and covariates with a probability greater than 50% were selected as important explanatory variables.

We suspect that there is correlation across space and responses that is not explained with the current list of explanatory variables in μ_k. A LMC model was applied to capture these correlations. We apply the use of latent factors with spatial correlation functions that designate the correlation between the response k across space. These factors represent unseen, independent processes and thus were not extracted to be explained. In this case, the factor loadings quantify the correlation between the responses at one site.

The spatial random effects are modeled for each kth response as a combination of spatially varying factors:

$$\omega_k(s_i, t) = \sum_{u=1}^{f} L_{k,u} F_u(s_i, t)$$

where f is the number of factors, $L_{k,u}$ is the factor loadings for response k on process u, $F_u(s_i, t)$ are independent over u and t spatial Gaussian processes with mean 0, variance 1, and spatial correlation functions $\rho_1, \ldots, \rho_f$, and we select exponential spatial correlation functions of distance d, $\rho_u(d) = e^{-d/\phi_u}$ for spatial range ϕ_u.

The factor loadings determine the cross-covariance between responses at the same location. In return, the cross-covariance matrix indicates how similar two responses co-vary using the equation:

$$\mathrm{Cov}(\omega_{i,k}(s,t), \omega_{i,j}(s,t)) = \sum_{u=1}^{f} L_{k,u} L_{j,u}$$

The degree of spatial variation is represented by $\sigma^2, L_{k,u}$, and ϕ_u. Uninformative priors were assigned for these parameters so the model was trained using the relationships in the data without prior knowledge. We use priors

$\beta_{0,k} \sim N(0,\ 100), \sigma^2{}_{i,k} \sim InvGamma(0.1,\ 0.1),\ \tau^2{}_{i,k} \sim InvGamma(0.1,\ 0.1)$, and $\phi_u \sim Gamma(0.1,\ 0.1)$.

After model specification, the multivariate, spatial model was built using 2 different MCMC chains and each chain containing 25000 MCMC iterations with 5000 iterations being removed as burn-in.

2.6 Model Selection

Once the covariates and data were processed, the multivariate, spatial Bayesian model was trained. Spatial models containing multivariate spatial effects were built using the {rjags} R software package. Several spatial models were trained with varying number of factors using all the processed data. Additionally, nonspatial models containing only the mean trend (excluding any multivariate, spatial random effects) were trained using all the covariate and response data. Nonspatial models were built using ordinary least squares to evaluate whether the spatial, multivariate model results were different. All models were tested for convergence using the Gelman-Rubin diagnostic, then evaluated using deviance information criterion (DIC) and Nash Sutcliffe Efficiency (NSE). The Gelman-Rubin diagnostic is an indicator of convergence, in which values less than 1.1 indicate convergence (Gelman & Rubin, 1992; Brooks & Gelman, 1998). DIC is a method of measuring Bayesian hierarchical model goodness-of-fit by calculating the posterior mean of the log likelihood and adding penalties for model complexity (Spiegelhalter et al., 2002). NSE is an accuracy metric (ranging from 0,1) commonly used in the hydrological sciences that compares the variance in observed and predicted responses, in which a higher NSE indicates a higher accuracy (Nash & Sutcliffe, 1970). Since all data were used for model building, the NSE accuracy metric

was calculated using the training dataset, which means the calculated accuracy for each nutrient response is a best-case-scenario. All models were compared across one another using the DIC and NSE metrics. The model with the smallest DIC and highest NSE was selected as the primary model for analysis.

3. RESULTS

3.1 Spatiotemporal variation in nutrient concentrations following major flooding

Raw nutrient concentrations during different sampling periods were investigated to understand the response variable observations (Figure 3). For TKN, the median and mean values were highest during phase 1 Hurricane Florence flood conditions (2.22 and 1.98 mg/L, respectively). Although the maximum TKN concentration was documented during phase 2 sampling. TKN distributions during non-storm conditions (phase 3 and 4) were very similar.

During phase 1 and 2, TAN concentrations were all below 1 mg/L. Phase 2 had the highest mean and median TAN concentrations at 0.27 and 0.24 mg/L, respectively. During phase 3, one site experienced the largest magnitude of TAN, 3.7 mg/L.

For NO_{2+3}^{-}, phase 1 experienced the lowest concentrations with a mean of 0.14 mg/L and median of 0.02 mg/L. NO_{2+3}^{-} concentrations after phase 1 were slightly higher than the floodwater concentrations, but values were very low across all temporal periods. The maximum NO_{2+3}^{-} concentration of 4.8 mg/L was during phase 3.

The mean concentrations of TP were consistent across all temporal periods. The maximum concentration (5.1 mg/L) was observed during phase 2, which also had the lowest median concentration of 0.13 mg/L. For OPO_4, the lowest mean and median concentrations were during phase 2 with values of 0.10 and 0.07 mg/L, respectively.

The highest OPO_4 concentration (2.3 mg/L) was during phase 1. While phase 3 and 4 had similar distributions.

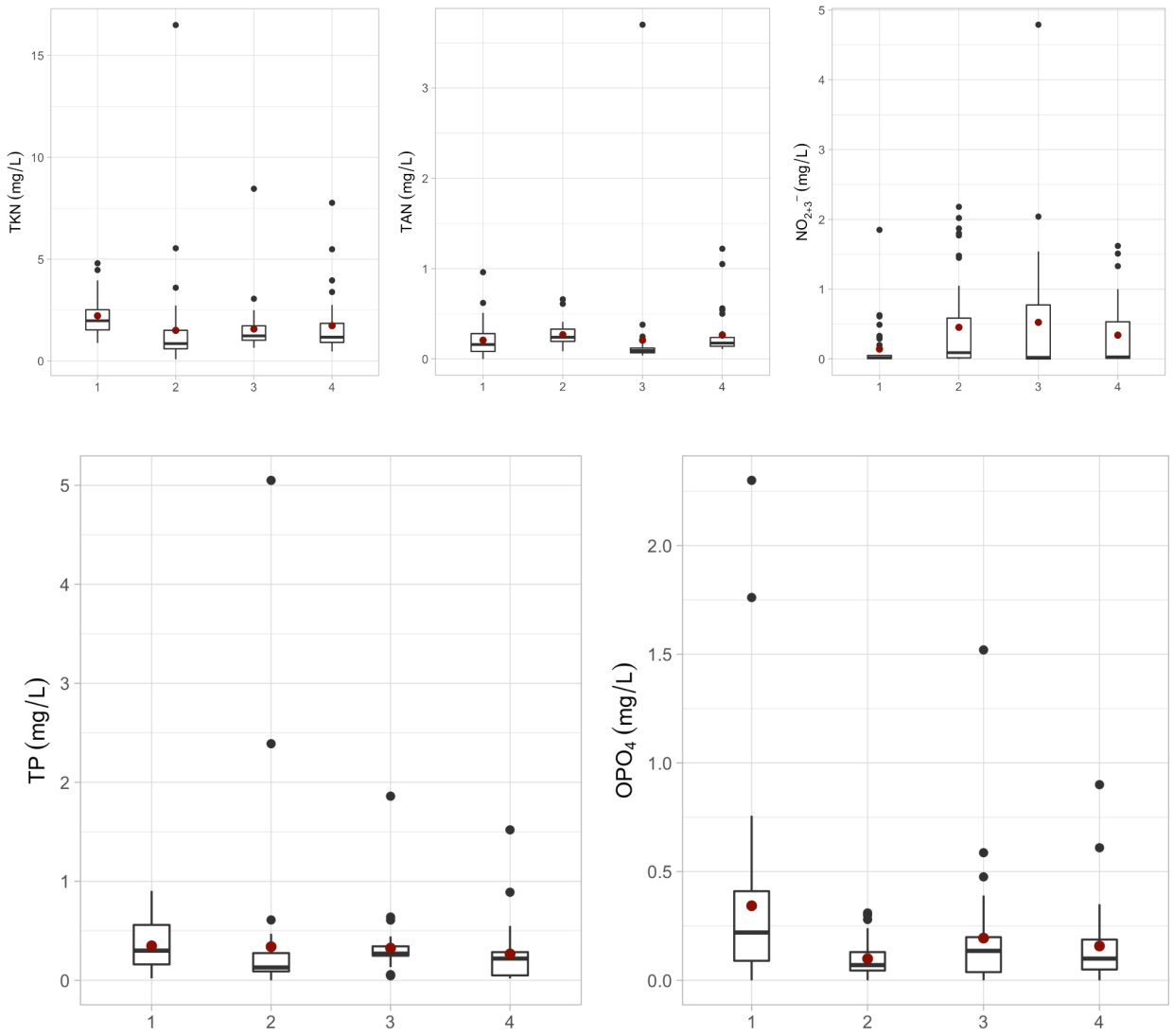

Figure 3- 3. Concentrations of TKN, TAN, NO_{2+3}^-, TP, and OPO_4 over all sampling periods. Red dots represent the mean value.

3.2 Model selection

Nonspatial and spatial models with varying numbers of latent factors were trained and compared using the model performance metrics: deviance information criterion (DIC) and Nash-Sutcliffe Efficiency (NSE). The nonspatial model performed the least

favorably, while the spatial model with four latent factors performed the best (Tables B-1 and B-2). Thus, the spatial model with four latent factors was used as the primary model for evaluation.

3.3 Explanatory variable importance

Results indicate that WWTP, CAFO, and rainfall variables are statistically significant variables in explaining nutrient concentrations (Figure 4). For TKN, generally speaking, hydroclimatic factors and pollution point sources were the most important variables in the model. CAFO presence, WWTP presence, distance to nearest CAFO within 7057 to 11807 m, day-of rainfall, number of CAFOs, distance to nearest CAFO within 8678 m, and distance to nearest WWTP over 19960 m away were important explanatory variables in predicting TKN across all temporal periods. In addition, during phase 1 specifically, CAFO presence, 2-day antecedent rainfall, day-of rainfall, WWTP presence, distance to nearest WWTP within 13152 to 17856 m, 3- day antecedent rainfall, and number of CAFOs variables were important in explaining the TKN response in floodwaters. During phase 2 conditions, when floodwaters were subsiding, 2 day antecedent rainfall, number of CAFOs, day-of rainfall, CAFO presence, distance to closest WTTP within 13152 to 17856 m, WWTP presence, 7-day antecedent rainfall, developed flooded area, distance to nearest WWTP within 8678 m, and distance to nearest CAFO within 5201 m were important explanatory variables.

For TAN, the model revealed that distance to nearest CAFO within 5201 m, 3-day antecedent rainfall, WWTP presence, 6-day antecedent rainfall, and distance to nearest WWTP within 8678 m were important in explaining TAN responses across all sampling periods. The interaction variables indicated that some explanatory variables

had a specific impact on TAN during flood conditions. During phase 1 flooding, distance to nearest CAFO within 5201 m, distance to nearest CAFO within 7057 to 11807 m, 3-day antecedent rainfall, distance to nearest WWTP over 19960 m away, distance to nearest WWTP within 13152 to 17856 m, 2-day antecedent rainfall, distance to nearest WWTP within 8678 m, developed flooded area, and day-of rainfall were important variables. While phase 2 conditions revealed that CAFO presence, number of CAFOs, cropland to wetland area, distance to nearest WWTP within 13152 to 17856 m, distance to WWTP over 19950 m away, 5-day antecedent rainfall, distance to nearest CAFO over 14691 m away, and distance to nearest WWTP within 8678 m were important in explaining the TAN response a month after Hurricane Florence.

For NO_{2+3}^{-}, the distance to nearest CAFO within 5201 m, 3-day antecedent rainfall, nearest WWTP within 13152 to 17856 m, developed flooded area, cropland to wetland area, 2-day antecedent rainfall, WWTP presence, and 6-day antecedent rainfall were important variables in explaining nitrite/nitrate concentrations across all temporal periods. In addition, the interaction explanatory variables revealed that some covariates were important in specifically explaining phase 1 and phase 2 flood conditions. During phase 1 sampling immediately after Hurricane Florence landfall, developed flooded area, 3-day antecedent rainfall, and distance to nearest WWTP within 8678 m, CAFO presence, WWTP presence, and 2-day antecedent rainfall were important in explaining the NO_{2+3}^{-} response. A month after Hurricane Florence, the model revealed that CAFO presence, 5-day antecedent rainfall, WWTP presence, 3-day antecedent rainfall, distance to nearest CAFO within 5201 m, cropland to wetland area, distance to nearest

WWTP within13152 to 17856 m, 6-day antecedent rainfall were important model covariates in explaining the NO_{2+3}^{-} concentration.

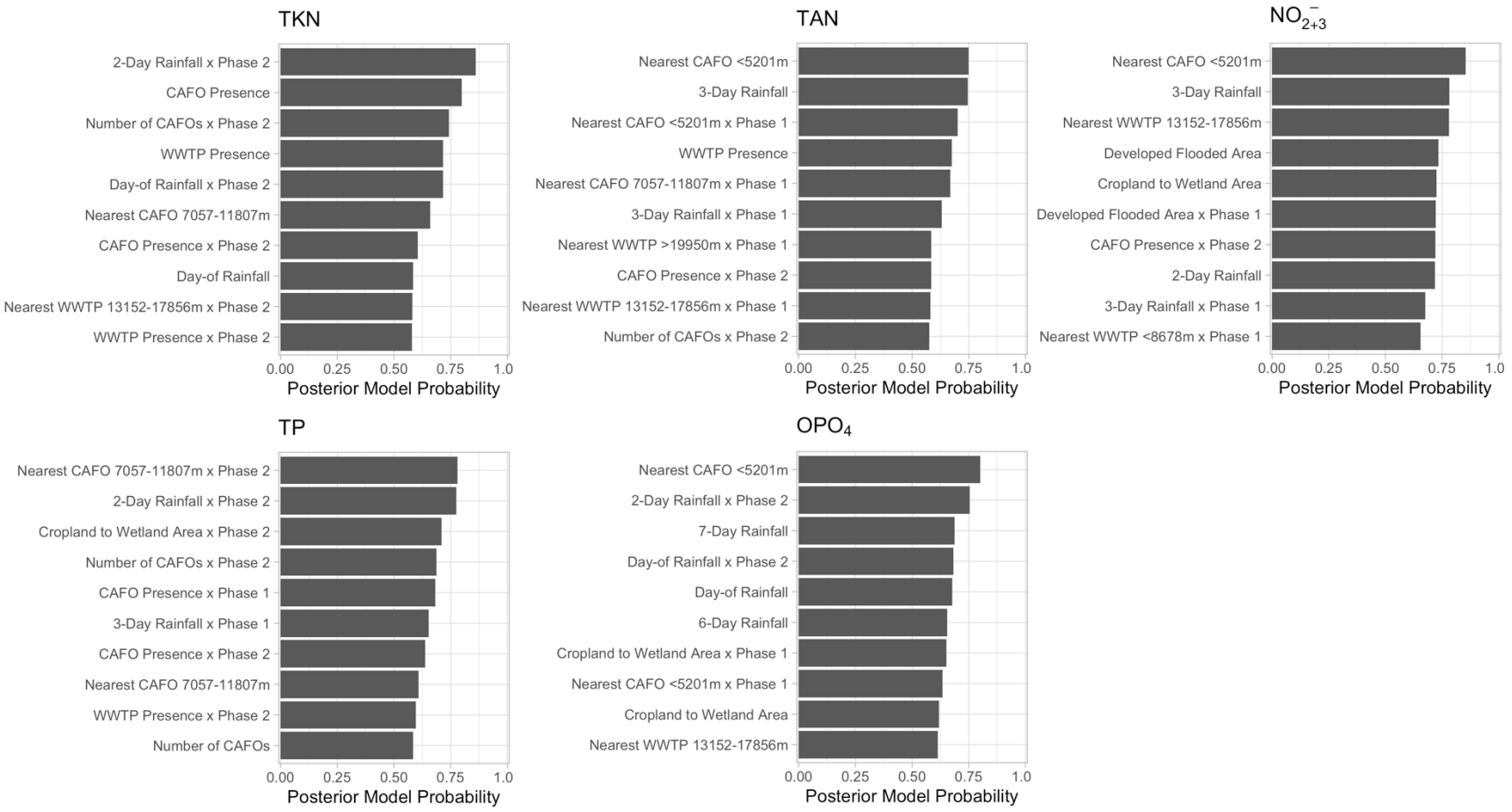

Figure 3- 4. Posterior probability of the ten most important model covariates for each nutrient response.

For TP, distance to nearest CAFO within 7057 to 11807 m, number of CAFOs, WWTP presence, 2-day antecedent rainfall, 3-day antecedent rainfall, distance to nearest WWTP within 13152 to 17856 m, and day-of rainfall were important explanatory variables during all sampling periods (phases 1-4). Some explanatory variables were important with only phase 1 or phase 2 interactions. This revealed that during phase 1 CAFO presence, 3-day antecedent rainfall, distance to nearest WWTP within 8678 m, developed flooded area, 2-day antecedent rainfall, number of CAFOs, distance to nearest WWTP within 13152 to 17856 m, and day-of rainfall were important covariates during flooding. While distance to nearest CAFO within 7057 to 11807 m, 2-day antecedent rainfall, cropland to wetland area, number of CAFOs, CAFO presence, WWTP presence, 3-day antecedent rainfall, day-of rainfall, distance to nearest WWTP over 19950 m away, 7-day antecedent rainfall, 5-day antecedent rainfall, and 6-day antecedent rainfall were important explanatory variables of TP concentration in post-flood conditions during phase 2 sampling.

The exploration of OPO_4 explanatory variables revealed the explanatory variables distance to nearest CAFO within 5201 m, 7-day antecedent rainfall, day-of rainfall, 6-day antecedent rainfall, cropland to wetland area, distance to nearest WWTP within 13152 to 17856 m, 2-day antecedent rainfall, 3-day antecedent rainfall, 5-day antecedent rainfall, developed flooded area, and WWTP presence were important during all phases of sampling, regardless of flood status. Phase 1 and 2 interactions revealed specific explanatory variables that are important during Hurricane Florence flood conditions. During phase 1 flooding, cropland to wetland area, distance to nearest CAFO within 5201 m, day-of rainfall, WWTP presence, 5-day antecedent rainfall,

distance to nearest WWTP over 19950 m away, 7-day antecedent rainfall, and 6-day antecedent rainfall were important. During phase 2 sampling, 2-day antecedent rainfall, day-of rainfall, CAFO presence, 7-day antecedent rainfall, 6-day antecedent rainfall, distance to WWTP within 13152 to 17856 m, and WWTP presence were important in explaining the OPO_4 conditions a month after Hurricane Florence.

3.4 Model variable magnitudes

The influence of each significant variable on the magnitude of the nutrient response is represented by the mean posterior regression coefficients (Table 3). The explanatory variables with the greatest magnitude in β have the greatest impact on the nutrient concentrations.

Table 3- 3. Top three explanatory variables for flood conditions a week after Hurricane Florence (phase 1), a month after Hurricane Florence landfall (phase 2), and throughout all sampling periods (phases 1-4). The β value represents the mean regression coefficient.

Nutrient	All Sampling Periods		Phase 1 Interactions		Phase 2 Interactions	
	Variable	β	Variable	β	Variable	β
TKN	CAFO Presence	0.080	2-Day Antecedent Rainfall x Phase 1	0.049	2-Day Antecedent Rainfall x Phase 2	1.878
	WWTP Presence	0.052	5-Day Antecedent Rainfall x Phase 1	0.032	Day-of Rainfall x Phase 2	0.822
	Distance to Nearest CAFO within 7057-11807 m	0.027	CAFO Presence x Phase 1	0.024	7-Day Antecedent Rainfall x Phase 2	0.171
TAN	Distance to Nearest CAFO within 5201 m	0.058	3-Day Antecedent Rainfall x Phase 1	0.132	CAFO Presence x Phase 2	0.026
	WWTP Presence	0.042	Distance to Nearest WWTP Over 19950 m Away x Phase 1	0.087	Number of CAFOs x Phase 2	0.023
	3-Day Antecedent Rainfall	0.041	Distance to Nearest CAFO within 5201 m x Phase 1	0.064	5-Day Antecedent Rainfall x Phase 2	0.017

Table 3- 3. (continued)

NO_{2+3}^-	Distance to Nearest CAFO within 5201 m	0.103	3-Day Antecedent Rainfall x Phase 1	0.193	3-Day Antecedent Rainfall x Phase 2	0.080
	Distance to Nearest WWTP within 13152 to 17856 m	0.054	Developed Flooded Area x Phase 1	0.189	CAFO Presence x Phase 2	0.077
	3-Day Antecedent Rainfall	0.052	Distance to Nearest WWTP within 8678 m x Phase 1	0.044	5-Day Antecedent Rainfall x Phase 2	0.057
TP	WWTP Presence	0.019	3-Day Antecedent Rainfall x Phase 1	0.122	2-Day Antecedent Rainfall x Phase 2	1.025
	Distance to Nearest CAFO within 7057-11807 m	0.016	CAFO Presence x Phase 1	0.061	Day-of Rainfall x Phase 2	0.214
	Number of CAFOs	0.014	2-Day Antecedent Rainfall x Phase 1	0.044	Distance to Nearest CAFO within 7057-11807 m x Phase 2	0.080
OPO_4	7-Day Antecedent Rainfall	0.125	Cropland to Wetland Area x Phase 1	0.048	2-Day Antecedent Rainfall x Phase 2	0.896
	Distance to Nearest CAFO within 5201 m	0.071	Distance to Nearest CAFO within 5201 m x Phase 1	0.036	Day-of Rainfall x Phase 2	0.489
	Day-of Rainfall	0.043	Day-of Rainfall x Phase 1	0.023	7-Day Antecedent Rainfall x Phase 2	0.150

4. DISCUSSION

Flooding can be detrimental to the health of citizens and the environment due to the destruction and pollution exported from these extreme events. Here, we modeled the drivers of flood water quality and characterized variables influencing N and P concentrations in surface waters during flood and non-flood conditions.

We found that TAN and NO_{2+3}^- values in phase 1 floodwaters were very low compared to historic averages, with mean concentrations being under the 25 percentile, according to Ecoregion XIV subecoregion 63 data (U.S. Environmental Protection Agency, 2000). Rainfall was an important factor in explaining TAN and NO_{2+3}^- concentrations, thus it is likely that the increased water volume created a dilution effect. Other studies found similar results, as hurricanes with extreme rainfall can dilute pollutant concentrations (Chen et al., 2018; Ching et al., 2015).

WWTP variables were relatively important explanatory variables for TKN, TAN, and NO_{2+3}^- concentrations in this analysis. Specifically, we found that the distance to the nearest WWTP was an important variable in explaining N concentrations during any sampling period. The stronger influence of WWTP variables on TAN and NO_{2+3}^-, suggests that humans may be a source of inorganic nitrogen entering the surface water system. This can be corroborated by reports of many wastewater plants discharging into tributaries for long periods after Hurricane Florence impact from the amount of severe flooding (Beeson, 2018). A study conducted in NC by Iverson et al. (2018) found that total nitrogen exports increased as the density of wastewater processing systems increased. It should be noted that many residents in rural areas of eastern NC use onsite wastewater systems that are prone to leaking and discharging during flood

events. Thus, we should better manage our sewage systems to withstand hurricane impacts, as it is anticipated that flooding and extreme events will only become worse with climate change progression (Milly et al., 2002).

Additionally, CAFO variables were consistently important in explaining N and P concentrations during flooding, but also during non-flood conditions. This suggests that CAFOs may have an influence on surface water quality outside of flood conditions, as suggested by Harris et al. (2021). Eastern NC has one of the densest CAFO industries in the US with most of them being on the floodplain (Montefiore et al., 2022), thus during Hurricane Florence many lagoons became flooded and caused waste to leach into floodwaters (Schaffer-Smith et al., 2020). This is important as underserved communities are more likely to become flooded and face the negative impacts associated with compromised water quality (Wing et al., 2002).

Rainfall was the most important driving factor for P concentrations. Furthermore, rainfall was important in explaining TP and OPO_4 during phase 1 flood conditions, but also had additional, stronger importance during phase 2 sampling a month after Hurricane Florence impact. P is typically bound to soil particles and immobilized from surface water runoff; thus, the high influence of precipitation during phase 2 likely represents the mechanistic transport of P from rainfall runoff after storm passage. Additionally, during flooding, OPO_4 concentrations were at an astonishingly high (maximum = 2.3 mg/L, mean = 0.3 mg/L, and median = 0.22 mg/L), while other sampling periods revealed concentrations a magnitude lower. As mentioned before, farmers will spray manure onto agricultural fields prior to hurricane impact, thus it is likely that flash losses of P occurred due to the heavy rainfall from Hurricane Florence

transporting P constituents from surface applications of manure. Moreover, research shows that P concentrations can be 100 times higher during these events compared to regular runoff (Wiederholt & Johnson, 2005).

It is important to consider that due to multicollinearity some variables were omitted from the model. Pearson's correlations between all continuous variables were calculated to inspect which candidate variables were highly correlated with covariates in the models (Figure 5). So while cropland to wetland area was kept in the model, any of the other variables that were multicollinear with cropland to wetland area (e.g., watershed area, total population, poor drainage area, and excessive drainage) could conceivably have been equally effective as cropland to wetland area in terms of explaining nutrient variance. However, the flooded developed land area, day of precipitation, and CAFO variables were not correlated with other variables, in turn giving us more confidence in interpreting these variables as descriptors of nutrient responses.

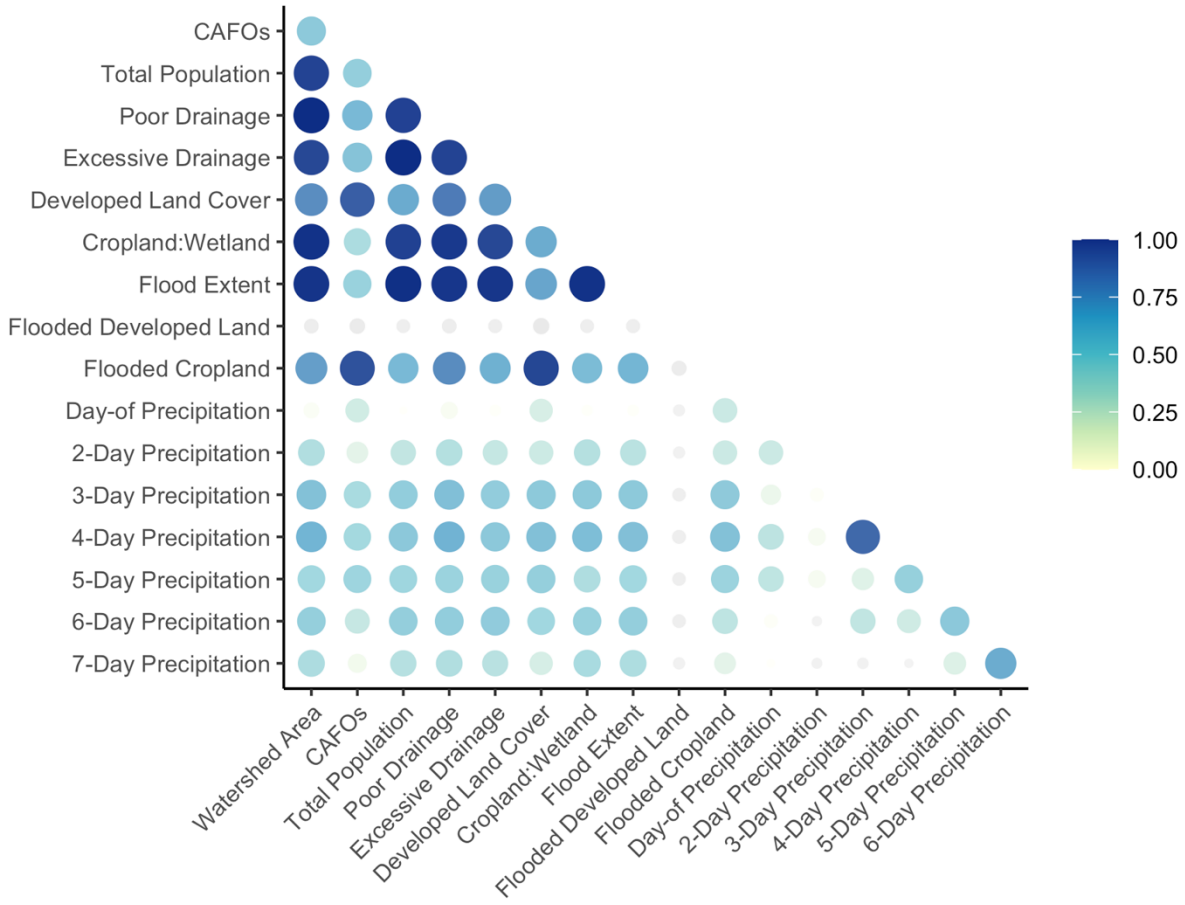

Figure 3- 5. Pearson's correlation plot of continuous candidate variables.

5. CONCLUSION

Extreme weather events associated with flooding are becoming more common and projected to increase in frequency and intensity (Hirabayashi et al., 2013). With surface waters being sensitive to nutrient enrichment, understanding of the drivers of nutrient runoff is important in explaining and managing factors that influence floodwater nutrient concentrations. Overall, this research shows that wastewater from CAFOs and WWTPs were likely sources of nutrient exports associated with Hurricane Florence, with rainfall amount being a primary driver. An investigation of flooded areas during Hurricane Florence highlighted that 190 swine CAFOs, 112 poultry CAFOs, and 299

WWTPs were flooded (Schaffer-Smith et al., 2020). Better management in development and implementation of CAFOs and WWTPs may be an additional measure to reduce nutrient pollution in floodwaters. Furthermore, many efforts have been made within eastern NC to reduce nutrient loading, ranging from stringent discharge regulations to best management practices within agricultural zones; however, most water quality control measures were designed for smaller storms that do not export as high of nutrient loads compared to extreme storm events, such as hurricanes (Humphrey et al., 2019). Further management of nutrient pollution should consider tackling potential wastewater runoff from extreme events. A potential strategy is to buyout CAFOs within flood-prone areas to prevent overtopping of swine waste lagoons and designing wastewater treatment plants for stronger storms.

6. REFERENCES

Arheimer, B., & Lidén, R. (2000). Nitrogen and phosphorus concentrations from agricultural catchments—Influence of spatial and temporal variables. *Journal of Hydrology*, *227*(1–4), 140–159. https://doi.org/10.1016/S0022-1694(99)00177-8

Beeson, S. (2018). *Pollution discharge from Hurricane Florence: Examining how North Carolina is Impacted by modern day storms* [Masters Thesis]. North Carolina State University. http://www.lib.ncsu.edu/resolver/1840.20/36304

Banerjee, S., Carlin, B.P., & Gelfand, A.E. (2014). Hierarchical Modeling and Analysis for Spatial Data (2nd ed.). Chapman and Hall/CRC. https://doi.org/10.1201/b17115

Burkholder, J., Eggleston, D., Glasgow, H., Brownie, C., Reed, R., Janowitz, G., Posey, M., Melia, G., Kinder, C., Corbett, R., Toms, D., Alphin, T., Deamer, N., & Springer, J. (2004). Comparative impacts of two major hurricane seasons on the Neuse River and western Pamlico Sound ecosystems. *Proceedings of the National Academy of Sciences*, *101*(25), 9291–9296. https://doi.org/10.1073/pnas.0306842101

Brooks, S. P., & Gelman, A. (1998). General methods for monitoring convergence of iterative simulations. *Journal of Computational and Graphical Statistics,* 7: 434–455.

Carey, R. O., Hochmuth, G. J., Martinez, C. J., Boyer, T. H., Dukes, M. D., Toor, G. S., & Cisar, J. L. (2013). Evaluating nutrient impacts in urban watersheds: Challenges and research opportunities. *Environmental Pollution*, *173*, 138–149. https://doi.org/10.1016/j.envpol.2012.10.004

Chen, N., Krom, M.D., Wu, Y., Yu, D., & Hong, H. (2018). Storm induced estuarine turbidity maxima and controls on nutrient fluxes across river-estuary-coast continuum. Science of The Total Environment, (628–629), 1108-1120. https://doi.org/10.1016/j.scitotenv.2018.02.060

Cherry, K. A., Shepherd, M., Withers, P. J. A., & Mooney, S. J. (2008). Assessing the effectiveness of actions to mitigate nutrient loss from agriculture: A review of methods. *Science of The Total Environment*, *406*(1–2), 1–23. https://doi.org/10.1016/j.scitotenv.2008.07.015

Ching, Y.C., Lee, Y.H., Toriman, M.E., Abdullah, M., & Yatim, B.B. (2015). Effect of the big flood events on the water quality of the Muar River, Malaysia. *Sustainable Water Resources Management,* 1, 97–110. https://doi.org/10.1007/s40899-015-0009-4

Clark, J.S. (2005). Why environmental scientists are becoming Bayesians. *Ecology Letters*, 8, 2–14. doi: 10.1111/j.1461-0248.2004.00702.x

Delkash, M., Al-Faraj, F. A. M., & Scholz, M. (2018). Impacts of Anthropogenic Land Use Changes on Nutrient Concentrations in Surface Waterbodies: A Review. *CLEAN – Soil, Air, Water*, *46*(5), 1800051. https://doi.org/10.1002/clen.201800051

Dewitz, J. (2019). National Land Cover Database (NLCD) 2016 Products: U.S. Geological Survey data release, https://doi.org/10.5066/P96HHBIE

Emanuel, R. & Wilkins, D.E. (2020). Breaching Barriers: The Fight for Indigenous Participation in Water Governance. *Water,* 12(8), 2113. https://doi.org/10.3390/w12082113

Gelman, A., & Rubin, D. B. (1992). Inference from iterative simulation using multiple sequences. *Statistical Science* 7: 457–472.

Ghosh, J. & Ghattas, A.E. (2015) Bayesian Variable Selection Under Collinearity, The American Statistician, 69:3, 165-173, DOI: 10.1080/00031305.2015.1031827

Hagy, J. D., Lehrter, J. C., & Murrell, M. C. (2006). Effects of Hurricane Ivan on water quality in Pensacola Bay, Florida. *Estuaries and Coasts*, *29*(6), 919–925. https://doi.org/10.1007/BF02798651

Haque, S. E. (2021). How Effective Are Existing Phosphorus Management Strategies in Mitigating Surface Water Quality Problems in the U.S.? *Sustainability*, *13*(12), Article 12. https://doi.org/10.3390/su13126565

Harris, A. R., Fidan, E. N., Nelson, N. G., Emanuel, R. E., Jass, T., Kathariou, S., Niedermeyer, J., Sharara, M., de los Reyes, F. L., Riveros-Iregui, D. A., & Stewart, J. R. (2021). Microbial Contamination in Environmental Waters of Rural and Agriculturally-Dominated Landscapes Following Hurricane Florence. *ACS ES&T Water*, *1*(9), 2012–2019. https://doi.org/10.1021/acsestwater.1c00103

Hirabayashi, Y., Mahendran, R., Koirala, S., Konoshima, L., Yamazaki, D., Watanabe, S., et al. (2013). Global flood risk under climate change. *Nature Climate Change*, 3(9), 816–821. https://doi.org/10.1038/nclimate1911

International Best Track Archive for Climate Stewardship (IBTrACS). (n.d.). 2018 Major Hurricane FLORENCE (2018242N13343). IBTrACS. https://ibtracs.unca.edu/index.php?name=v04r00-2018242N13343

Iverson, G., Humphrey, C.P., O'Driscoll, M.A., Sanderford, C., Jernigan, J., & Serozi, B. (2018). Nutrient exports from watersheds with varying septic system densities in

the North Carolina Piedmont. Journal of Environmental Management, 211, 206-217. https://doi.org/10.1016/j.jenvman.2018.01.063.

Jiang, C., Zhou, J., Wang, J., Fu, G., & Zhou, J. (2020). Characteristics and Causes of Long-Term Water Quality Variation in Lixiahe Abdominal Area, China. *Water*, *12*(6), Article 6. https://doi.org/10.3390/w12061694

Jongman, B., Ward, P. J., & Aerts, J. C. J. H. (2012). Global exposure to river and coastal flooding: Long term trends and changes. *Global Environmental Change*, 22(4), 823–835. https://doi.org/10.1016/j.gloenvcha.2012.07.004

Khajehei, S. (2019). *Recovery challenges of public housing residents after disasters: Lumberton, North Carolina after Hurricane Matthew* [Masters Thesis], Iowa State University. https://dr.lib.iastate.edu/handle/20.500.12876/31666

Kiaghadi, A., & Rifai, H. S. (2019). Physical, Chemical, and Microbial Quality of Floodwaters in Houston Following Hurricane Harvey. *Environmental Science & Technology*, *53*(9), 4832–4840. https://doi.org/10.1021/acs.est.9b00792

Lintern, A., Webb, J. a., Ryu, D., Liu, S., Bende-Michl, U., Waters, D., Leahy, P., Wilson, P., & Western, A. W. (2018). Key factors influencing differences in stream water quality across space. *WIREs Water*, *5*(1), e1260. https://doi.org/10.1002/wat2.1260

Liu, X., Wang, M., & Shi, W. (2009). A study of a Hurricane Katrina–induced phytoplankton bloom using satellite observations and model simulations. *Journal of Geophysical Research: Oceans*, *114*(C3). https://doi.org/10.1029/2008JC004934

Lloyd, S. P. (1957). Least squares quantization in PCM. Technical Report RR-5497, Bell Lab, September 1957.

Malaviya, P., & Singh, A. (2012). Constructed Wetlands for Management of Urban Stormwater Runoff. *Critical Reviews in Environmental Science and Technology*, *42*(20), 2153–2214. https://doi.org/10.1080/10643389.2011.574107

Mallin, M. A., & Cahoon, L. B. (2003). Industrialized Animal Production—A Major Source of Nutrient and Microbial Pollution to Aquatic Ecosystems. *Population and TheEnvironment*, *24*(5), 369–385.

Mallin, M. A., Posey, M. H., Shank, G. C., McIver, M. R., Ensign, S. H., & Alphin, T. D. (1999). Hurricane Effects on Water Quality and Benthos in the Cape Fear Watershed: Natural and Anthropogenic Impacts. *Ecological Applications*, *9*(1), 350–362. https://doi.org/10.1890/1051-0761(1999)009[0350:HEOWQA]2.0.CO;2

Marquardt, D. W. (1970). Generalized inverses, ridge regression, biased linear estimation, and nonlinear estimation. Technometrics, 12, 591–256.

Meybeck, M., & Helmer, R. (1989). The Quality of Rivers: From Pristine Stage to Global Pollution. *Global and Planetary Change*, *75*(4), 283–309. https://doi.org/10.1016/0921-8181(89)90007-6

Milly, P. C. D., Wetherald, R. T., Dunne, K. A., & Delworth, T. L. (2002). Increasing Risk of Great Floods in a Changing Climate. *Nature*, 415, 514−517.

Montefiore, L. R., Nelson, N. G., Dean, A., & Sharara, M. (2022). Reconstructing the historical expansion of industrial swine production from Landsat imagery. *Scientific Reports*, *12*(1), 1736. https://doi.org/10.1038/s41598-022-05789-5

Nash, J. E. & Sutcliffe, J. V. (1970), River flow forecasting through conceptual models part I -A discussion of principles. *Journal of Hydrology*, 10 (3), 282-290.

Neter, J., Wasserman, W. & Kutner, M. H. (1989). Applied Linear Regression Models. Homewood, IL: Irwin.

Newcomer Johnson, T. A., Kaushal, S. S., Mayer, P. M., Smith, R. M., & Sivirichi, G. M. (2016). Nutrient Retention in Restored Streams and Rivers: A Global Review and Synthesis. *Water*, *8*(4), Article 4. https://doi.org/10.3390/w8040116

Olszewska, D. O. (2005). *Wetland planning in agricultural landscape using Geographical Information System. A case study of Lake Ringsjön basin in South Sweden.* [Masters Thesis]. Linköping University. http://liu.diva-portal.org/smash/record.jsf?pid=diva2%3A20353&dswid=-8409

Paerl, H. W., Hall, N. S., Hounshell, A. G., Rossignol, K. L., Barnard, M. A., Luettich Jr., R. A., Rudolph, J. C., Osburn, C. L., Bales, J., & Harding Jr., L. W. (2020). *Recent increases of rainfall and flooding from tropical cyclones (TCs) in North Carolina (USA): Implications for organic matter and nutrient cycling in coastal watersheds*. *150*, 197–216.

Paerl, H. W., Valdes, L. M., Joyner, A. R., Peierls, B. L., Piehler, M. F., Riggs, S. R., Christian, R. R., Eby, L. A., Crowder, L. B., Ramus, J. S., Clesceri, E. J., Buzzelli, C. P., & Luettich, R. A. (2006). Ecological response to hurricane events in the Pamlico Sound system, North Carolina, and implications for assessment and management in a regime of increased frequency. *Estuaries and Coasts*, *29*(6), 1033–1045. https://doi.org/10.1007/BF02798666

Peierls, B. L., Christian, R. R., & Paerl, H. W. (2003). Water quality and phytoplankton as indicators of hurricane impacts on a large estuarine ecosystem. *Estuaries*, *26*(5), 1329–1343. https://doi.org/10.1007/BF02803635

Powell, M. (2020, September 14). *Hurricane Florence: What the Carolinas Learned.* National Flood Services. https://nationalfloodservices.com/blog/hurricane-florence-what-the-carolinas-learned-from-the-second-1000-year-flood-in-two-years/

Roetman, S. L. (2016, October 20). *Lumbee Tribe of NC Emerges Slowly From Hurricane Matthew Flood Waters.* Indian Country Today. https://indiancountrytoday.com/archive/lumbee-tribe-of-nc-emerges-slowly-from-hurricane-matthew-flood-waters

Rose, A. N., McKee, J.J.,Sims, K.M.,Bright, E.A.,Reith, A. E., & Urban, M.L. (2020). LandScan 2019. Oak Ridge National Laboratory.

Schaffer-Smith, D., Myint, S. W., Muenich, R. L., Tong, D., & DeMeester, J. E. (2020). Repeated Hurricanes Reveal Risks and Opportunities for Social-Ecological Resilience to Flooding and Water Quality Problems. *Environmental Science & Technology*, *54*(12), 7194–7204. https://doi.org/10.1021/acs.est.9b07815

Smith, L. M., Macauley, J. M., Harwell, L. C., & Chancy, C. A. (2009). Water Quality in the Near Coastal Waters of the Gulf of Mexico Affected by Hurricane Katrina: Before and After the Storm. *Environmental Management*, *44*(1), 149–162. https://doi.org/10.1007/s00267-009-9300-1

Song, Z., Chomicki, K. M., Drouillard, K., & Weidman, R. P. (2022). A statistical framework for testing impacts of multiple drivers of surface water quality in

nearshore regions of large lakes. *Science of The Total Environment*, *811*, 152362. https://doi.org/10.1016/j.scitotenv.2021.152362

Simpson, A. G. (2018, September 16). *Florence Floods Cause Sewage, Coal Ash Spills*. Insurance Journal. https://www.insurancejournal.com/news/southeast/2018/09/16/501423.htm

Soil Survey Staff. (2019). Gridded Soil Survey Geographic (gSSURGO) Database for North Carolina. United States Department of Agriculture, Natural Resources Conservation Service. http://datagateway.nrcs.usda.gov/

Spiegelhalter, D.J., Best, N.G., Carlin, B.P., & Van der Linde, A. (2002). Bayesian Measures of Model Complexity and Fit (with Discussion). *Journal of the Royal Statistical Society*, Series B, 64(4):583-616.

Steichen, J. L., Labonté, J. M., Windham, R., Hala, D., Kaiser, K., Setta, S., Faulkner, P. C., Bacosa, H., Yan, G., Kamalanathan, M., & Quigg, A. (2020). Microbial, Physical, and Chemical Changes in Galveston Bay Following an Extreme Flooding Event, Hurricane Harvey. *Frontiers in Marine Science*, *7*. https://www.frontiersin.org/articles/10.3389/fmars.2020.00186

Tomasko, D. A., Anastasiou, C., & Kovach, C. (2006). Dissolved oxygen dynamics in Charlotte Harbor and its contributing watershed, in response to hurricanes Charley, Frances, and Jeanne—Impacts and recovery. *Estuaries and Coasts*, *29*(6), 932–938. https://doi.org/10.1007/BF02798653

U.S. Department of Agriculture National Agricultural Statistics Service (NASS). (2022). *2021 State Agriculture Overview: North Carolina.*

https://www.nass.usda.gov/Quick_Stats/Ag_Overview/stateOverview.php?state=NORTH%20CAROLINA

U.S. Department of Commerce. (2018). *Historical Hurricane Florence, September 12-15, 2018*. National Weather Service. https://www.weather.gov/mhx/Florence2018

U.S. Environmental Protection Agency. (2000). *Ambient Water Quality Criteria Recommendations Information Supporting the Development of State and Tribal Nutrient Criteria: Rivers and Streams in Nutrient Ecoregion XIV.* https://www.epa.gov/sites/default/files/documents/rivers14.pdf

U.S. Geological Survey. (2016). The StreamStats program, online at http://streamstats.usgs.gov

U.S. Geological Survey. (n.d.). *Stream Grid Download*. StreamStats. https://streamstatsags.cr.usgs.gov/StreamGrids/directoryBrowsing.asp

Varanka, S., Hjort, J., & Luoto, M. (2015). Geomorphological factors predict water quality in boreal rivers. *Earth Surface Processes and Landforms*, *40*(15), 1989–1999. https://doi.org/10.1002/esp.3601

Wachnicka, A., Armitage, A. R., Zink, I., Browder, J., & Fourqurean, J. W. (2020). Major 2017 Hurricanes and their Cumulative Impacts on Coastal Waters of the USA and the Caribbean. *Estuaries and Coasts*, *43*(5), 941–942. https://doi.org/10.1007/s12237-020-00702-7

West, B. M., Liggit, P., Clemans, D. L., & Francoeur, S. N. (2011). Antibiotic Resistance, Gene Transfer, and Water Quality Patterns Observed in Waterways near CAFO Farms and Wastewater Treatment Facilities. *Water, Air, & Soil Pollution*, *217*(1–4), 473–489. https://doi.org/10.1007/s11270-010-0602-y

Wiederholt, R., & Johnson, B. (2005). Phosphorus Behavior in the Environment. *North Dakota State University Extension.* https://library.ndsu.edu/ir/bitstream/handle/10365/5360/nm1298.pdf?sequence=1

Wing, S., Freedman, S., & Band, L. (2002). The potential impact of flooding on confined animal feeding operations in eastern North Carolina. *Environmental Health Perspectives*, *110*(4), 387–391. https://doi.org/10.1289/ehp.02110387

Yang, S.-H., Chen, C.-H., & Chu, K.-H. (2021). Fecal indicators, pathogens, antibiotic resistance genes, and ecotoxicity in Galveston Bay after Hurricane Harvey. *Journal of Hazardous Materials*, *411*, 124953. https://doi.org/10.1016/j.jhazmat.2020.124953

Zhao, A., Cornish, K., & Gonsenhauser, R. (2020). *Environmental Justice Analysis of Post-Hurricane Funding and Planning.* [Master's Thesis], Duke University. Retrieved from https://hdl.handle.net/10161/20481

Zhao, H., Tang, D., & Wang, Y. (2008). Comparison of phytoplankton blooms triggered by two typhoons with different intensities and translation speeds in the South China Sea. *Marine Ecology Progress Series*, *365*, 57–65. https://doi.org/10.3354/meps07488

CHAPTER 4: THE IMPACTS OF HURRICANE STRENGTH AND WATERSHED CHARACTERISTICS ON ESTUARINE DISSOLVED OXYGEN DYNAMICS

Abstract

Hurricane events have the potential to alter the biogeochemical cycling of DO in estuaries and influence the ecological health of aquatic ecosystems. Prior studies demonstrate how estuarine DO response varies widely in response to tropical cyclones (e.g., hypoxia, increases in DO, no change). However, the majority of existing research focused on singular hurricane events or estuary sites, making it difficult to assess the extent to which previously reported results are unique to a given event or study system, and if there are generalizable and consistent post-storm patterns across estuaries and hurricanes. Our goal was to quantify the trends, if any, in DO dynamics after hurricane events across different estuarine systems. Within this study, we evaluated the trends in DO before, during, and after hurricane impact in different tidal estuaries spanning the southeast Atlantic coast of the US, a region routinely impacted by hurricanes and where long-term water quality data are available. Results indicate minor changes in DO trends upon hurricane impact; however, further findings revealed no indication of hypoxia or long-lasting impacts on estuarine DO.

Keywords: water quality, cyclones, tropical storms, near-shore environment

1. INTRODUCTION

Dissolved oxygen (DO) is a common indicator of water quality and ecological health in aquatic systems. However, estuarine DO dynamics are highly variable because they are driven by the balance of biological processes including primary productivity and respiration, as well as physical processes like tidal cycling (Kemp and Boynton, 1980). Net primary production is an important mechanism controlling DO cycles, in which aerobic respiration removes oxygen from the system to break down organic carbon, while photosynthesis contributes oxygen to the system by processing inorganic matter (Kemp and Testa, 2012). This balance in biological processes creates diurnal peaks in DO during daylight hours and steady decreases in DO during nighttime when oxygen is consumed and photosynthesis is not occurring (Bianchi, 2007). Tidal cycling also affects DO by mixing oxygen within the air into the water (via diffusion) through turbulence, and driving the exchange of relatively DO-rich and DO-poor waters from open and shallow waters, respectively (Eldridge & Roelke, 2011). Thus, tidal forcing typically creates a distinct tidal signal in DO concentration time series. Throughout the day, these processes play an important role in balancing DO in estuaries.

Large storm events, such as hurricanes, have the potential to alter the typical biogeochemical cycling of DO in estuaries due to both their high wind speeds and precipitation volumes. Numerous studies have revealed that hurricanes can create widespread hypoxia/anoxia in coastal basins (Burkholder et al., 2004; González-De Zayas et al., 2022; Mallin et al., 1999; Peierls et al., 2003; Schafer et al., 2020). Hypoxia and anoxia following tropical cyclones is largely explained as driven by the transport of

nutrients on the landscape to downstream systems from increased rainfall-driven river discharge and runoff. Additionally, increased fluvial forcing and wind disturbances from hurricanes can cause the resuspension of settled material, which can also contribute additional nutrients and promote increased rates of photosynthesis (Bianucci et al., 2018). In return, increased biomass of primary producers and organic matter create large and rapid decreases in DO due to respiration and decomposition, causing hypoxic/anoxic conditions.

Although less commonly reported, several studies have found increases or no change in DO after hurricane impact. Research by Barik et al. (2017) found an increase in DO in a shallow, bar-built estuary with little tidal influence after Cyclone Phailin, which was attributed to wind-induced mixing and resuspension of buried chlorophyll. A longitudinal study by Chen et al. (2017) also noted increases in DO after storm passage within three estuarine lagoons located in Big Lagoon Sound, Florida, USA. The authors propose that, although increased nutrient loading following the storms was observed, hypoxia may not have occurred due to high freshwater replacement rates and/or short residence times in the estuary, though this hypothesis was not proven. Meanwhile, Walker et al. (2021) found that Hurricane Harvey did not significantly change DO within the Guadalupe, Lavaca-Colorado, and Nueces-Corpus estuaries in Texas, USA. A possible reason suggested by the authors is that the increased availability of nutrients were counterbalanced by increased flushing, thus creating a circumstance in which DO concentrations were not significantly changed by the storm passage. Moreover, Taghon et al. (2016) found that Hurricane Sandy had no effect on DO in the Barnegat Bay in New Jersey, USA, likely due to little freshwater delivery to the estuary.

Combined, prior studies demonstrate how estuarine DO response varies widely in response to tropical cyclones (e.g., hypoxia, increases in DO, no change). The majority of existing research focused on singular hurricane events or estuary sites, making it difficult to assess the extent to which previously reported results are unique to a given event or study system, and if there are generalizable and consistent post-storm patterns across estuaries and hurricanes. Our goal was to quantify the trends, if any, in DO dynamics after hurricane events across different estuarine systems. Specifically, we evaluated the trends in DO before, during, and after hurricane impact in different tidal estuaries spanning the southeast Atlantic coast of the US, a region routinely impacted by hurricanes and where long-term water quality data are available. We hypothesized that the direction of an estuarine site's post-hurricane DO response (i.e., positive/increase, negative/decrease, no change) is primarily explained by the strength of the affecting cyclone as defined by wind speed, and whether an estuarine site is located in a developed watershed.

2. METHODS

2.1 Study area and data description

The east coast of the United States (US) is an area frequented by hurricanes and tropical storms due to the warm tropical waters. For this study, we focused on estuaries on the southeast Atlantic coast, which are similar in climate and ecoregion (8.5.1: Middle Atlantic Coastal Plain, 8.5.3: Southern Coastal Plain; US Environmental Protection Agency, 2022). A study region with some uniformity between sites allows us to focus on the influence of storm strength and watershed type on DO dynamics. In

addition, many hurricanes travel up the east coast of the US, which allows us to assess how different estuary systems were impacted by the same hurricane.

The National Estuarine Research Reserve System (NERRS) is a part of the National Oceanic and Atmospheric Administration (NOAA) and consists of 30 estuary sites. NERRS estuary systems are shallow, tidally influenced estuaries and typically have a short residence time. Longitudinal estuary water quality and meteorological data are available from the NERRS System-Wide Monitoring Program (SWMP) as far back as the 1990s (NOAA National Estuarine Research Reserve System, n.d.). The SWMP database contains continuous water quality (e.g., DO, water temperature, depth, salinity) and meteorological (e.g., wind speed, barometric pressure, air temperature) data at 15-30 minute intervals. Each NERRS reserve contains multiple sites for measuring water quality data and one site for recording meteorological data. The water quality sensors are placed in different developed and undeveloped estuary watersheds to compare long-term changes in land use and associated water quality. Estuary type and watershed condition were determined for each site using metadata accompanied with the DO observations. Stations were selected considering an even distribution of sites with developed and undeveloped watersheds, freshwater and marine influence, and tidal creeks and open water (Table 1; Figure 1). At some NERRS reserves, two quality sites would be in extreme proximity to one another; for example, East Cribbing and Zeke's Basin are located beside one another in Bald Head Island, North Carolina (Figure C-1). In this case, the site with more data was chosen for analysis. Hereafter, we refer to undeveloped watersheds as natural estuary systems within the text.

Table 4- 1. Southeast Atlantic NERRS sites with corresponding estuary characteristics. Residence time was determined from Moorman et al. (2002). Salinity and depth values are averages for the 2021 calendar year.

NERRS Reserve	Residence time	Site Name	Site Abbreviation	Estuary Type	Watershed Condition	Depth (m)	Salinity (psu)
North Carolina	2 days	Research Creek	nocrc	tidal creek and salt marsh with primarily marine influence	natural	1.2	29.7
North Carolina		East Cribbing	nocec	open water lagoon with primarily marine influence	natural	0.8	20.3
North Inlet – Winyah Bay	7 days	Oyster Landing	niwol	tidal creek with primarily marine influence	natural	1.9	31.2
North Inlet – Winyah Bay		Debidue Creek	niwdc	tidal marsh with primarily marine influence	developed	2.6	31.0
North Inlet – Winyah Bay		Thousand Acre	niwta	large tidal creek with freshwater influence	developed	2.5	8.1
ACE Basin	2 days	Mosquito Creek	acemc	micro tidal creek with primarily freshwater influence	developed	4.0	15.0

Table 4- 1. (continued)

ACE Basin		St. Pierre	acesp	tidal creek with primarily marine influence	natural	1.9	26.4
Sapelo Island	1 day	Dean Creek	sapdc	tidal creek with primarily marine influence	natural	0.9	19.3
Guana Tolomato Matanzas	6 days	Pellicer Creek	gtmpc	tidal creek with primarily freshwater influence	natural but developing	1.1	12.7
Guana Tolomato Matanzas		San Sebastian	gtmss	tidal inlet and open water lagoon with primarily marine influence	developed	5.2	32.3

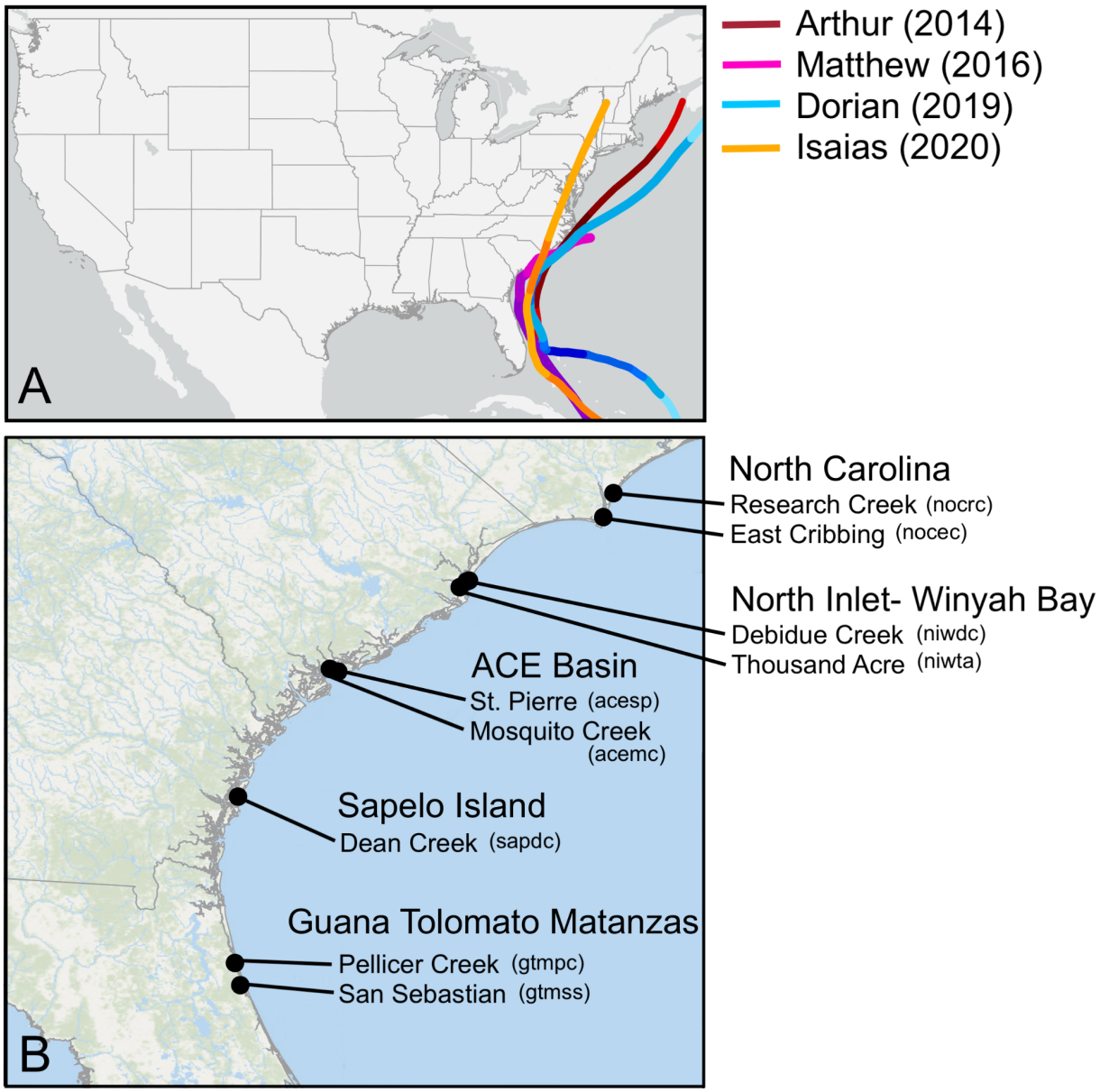

Figure 4- 1. A) Map of the U.S. with select hurricanes that have impacted the Atlantic coast. Each line color represents a different hurricane path, and the darker hues in color indicate instances in which the hurricane was a higher category. B) Map of study area and corresponding water quality sites within each NERRS reserve. Site abbreviations are shown in parentheses.

2.2 Data processing

Hurricane track data was obtained from the International Best Track Archive for Climate Stewardship (IBTrACS) (Knapp et al., 2010; Knapp et al., 2018). Similar to

Bianucci et al. (2018), all hurricanes within 200 km of each study site were delineated and dissolved oxygen data 15 days prior to and after landfall were imported. Here, landfall and hurricane impact both refer to when a hurricane reached 200 km of an estuary site. Due to extreme weather conditions, many hurricane events did not have continuous data available. Thus, for each site, hurricane events with greater than 20% missing DO data were thrown out. Additionally, to ensure that DO data was not missing during hurricane impact, hurricane events with over 1% data missing within 5 days of the storm were also thrown out. Any leftover missing data was linearly interpolated using the {SWMPr} R package (Beck, 2016).

Next, the dissolved oxygen data was detrended to reduce the effect of tidal advection on dissolved oxygen trends. By removing the tidal advection influence on DO, we can overlook the influence of tides on dissolved oxygen mixing and focus on other mechanisms that influence DO, such as primary production. The {oce} R package was used to generate fitted tidal harmonic constituents by providing depth, time, and location data (Kelley & Richards, 2022). The output from the {oce} package was tidal height information, which was used as an input in the {WtRegDO} R package (Beck et al., 2015). Continuous tidal height, DO, water temperature, salinity, air temperature, barometric pressure, and wind speed data are required to de-tide the DO values, which were obtained from the meteorological NERRS stations. A weighted regression approach was used to de-tide the DO values, as this method considers the complex and dynamic patterns of DO relative to advection and metabolism. After detrending, 19 different hurricane and site combinations were left in our dataset (Figure C-1).

2.3 Hurricane descriptions

After data processing, DO data for four hurricanes and 10 estuary sites were available for statistical analysis. The hurricanes included in this analysis were Hurricanes Arthur, Matthew, Doran, and Isaias (Figure 1B). The estuary sites that we were able to obtain continuous data are listed in Table 4-1.

Hurricane Arthur originated in the US east coast as a small tropical depression and increased to a category 2 hurricane upon reaching North Carolina on July 4, 2014 (Berg, 2015). Hurricane Arthur was not a wet storm and only brought 2-4 inches of rain upon landfall. The hurricane had a minimum pressure of 972 mb and maximum wind speed of 44 m/s.

Hurricane Matthew originated in Barbados as a category 5 hurricane and moved north to the Atlantic coast (Stewart, 2016). Upon reaching south Florida on October 6, 2016, Hurricane Matthew was a category 4 hurricane. By the time Hurricane Matthew reached North Carolina on October 8, it was downgraded to a category 1 hurricane. Despite this, Hurricane Matthew brought record-breaking rainfall along with it. Areas of South and North Carolina received 6-17 inches of rain, with some cities receiving 20 inches. Wind speed decreased from 54 to 36 m/s across Florida to North Carolina, respectively. Similarly, pressure increased from 944 mb in Florida to 981 mb in the North Carolina area.

Hurricane Dorian originated in the Caribbean and moved up the east coast of the US (Avila et al., 2020). Upon reaching the Bahamas on September 1, 2019, Dorian was a category 5 storm. As Hurricane Dorian migrated north, the storm downgraded to a category 2/3 hurricane. When hugging the southeast coast, the wind speed and

pressure hovered between 46-51 m/s and 955-960 mb, respectively. While the hurricane moved toward South and North Carolina on September 5-6, it produced large amounts of rainfall ranging from 5-10 inches and a peak of 15 inches.

Hurricane Isaias was a small hurricane that alternated between tropical storm and category 1 status (Latto et al., 2021). Isaias originated in the Caribbean and moved north up the US Atlantic coastline. Upon reaching south Florida on August 1, 2020, Hurricane Isaias was a tropical storm, but increased to a category 1 hurricane with 33 m/s winds and 991 mb pressure after migrating to the Georgia area on August 3. Isaias was not a wet hurricane and brought 1-3 inches of rain to the Carolinas, with some areas reportedly receiving up to 7 inches. Further detailed information on all hurricanes is available at: https://coast.noaa.gov/hurricanes.

2.4 Statistical analyses

In order to understand the changing trends between pre-storm and post-storm conditions, we analyzed estuarine DO during three time periods: 15 days prior to impact, 0-5 days after hurricane impact, and 5-15 days after impact (Bianucci et al., 2018). Here, we focus on DO trends up to two weeks after the storm since the typical residence time within these tidal estuaries is less than a week. Detrended DO data were analyzed for mean, standard deviation, range, and rate of change during the three time periods of interest, and comparisons were made between hurricane categories and different estuary systems.

Ordinary least squares regression models were built for the three time periods of interest for each site and hurricane combination. We chose to regress detrended DO concentrations against time to capture the rate of change and mean trend of DO before

and after hurricane impact (Figure 2). The regression coefficient (slope) and corresponding p values ($p < 0.05$) were used to evaluate the DO trend pre- and post-storm landfall and test for significant differences from zero. Slope values that were not significant indicated no change in DO trends, while positive and negative values showed increasing and decreasing DO trends, respectively.

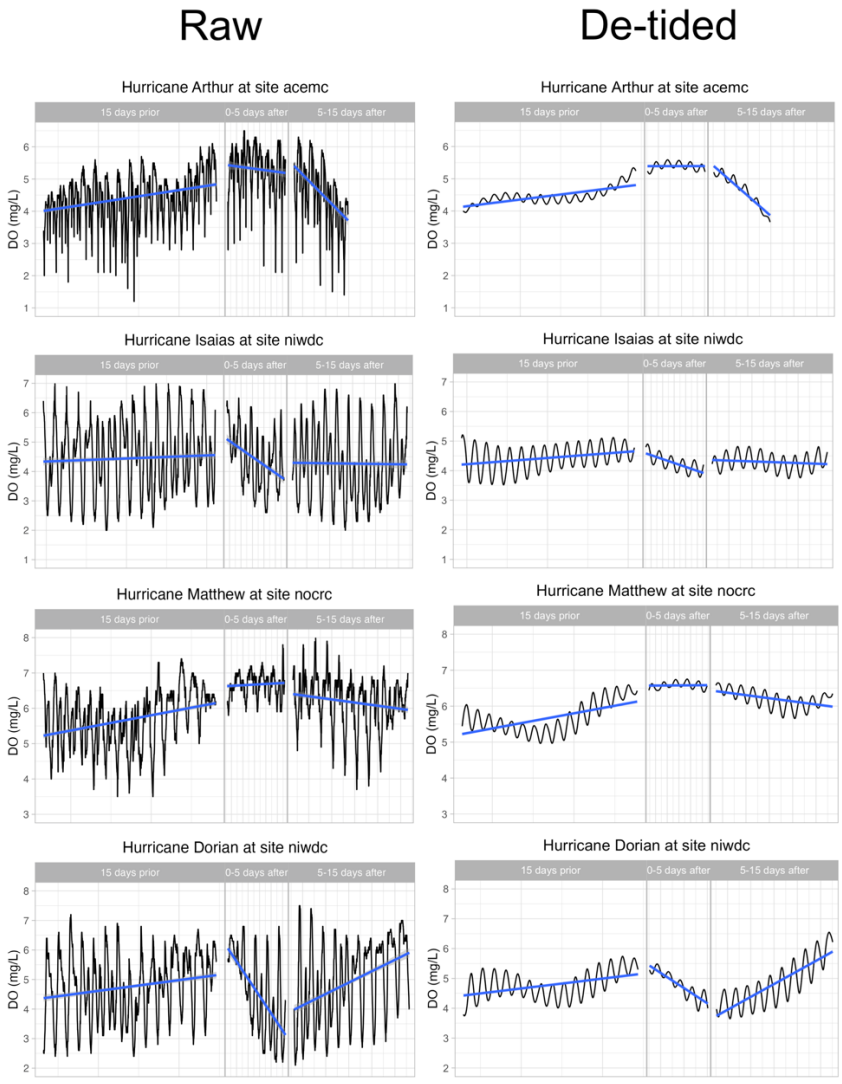

Figure 4- 2. Time series raw (left) and detided (right) dissolved oxygen concentrations for different hurricane events at select estuary sites. Each linear regression trendline (blue) within a plot panel corresponds to the three study periods: 15 days prior to storm impact, 0-5 days after storm impact, and 5-15 days after storm impact, respectively.

Additionally, to evaluate the change in DO at the time of hurricane impact, DO concentration was predicted at landfall using the pre-storm (15 days prior to landfall) regression model and post-storm (0-5 days after landfall) regression model. The difference in DO between the two model predictions represented how DO changed at the time of hurricane impact.

3. RESULTS

Mean DO values during the three different temporal periods were investigated. The estuary sites revealed low mean DO conditions (ranging from 3.6 to 5.9 mg/L) prior to storm landfall. The range of mean DO values in sites with developed and natural watersheds are highlighted in Table 4-2. Natural estuary sites demonstrated a greater range in DO values compared to developed estuary watersheds. Additionally, many estuary sites with developed watersheds experienced a decrease in DO, while most estuaries with natural watersheds experienced an increase in average DO after hurricane impact. However, these changes in mean DO between temporal periods were small and returned to pre-storm conditions within the 5-15 day period. Similarly, no trend was observed between mean DO and varying hurricane strength (Figure C-2).

Table 4- 2. Summary of mean DO values in developed and natural estuary watersheds. All DO units are in mg/L.

	Developed			Natural		
	15 days prior	0-5 days after	5-15 days after	15 days prior	0-5 days after	5-15 days after
Mean	4.77	4.90	4.73	4.74	5.07	4.86
Min	4.32	4.02	4.20	3.63	3.41	3.44
Max	5.49	5.57	5.65	5.89	6.58	6.20

DO variance decreased across all sites and storms after hurricane passage, with the exception of acesp during Tropical Storm Isaias. All sites impacted by category 2 and 3 storms had decreased DO variance immediately after the hurricane (0-5 days), then increased to pre-storm conditions later (5-15 days). Natural estuary systems appeared to experience a greater change in standard deviation from storm impact when compared to developed sites, however the changes in standard deviation were very small.

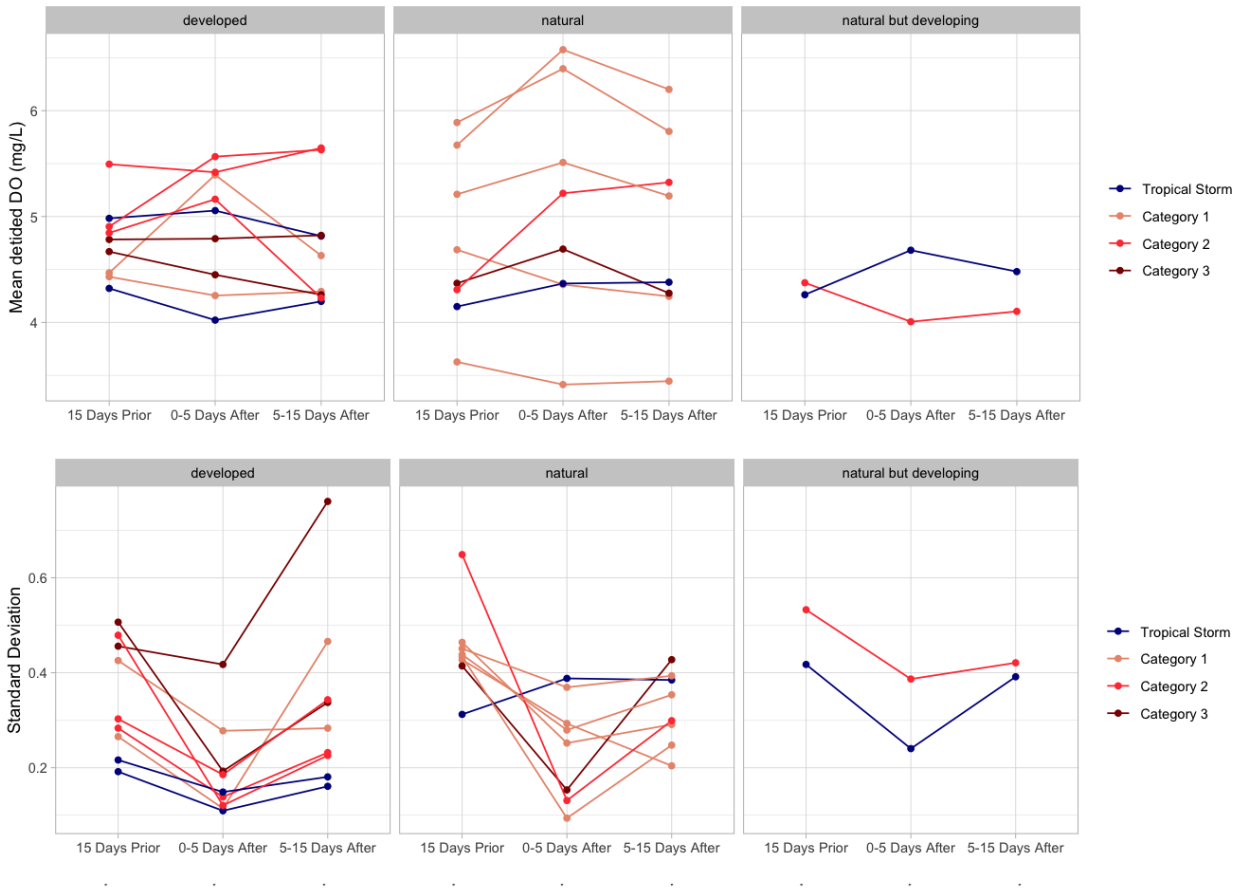

Figure 4- 3. Mean (top) and standard deviation (bottom) of DO values during three temporal periods. Color corresponds to the Saffir-Simpson Hurricane Scale category upon local impact.

To evaluate whether there was a step change in DO concentrations following storm landfall, DO concentration was predicted at landfall using the regression model built for 15 days prior to storm and 0-5 days after storm (Figure 4). This showed that at landfall, most sites experienced an increase in DO, although the increases were small. The greatest “jump” in DO was for a category 3 storm. Interestingly, Hurricane Isaias was the only storm for which immediate decreases in DO after landfall were observed across all affected sites.

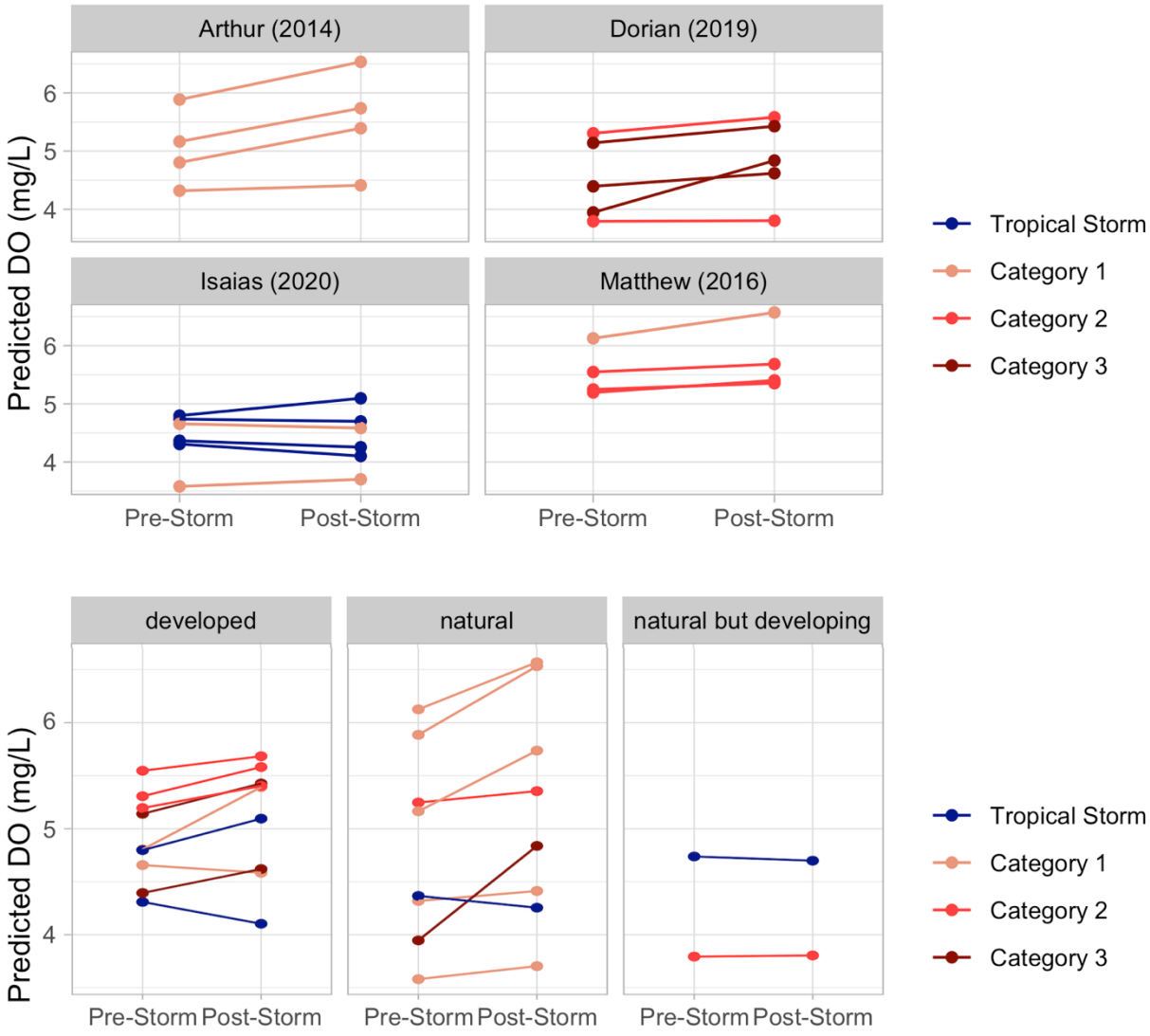

Figure 4- 4. Predictions of DO (mg/L) at landfall using the pre-storm and post-storm linear regression models. Top figure displays the predicted DO within different watershed types, while the bottom figure displays the same information by hurricane.

Slope was assessed to understand the linear trend of DO during the three different time periods (Figure 5). Results show that for tropical storms the change in slope after storm passage was relatively small across different sites and the greatest change in slope was after a category 3 hurricane impact. P values were calculated to further determine if the DO trends were significantly different from zero (Figure 6). This

demonstrated that nearly all sites experienced a decreasing trend in DO after landfall. An evaluation of slope across different sites did not indicate a clear trend, although there appears to be consistency within each site's response to different hurricanes.

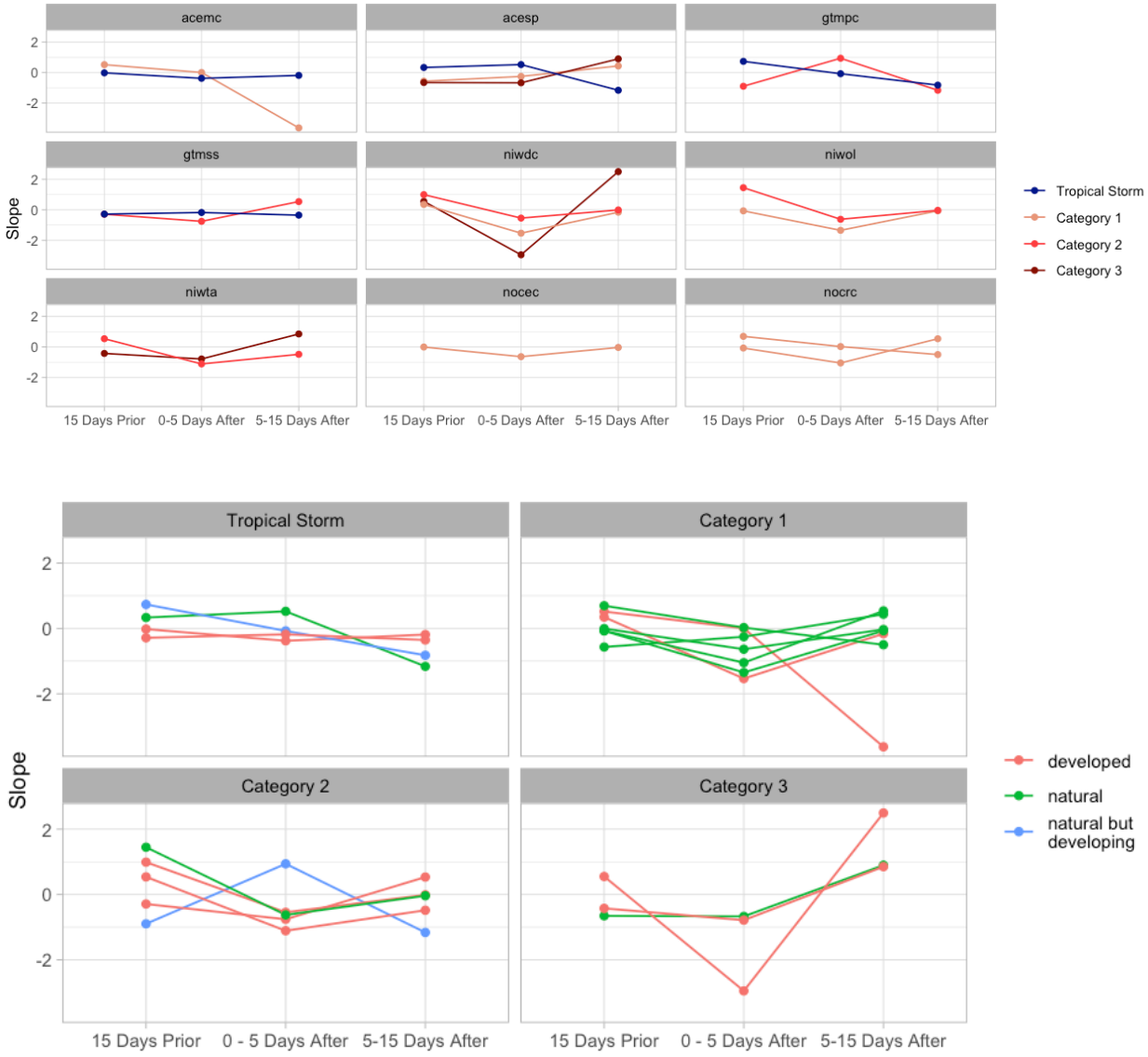

Figure 4- 5. Slope values are represented for each site with color corresponding to hurricane category upon impact (top) and for each hurricane category with color corresponding to the level of development within the site's watershed (bottom). Due to representation of time being in seconds, slope values were extremely small (with an order of magnitude of 10-6); therefore, slope values were multiplied by 106 for plotting purposes.

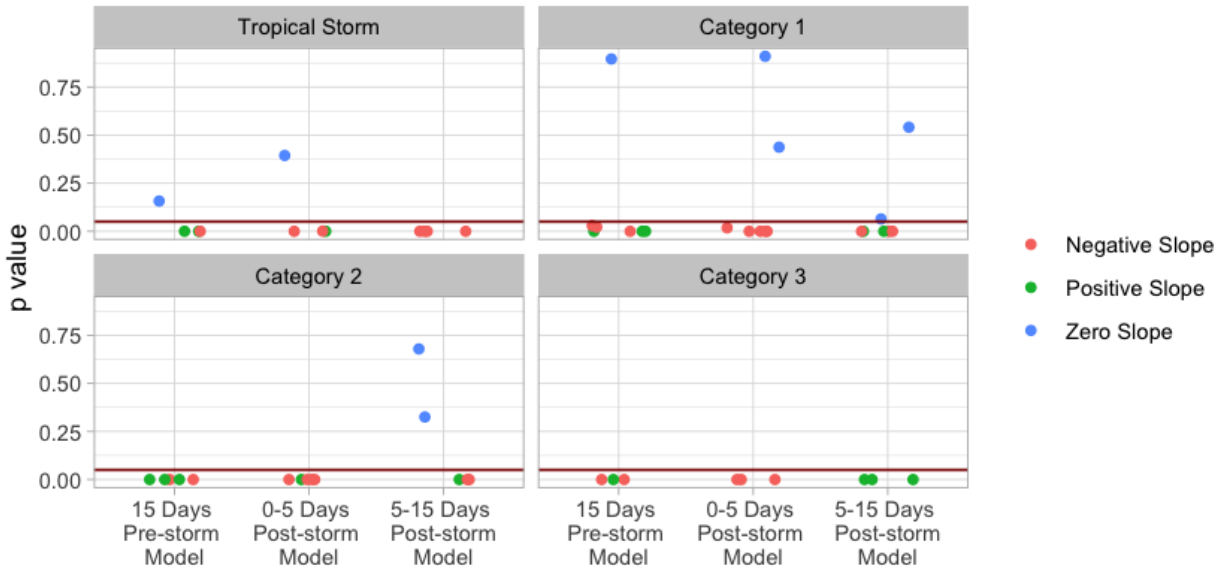

Figure 4- 6. P values for each linear regression model and the corresponding direction of DO trend.

4. DISCUSSION

Post-hurricane DO cycling is dependent on many factors including rainfall delivery of nutrients, resuspension of sediment and organic matter from winds, changes in temperature and salinity, metabolic activity, and light limitation. These processes are complex and no estuary is exactly the same, however, previous research indicates that hurricane and estuary characteristics have a strong influence on coastal water quality. Despite this, our understanding of DO dynamics induced by different storms across estuary types is still unknown.

This study analyzed DO trends prior to, during, and after hurricane passage within different estuaries along the south Atlantic coast of the U.S. Because of the known connections between runoff, nutrient loading, and DO concentrations in estuaries, we investigated if developed and undeveloped estuaries had clear differences in DO trends following cyclone impact and whether hurricane category had

an influence on the DO magnitude and response. Overall, we found that changes in DO dynamics were minute and short-lived, with no clear differentiation between different estuaries and hurricane categories.

4.1 Hurricane influence

We found that hurricane strength changed DO dynamics upon landfall, but the disturbance is minor and temporary. The highest category hurricanes created the largest decrease in DO variance during hurricane passage, which returned to pre-storm concentrations after 5-15 days. Tropical storms hardly impacted the trends in DO, while category 3 hurricanes (max wind speeds of 178-208 km/h) created the largest change between pre- and post-storm conditions. However, these trends between the rate of DO change and hurricane strength are not as pronounced for category 1 and 2 hurricanes (wind speeds of 119-153 and 154-177 km/h, respectively). Similar findings were presented in Walker et al. (2021), which found that a category 4 hurricane instigated short-term changes in DO that returned to pre-storm conditions within 9 days, despite the devastating destruction incurred inland from the catastrophic hurricane.

In this analysis, the highest category hurricanes (category 2 and 3 in this case) were also wet hurricanes with heavy rainfall. Thus, it is likely that high nutrient inputs were delivered to the estuaries; however, increased flushing and shorter residence times may have overshadowed the increased nutrient availability. A study conducted in an embayed estuary with restricted water exchange and long residence time (~1 year) found that increased hurricane activity fueled widespread hypoxia (Paerl et al., 2018). The long retention time within this estuary allowed existing phytoplankton groups to accumulate in nutrient rich waters and induce long-lasting hypoxia. Thus, embayed

estuaries, unlike the tidally-dominated estuaries in this study, may be more likely to experience large changes in DO from severe hurricanes.

In addition, within this analysis, hurricane strength is measured according to the Saffir-Simpson hurricane category scale. The Saffir-Simpson scale only considers the maximum sustained wind speed of a hurricane. Thus, the more noticeable changes in DO within high category storms may be a result of the heavy rainfall and not necessarily the storm strength. Overall, there is a potential relationship between hurricane strength and DO response; however, future work should explore how rainfall and residence time influence the DO dynamics in estuaries.

4.2 Estuary watershed influence

We found that natural estuaries experienced a greater change in DO standard deviation after storm impact, compared to developed estuary systems. However, the variation in standard deviation was on such a small scale that the impact on DO is nearly negligible. Park et al. (2007) found that diel DO patterns disappeared during hurricane passage and (Taghon et al., 2016) noted the dampening of diurnal signals, which may explain the decrease in variance within the days of hurricane impact. Although the mechanisms behind the disappearance of diel DO signals are not clear, hurricane impact may have created disturbances, like light limitation due to turbidity and cloud cover, that inhibited growth among phytoplankton groups. However, the raw and detided DO observations (Figure 2) show that diel patterns were largely not disrupted, although a few cases showed that diel patterns were muted for a brief period. Thus, our results agree with prior findings, but also show that dampening of diel variation varies by site and event.

Previous studies found that estuaries with development received large nutrient load pulses and consequently experienced decreased DO and hypoxia following hurricanes (Chen et al., 2017; González-De Zayas et al., 2022). However, post-storm DO declines were not observed in our study, as we found that DO changes were short-lived and none of the sites experienced hypoxia (≤ 3 mg/L) after hurricane impact. The rapid return to pre-storm conditions demonstrates that water quality, specifically DO, in estuaries such as those studied here can be resilient in the face of acute and short-term change. Similar findings were reported in a recent study by Walker et al. (2021), who showed that lagoonal systems with minimal tidal influence did not experience negative DO impacts from a catastrophic hurricane, despite previous studies suggesting that these systems are susceptible to hypoxia. Wetz and Yoskowitz (2013) explain that high turbidity and flow after hurricanes can create unfavorable conditions for biomass growth. This may explain why the estuaries within this study did not experience severe changes in DO. Specifically, the short residence time within the tidally-influenced estuaries likely induced freshwater flushing and dilution of nutrients and organic matter entering the coastal basins; this effect may have feasibly muted the DO response. Findings from this study can help explain, in part, why seagrass and fish communities across the Atlantic coast are not severely impacted by hurricanes (Anton et al., 2009; Wilson et al., 2020; Zhang et al., 2022).

In summary, previous work has highlighted case studies of hurricanes creating widespread hypoxic conditions, however, a majority of these studies focus on an estuary's response to a singular hurricane event. It is important to evaluate DO dynamics considering different storms and estuary systems, as different estuary types,

watershed conditions, and hurricane characteristics impact coastal DO in different ways that aren't limited to hypoxia. Choked estuaries with high development and slow residence time showed long lasting hypoxia (González-De Zayas et al., 2022; Paerl et al., 2006), while some shallow bar-built estuaries surrounded by barrier islands showed no response (Taghon et al., 2016; Walker et al., 2021). In some cases, the literature revealed that sites with similar estuary type and watershed characteristics exhibited opposite trends in DO, which may be potentially explained by hurricane characteristics (e.g., windy hurricanes can inhibit stratification, rainy hurricanes may deliver increased nutrient loads). Overall, our findings align with other studies that found no revealing change in water quality after hurricane impact. In the future, the DO response to differences in estuary residence time should be further investigated to understand if flushing is the mechanism explaining the lack of DO response. In particular, the Atlantic estuaries within this study were tidally influenced and had short residence times, thus it is reasonable for estuaries with long residence times and little water exchange to experience more severe DO responses after hurricanes, as a result of runoff and retention.

5. REFERENCES

Anton, A., Cebrian, J., Duarte, C. M., Jr, K. L. H., & Goff, J. (2009). Low Impact of Hurricane Katrina on Seagrass Community Structure and Functioning in the Northern Gulf of Mexico. *Bulletin Of Marine Science*, *85*(1), 15.

Avila, L., Stewart, S., Berg, R., & Hagen, A. (2020). Hurricane Dorian. In *National Hurricane Center Tropical Cyclone Report*. https://www.nhc.noaa.gov/data/tcr/al052019_dorian.pdf

Barik, S. K., Muduli, P. R., Mohanty, B., Behera, A. T., Mallick, S., Das, A., Samal, R. N., Rastogi, G., & Pattnaik, A. K. (2017). Spatio-temporal variability and the impact of Phailin on water quality of Chilika lagoon. *Continental Shelf Research*, *136*, 39–56. https://doi.org/10.1016/j.csr.2017.01.019

Beck, M.W. (2016). "SWMPr: An R Package for Retrieving, Organizing, and Analyzing Environmental Data for Estuaries." *The R Journal*, 8(1), 219-232.

Beck, M.W., Hagy III, J.D., & Murrell, M.C. (2015). Improving estimates of ecosystem metabolism by reducing effects of tidal advection on dissolved oxygen time series. *Limnology and Oceanography Methods*, 13(12), 731-745. DOI: 10.1002/lom3.10062

Berg, R. (2015). Hurricane Arthur. In *National Hurricane Center Tropical Cyclone Report.* https://www.nhc.noaa.gov/data/tcr/al012014_arthur.pdf

Bianucci, L., Balaguru, K., Smith, R. W., Leung, L. R., & Moriarty, J. M. (2018). Contribution of hurricane-induced sediment resuspension to coastal oxygen dynamics. *Scientific Reports*, *8*(1), 15740. https://doi.org/10.1038/s41598-018-33640-3

Chen, Y., Cebrian, J., Lehrter, J., Christiaen, B., Stutes, J., & Goff, J. (2017). Storms do not alter long-term watershed development influences on coastal water quality. *Marine Pollution Bulletin*, *122*(1–2), 207–216. https://doi.org/10.1016/j.marpolbul.2017.06.038

González-De Zayas, R., Merino-Ibarra, M., Lestayo González, J. A., Chaviano-Fernández, Y., Alatorre Mendieta, M. A., Pupo, F. M., & Castillo-Sandoval, F. S. (2022). Biogeochemical responses of a highly polluted tropical coastal lagoon after the passage of a strong hurricane (Hurricane Irma). *Journal of Water and Climate Change*, *13*(2), 1089–1105. https://doi.org/10.2166/wcc.2021.178

Kelley, D. & Richards, C. (2022). oce: Analysis of Oceanographic Data. R package version 1.7-10, https://dankelley.github.io/oce/.

Kemp, W. M., & Boynton, W. R. (1980), Influence of biological and physical processes on dissolved oxygen dynamics in an estuarine system: Implications for measurement of community metabolism. *Estuarine and Coastal Marine Science*, 11(4), 407–431, https://doi.org/10.1016/S0302-3524(80)80065-X

Kemp, W. M., & Testa, J. M. (2012). Metabolic balance between ecosystem production and consumption, p. 83118. In E. Wolanski, and D. S. McLusky [eds.], *Treatise on estuarine and coastal science.* Academic Press.

Knapp, K. R., Diamond, H. J., Kossin, J. P., Kruk, M. C., & Schreck, C. J. (2018). International Best Track Archive for Climate Stewardship (IBTrACS) Project, Version 4. NOAA National Centers for Environmental Information. doi:10.25921/82ty-9e16

Knapp, K. R., Kruk, M. C., Levinson, D. H., Diamond, H. J., & Neumann, C. J. (2010). The International Best Track Archive for Climate Stewardship (IBTrACS): Unifying tropical cyclone best track data. *Bulletin of the American Meteorological Society*, 91, 363-376. doi:10.1175/2009BAMS2755.1

Latto, A., Hagen, A., & Berg, R. (2021). Hurricane Isaias. In *National Hurricane Center Tropical Cyclone Report*. https://www.nhc.noaa.gov/data/tcr/al092020_isaias.pdf

Moorman, M.C., Hoos, A.B., Bricker, S.B., Moore, R.B., García, A.M., & Ator, S.W. (2002) Nutrient Load Summaries for Major Lakes and Estuaries of the Eastern United States. National Water-Quality Assessment Program. Data Series 820. https://pubs.usgs.gov/ds/0820/pdf/ds820.pdf

NOAA National Estuarine Research Reserve System (NERRS). System-wide Monitoring Program. Data accessed from the NOAA NERRS Centralized Data Management Office website: http://www.nerrsdata.org

Paerl, H. W., Crosswell, J. R., Van Dam, B., Hall, N. S., Rossignol, K. L., Osburn, C. L., Hounshell, A. G., Sloup, R. S., & Harding, L. W. (2018). Two decades of tropical cyclone impacts on North Carolina's estuarine carbon, nutrient and phytoplankton dynamics: Implications for biogeochemical cycling and water quality in a stormier world. *Biogeochemistry*, *141*(3), 307–332. https://doi.org/10.1007/s10533-018-0438-x

Paerl, H. W., Valdes, L. M., Joyner, A. R., Peierls, B. L., Piehler, M. F., Riggs, S. R., Christian, R. R., Eby, L. A., Crowder, L. B., Ramus, J. S., Clesceri, E. J., Buzzelli, C. P., & Luettich, R. A. (2006). Ecological response to hurricane events in the Pamlico Sound system, North Carolina, and implications for assessment and

management in a regime of increased frequency. *Estuaries and Coasts*, *29*(6), 1033–1045. https://doi.org/10.1007/BF02798666

Park, K., Valentine, J. F., Sklenar, S., Weis, K. R., & Dardeau, M. R. (2007). The Effects of Hurricane Ivan in the Inner Part of Mobile Bay, Alabama. *Journal of Coastal Research*, *23*(5), 1332–1336. https://doi.org/10.2112/06-0686.1

Schafer, T., Ward, N., Julian, P., Reddy, K.R., Osborne, T.Z. (2020). Impacts of Hurricane Disturbance on Water Quality across the Aquatic Continuum of a Blackwater River to Estuary Complex. *Journal of Marine Science and Engineering*, 8(6), 412. doi.org/ 10.3390/jmse8060412

Stewart, S. (2016). Hurricane Matthew. In *National Hurricane Center Tropical Cyclone Report.* https://www.nhc.noaa.gov/data/tcr/al142016_matthew.pdf

Taghon, G. L., Ramey, P. A., Fuller, C. M., Petrecca, R. F., & Grassle, J. P. (2016). Benthic Community Structure and Sediment Properties in Barnegat Bay, New Jersey, Before and After Hurricane Sandy. *Estuaries and Coasts*, *40*(1), 160–172. https://doi.org/10.1007/s12237-016-0133-x

US Environmental Protection Agency. (2022, July 26). *Ecoregions of North America*. US EPA. https://www.epa.gov/eco-research/ecoregions-north-america

Walker, L. M., Montagna, P. A., Hu, X., & Wetz, M. S. (2021). Timescales and Magnitude of Water Quality Change in Three Texas Estuaries Induced by Passage of Hurricane Harvey. *Estuaries and Coasts*, *44*(4), 960–971. https://doi.org/10.1007/s12237-020-00846-6

Wetz, M. S., & Yoskowitz, D. W. (2013). An ‘extreme’ future for estuaries? Effects of extreme climatic events on estuarine water quality and ecology. *Marine Pollution Bulletin*, *69*(1–2), 7–18. https://doi.org/10.1016/j.marpolbul.2013.01.020

Wilson, S. S., Furman, B. T., Hall, M. O., & Fourqurean, J. W. (2020). Assessment of Hurricane Irma Impacts on South Florida Seagrass Communities Using Long-Term Monitoring Programs. *Estuaries and Coasts*, *43*(5), 1119–1132. https://doi.org/10.1007/s12237-019-00623-0

Zhang, Q., Bostic, J. T., & Sabo, R. D. (2022). Regional patterns and drivers of total nitrogen trends in the Chesapeake Bay watershed: Insights from machine learning approaches and management implications. *Water Research*, *218*, 118443. https://doi.org/10.1016/j.watres.2022.118443

CHAPTER 5: SUMMARY OF STUDIES AND FUTURE RESEARCH

This dissertation presents research on the application of data science tools in understanding the hurricane impacts on flood extent and flood-impacted surface water quality.

In chapter 2, a Random Forest machine learning model was trained using remotely sensed imagery and geospatial characteristics to predict pluvial flooding within a region of the North Carolina Coastal Plain. The trained model was used to generate a timeline of pluvial flooding during Hurricanes Matthew (2016) and Florence (2018) at 10-m resolution. Results of model evaluation indicated high accuracy, with physically-based predictor variables, distance to the nearest stream, distance to the nearest road, and height above nearest drainage, being the most important in flood extent prediction. Further analysis of model outputs highlighted that croplands, specifically corn, soybean, and tobacco fields, were most impacted by the pluvial flooding. Therefore, the model may be used to emphasize agricultural areas susceptible to pluvial flooding, crops that may be potentially impacted, and characteristics of areas that experience pluvial flooding.

In chapter 3, we aimed to explain nutrient concentrations in flood-impacted surface waters as a function of different environmental variables. Data were gathered at four time points after Hurricane Florence (2018) impacted the North Carolina Coastal Plain and analyzed for total Kjeldahl nitrogen, total ammonia nitrogen, nitrite and nitrate, total phosphorus, and orthophosphate. A geostatistical model was trained to explain nitrogen and phosphorus concentrations in relation to different land characteristics, pollution point sources, and hydroclimatic factors. Results indicate that concentrated

animal feeding operations, croplands, and wastewater treatment plants were likely sources of nutrient exports associated with Hurricane Florence. Better management of agricultural resources for extreme storm events may be an additional measure to reduce nutrient pollution in floodwaters.

In chapter 4, our goal was to quantify trends in estuarine dissolved oxygen dynamics after hurricane impacts. Tidal estuaries within the Atlantic coast were evaluated for trends 15-days before, 5 days after, and 5-15 days after hurricane impact using least squared regression analysis. Overall, we found that changes in dissolved oxygen dynamics were minute and short-lived, with no clear differentiation between different estuaries and hurricane categories. However, future work should explore how differences in rainfall and estuary residence time influences changes in dissolved oxygen upon hurricane impact.

Overall, this dissertation applies different analytical tools and methods to quantify the hurricane impacts on surface water quantity and quality. The research presented contributes to the understanding of hurricane influence on flood extent and flood-impacted surface water quality, and presents potential drivers that explain the trends in surface water dynamics. This research is only a step forward toward uncovering the interactions between anthropogenic activities, hydroclimatic conditions, landscape characteristics, and surface water resources. Future research should leverage advances in data science methods to inform mechanistic understanding of surface water dynamics, improve modeling approaches through process-informed machine learning, and create analytical systems for real-time assessment of hurricane impacts.

APPENDICES

APPENDIX A

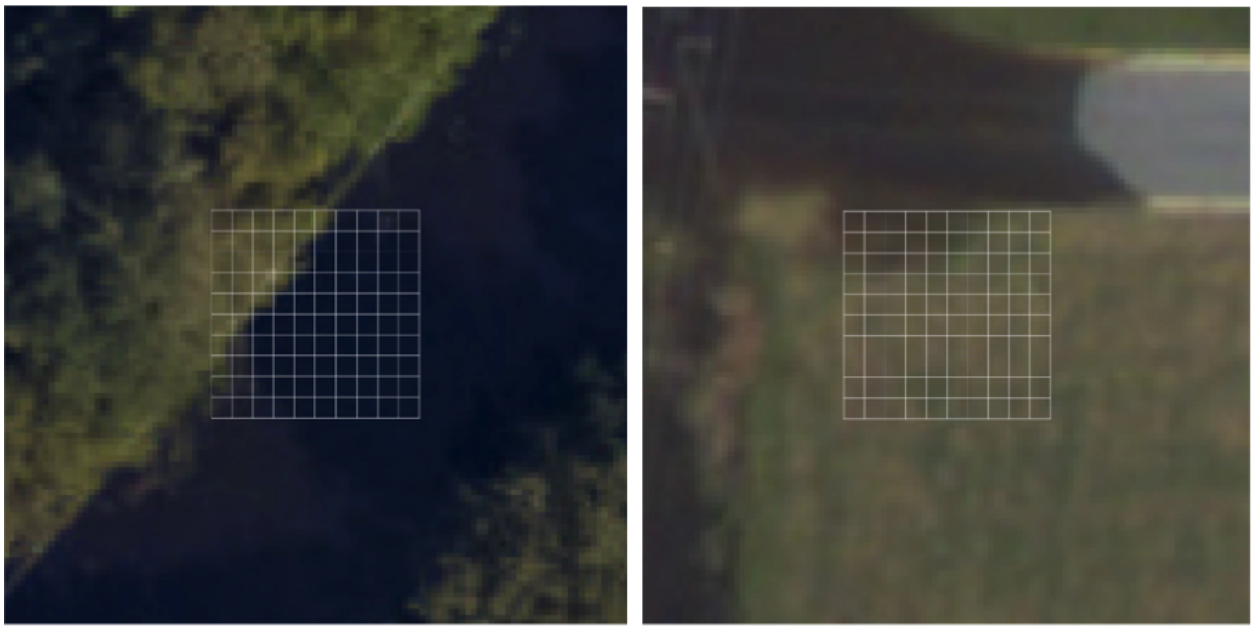

Figure A- 1. Examples of sample tiles used for the NDWI threshold determination. The left image shows a sample tile labeled as flooded, and the right image shows a sample tile labeled as non-flooded.

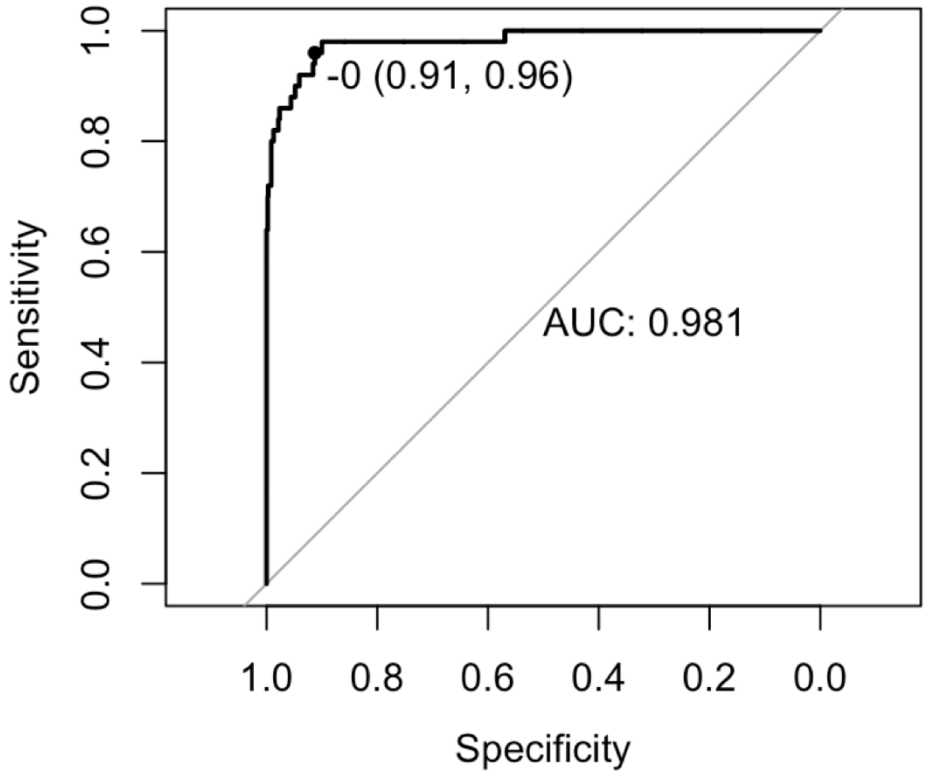

Figure A- 2. The resulting summary graphic of the ROC analysis.

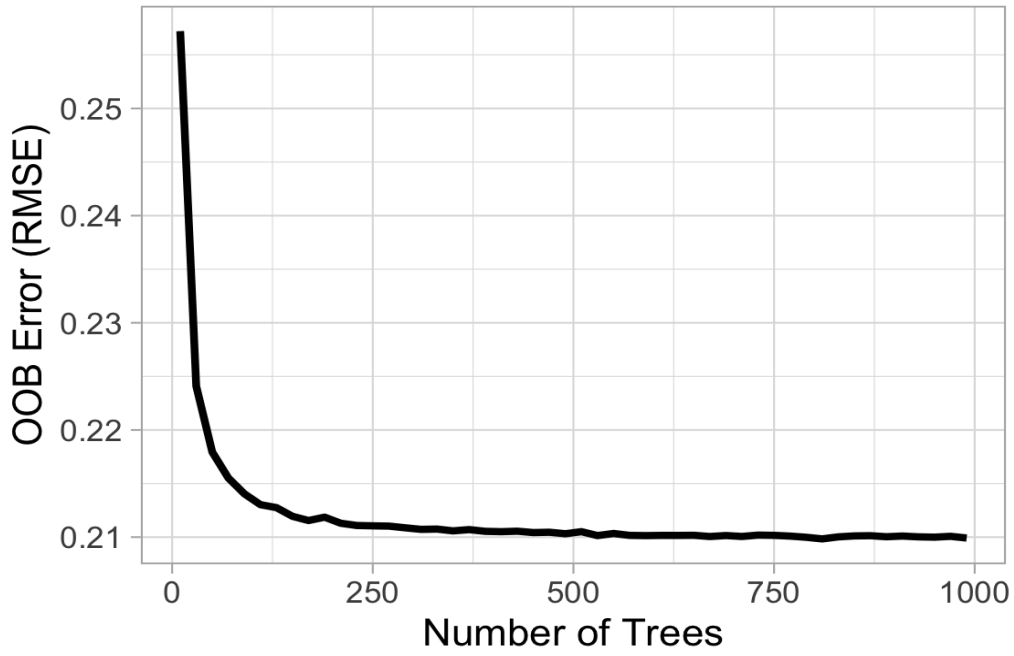

Figure A- 3. The out of bag (OOB) error associated with Random Forest models trained with varying numbers of trees.

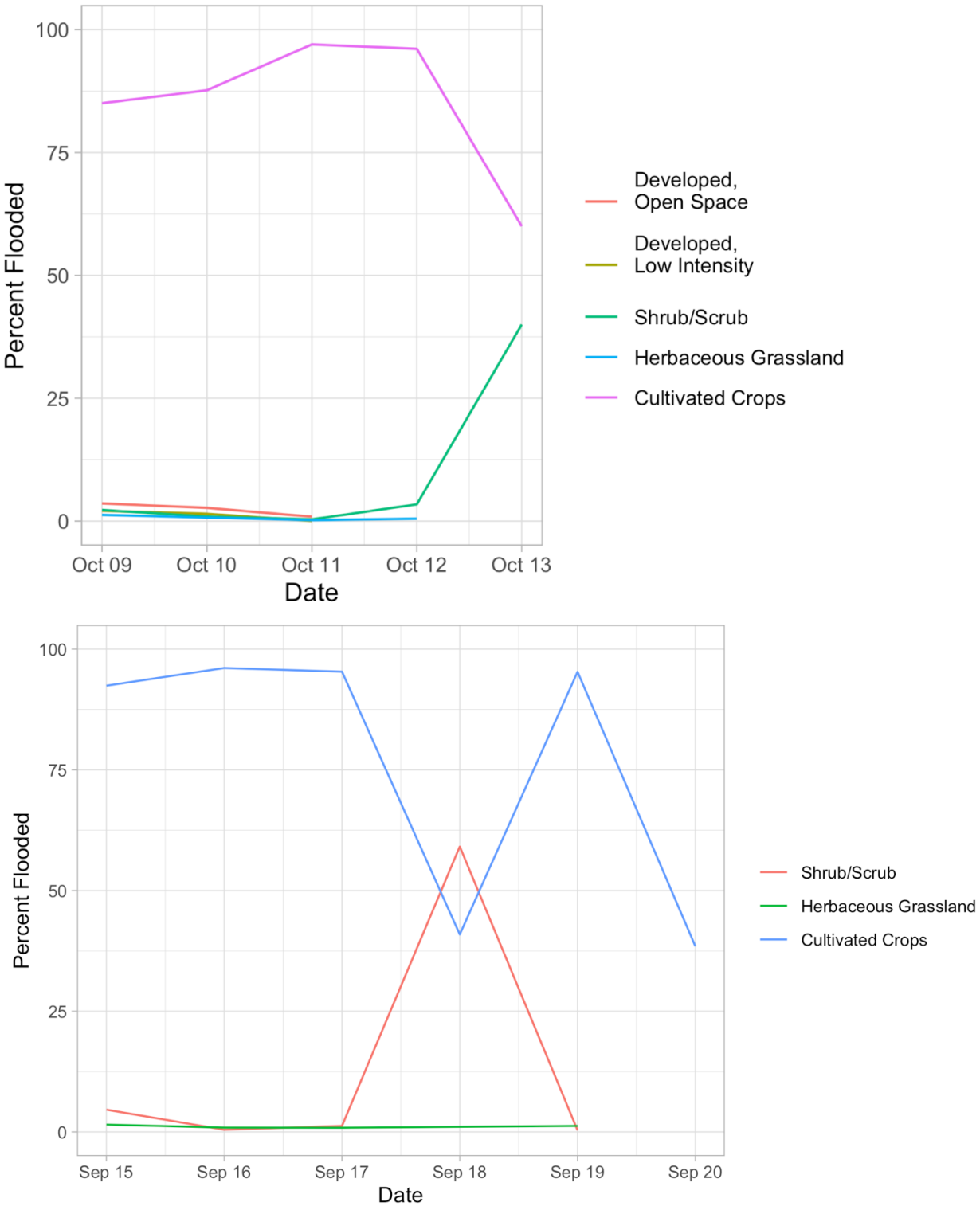

Figure A- 4. Percent of flooded area for each dominant land cover classification for Hurricanes Matthew (top figure) and Florence (bottom figure).

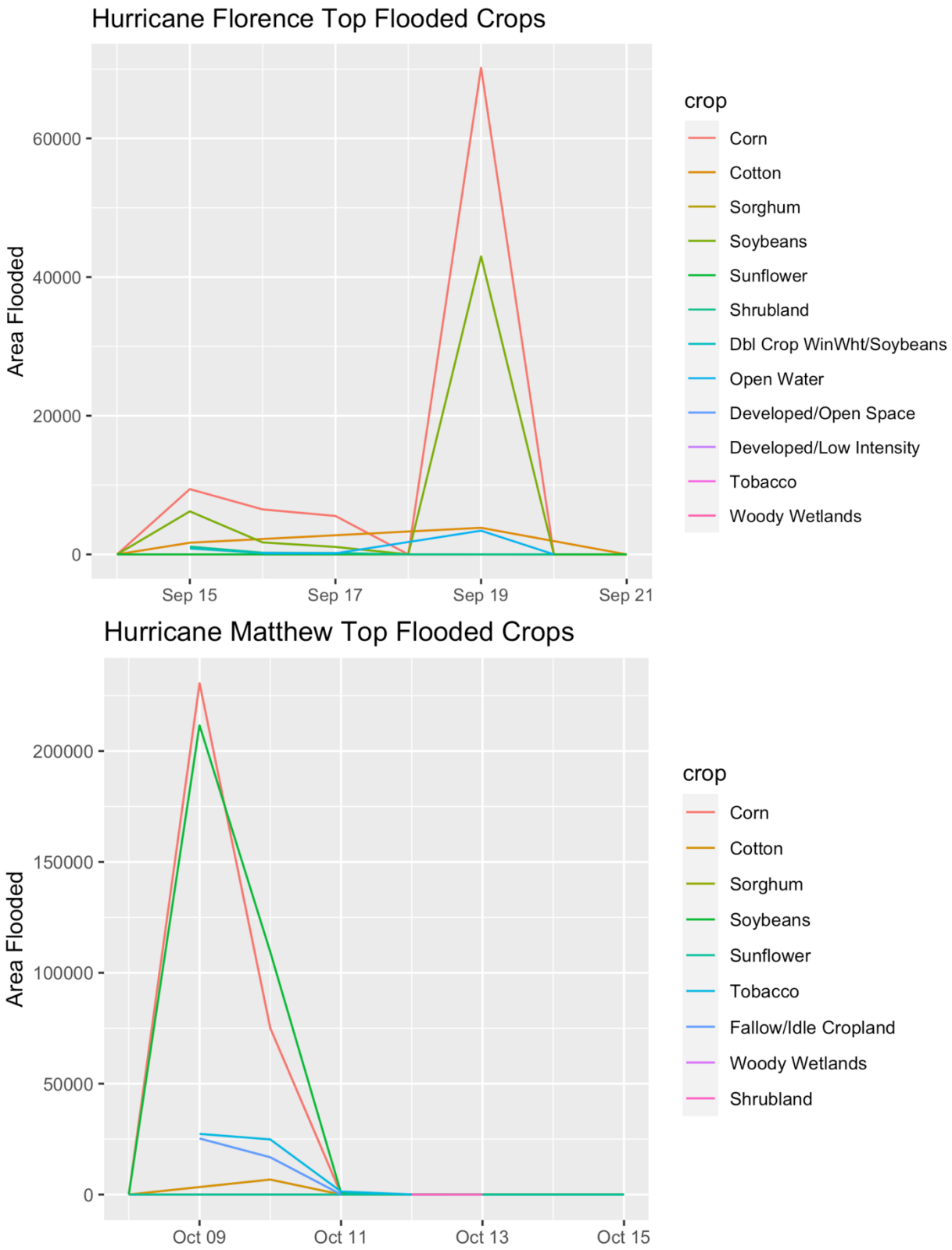

Figure A- 5. Timeline of the croplands that were flooded during Hurricanes Florene and Matthew.

APPENDIX B

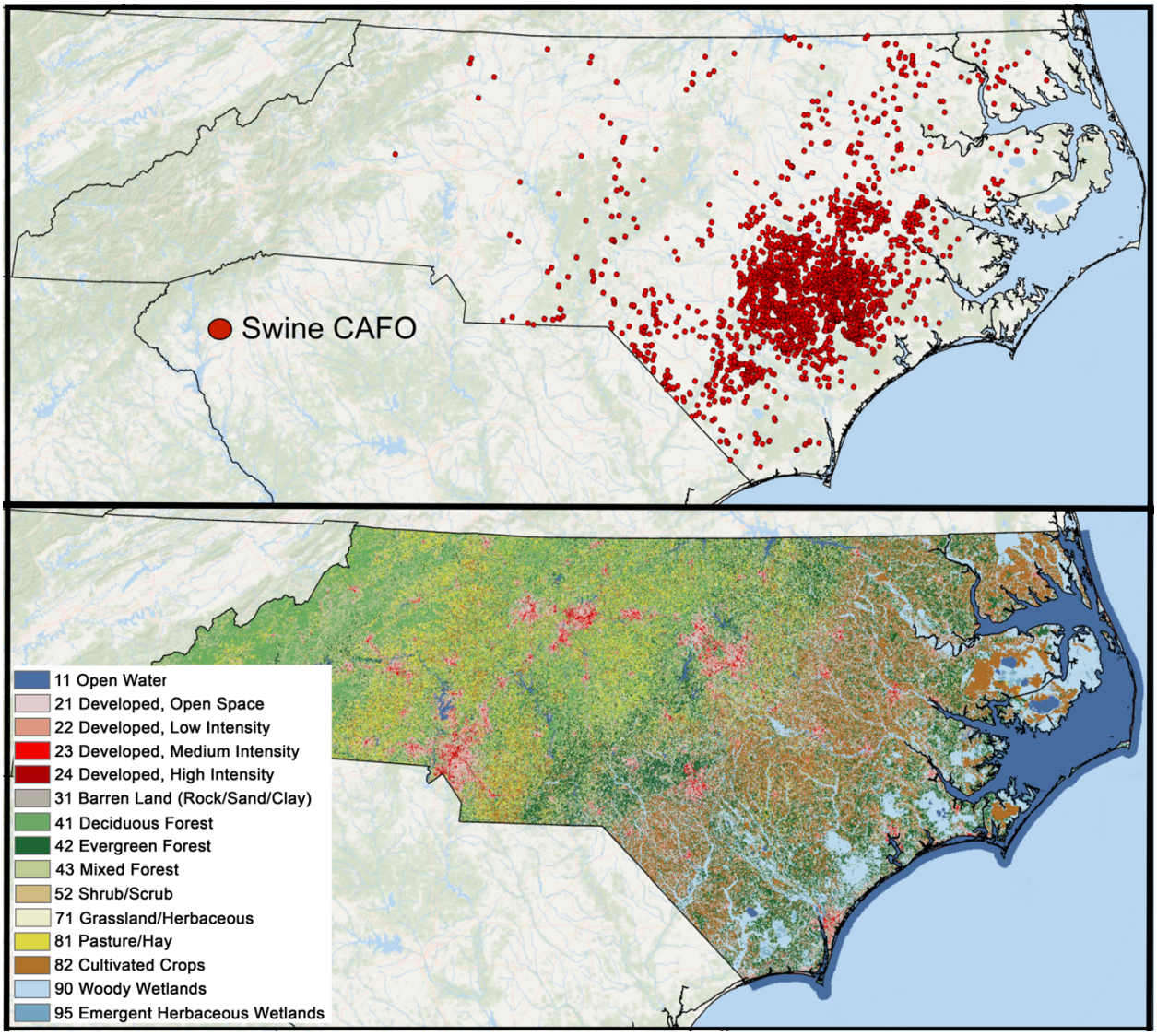

Figure B- 1. Swine CAFO locations (top figure) and landcover characteristics (bottom figure) in NC.

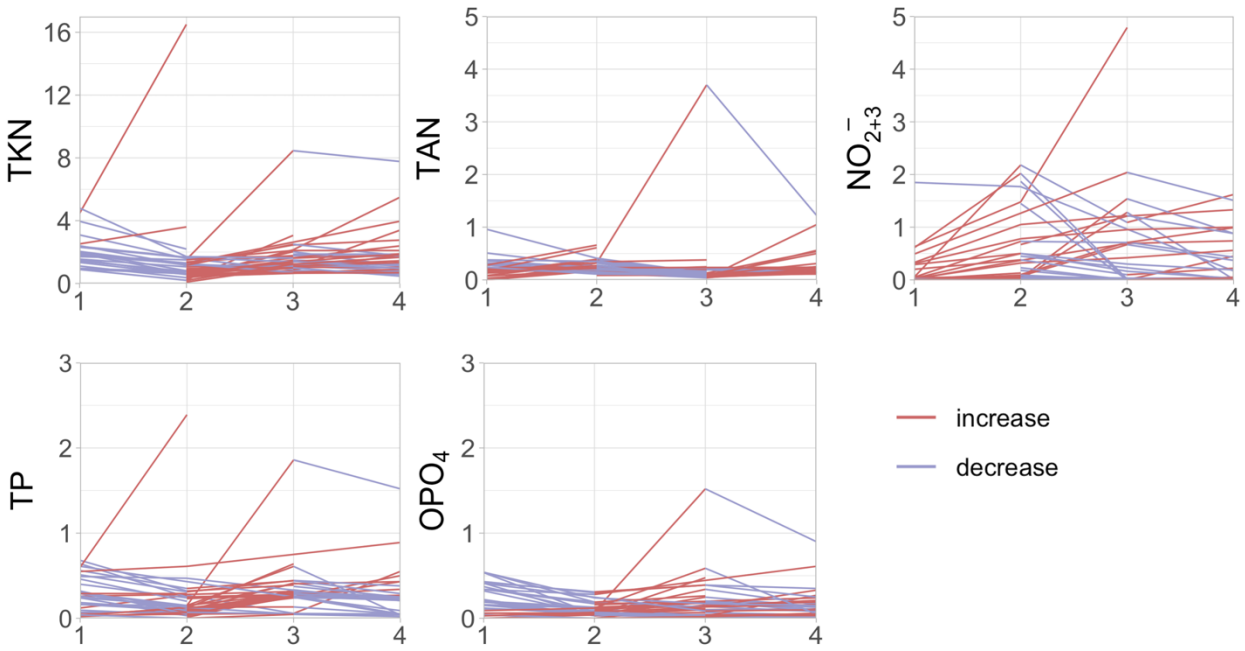

Figure B- 2. Site by site variability of TKN, TAN, NO_{2+3}^-, TP, and OPO_4 concentrations in mg/L. Colors indicate increasing and decreasing trends across sampling phases.

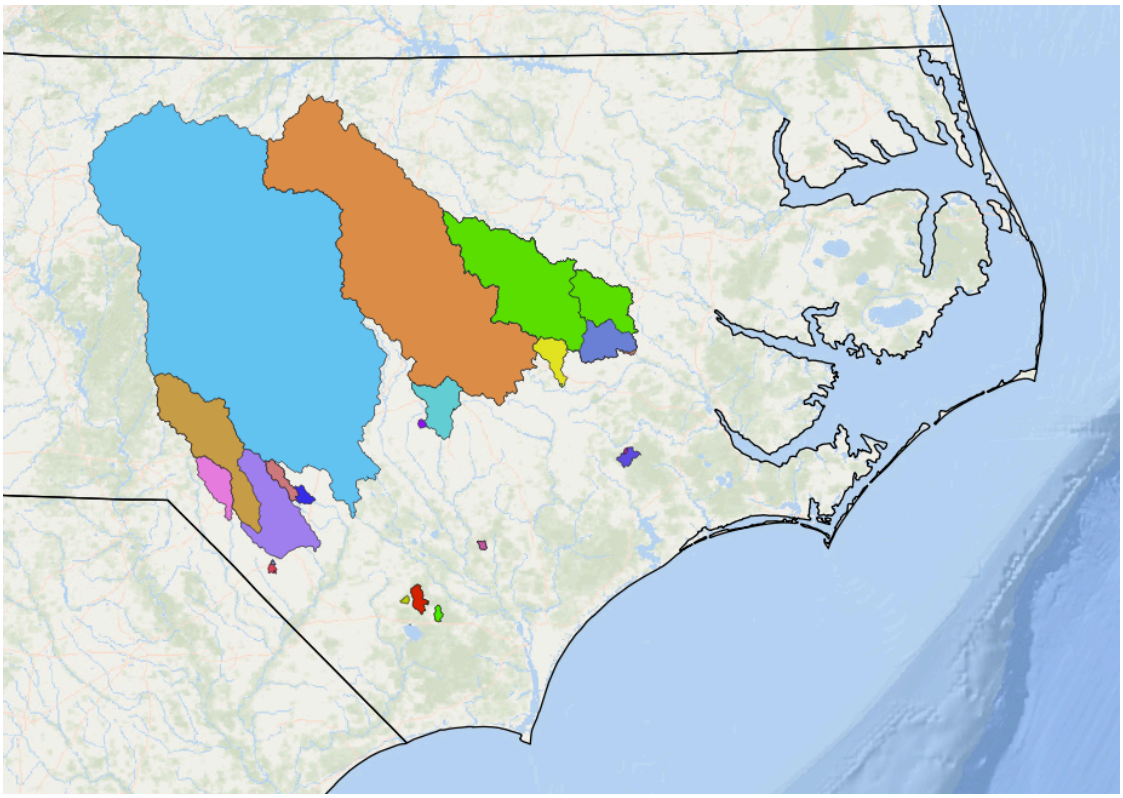

Figure B- 3. Watersheds delineated for each sampled site. Colors indicate different site drainage areas.

Table B- 1. Comparison of DIC values between different models.

Spatial/NonSpatial	Factors	Mean DIC
Spatial	1	1334
Spatial	2	1016
Spatial	3	840
Spatial	4	643
Spatial	5	1335
NonSpatial	NA	1859

Table B- 2. NSE values for each nutrient response using the final trained model.

Nutrient	NSE value
TKN	0.92
TAN	0.83
NO_{2+3}^{-}	0.95
TP	0.91
OPO_4	0.97

APPENDIX C

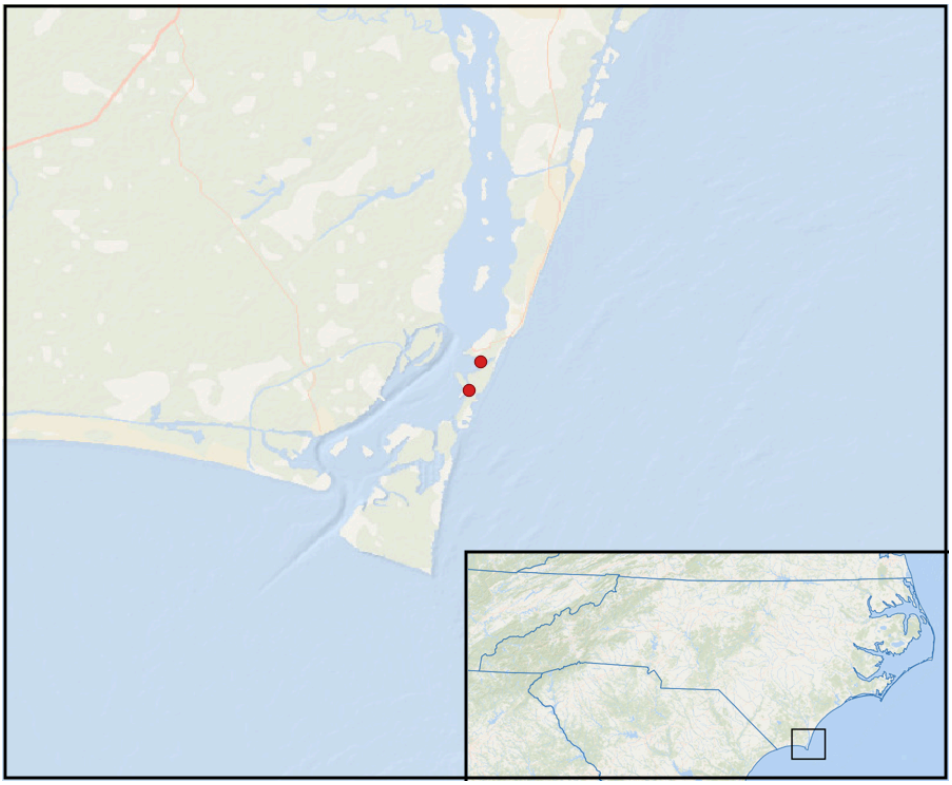

Figure C- 1. Proximity of NERRS sites at East Cribbing and Zeke's Basin.

Table C- 1. Delineated hurricanes for each site. Category represents the Saffir-Simpson Hurricane Scale at the time of impact, in which 0 indicates a tropical storm.

NERRS Site	Hurricane (Year)	Category
acemc	Arthur (2014)	1
acesp	Arthur (2014)	1
nocec	Arthur (2014)	1
nocrc	Arthur (2014)	1
acesp	Dorian (2019)	3
gtmpc	Dorian (2019)	2
gtmss	Dorian (2019)	2
niwdc	Dorian (2019)	3
niwta	Dorian (2019)	3
acemc	Isaias (2020)	0
acesp	Isaias (2020)	0
gtmpc	Isaias (2020)	0
gtmss	Isaias (2020)	0
niwdc	Isaias (2020)	1
niwol	Isaias (2020)	1
niwdc	Matthew (2016)	2
niwol	Matthew (2016)	2
niwta	Matthew (2016)	2
nocrc	Matthew (2016)	1

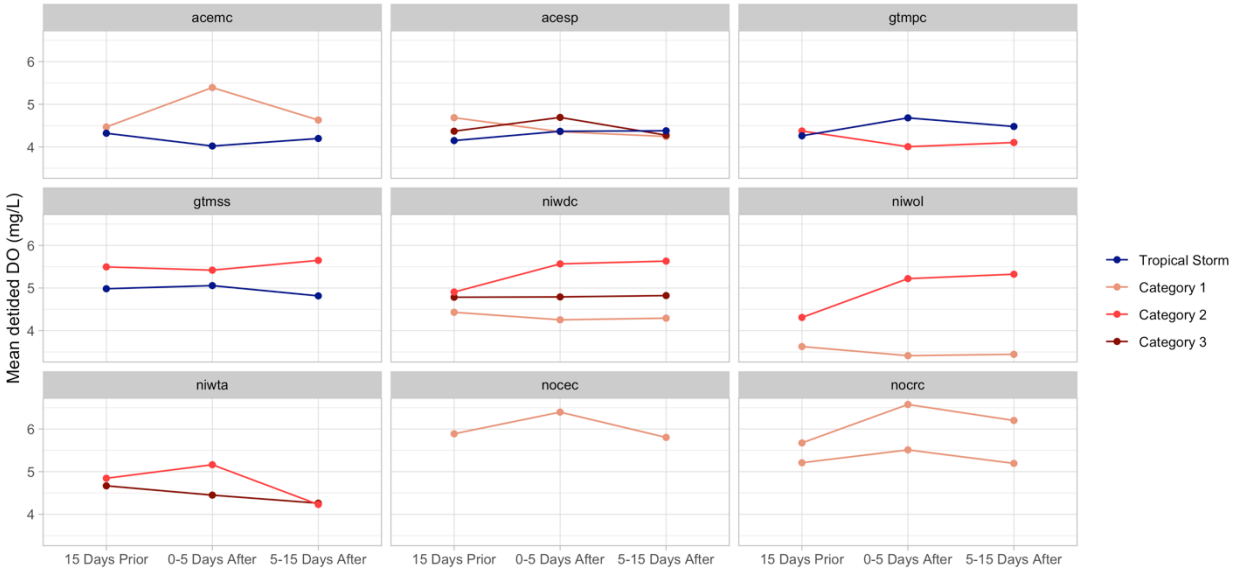

Figure C- 2. Mean DO (mg/L) for each estuary site. Colors represent hurricane category.